



**Politecnico
di Torino**

Politecnico di Torino

Automotive engineering

A.Y. 2022/2023

17/10/2023

**Piston system definition and verification
in CNG engine for truck application**

Relatori: Carlo Rosso

Candidato: Lorenzo Ridolfi

Tutor aziendale: Luca Tiezzi

Abstract

The work of the thesis has been focused on the study of the PCU system, which consists of piston, piston rings and liner, of a 12,9 L 6-cylinders in-line natural gas internal combustion engine for heavy duty application. The final goal is the evaluation of the friction of the PCU system and blow-by flowrate through a predictive model implemented in the program GT Power representative of a single crank.

The thesis is organized starting from the current scenario about air pollution and emission regulations with a theoretical description of the phenomenon and the part of the engine contributing to friction and blow-by, with a focus on the part modeled in GT Power. At the beginning is also introduced the system engineering discipline, whose guidelines have been followed to verify the targets of friction and blow-by. The results obtained in GT Power was analyzed comparing different alternatives of piston rings provided by the supplier evaluating their impact in terms of friction and subsequently the weight in CO₂ emissions in the VECTO cycle used for homologation. Some of the results have been compared with experimental data from bench test when available.

Contents

- List of Figures 5
- List of Tables..... 11
- Nomenclature 13
- 1. Introduction 18
 - 1.1 Organization of the thesis 18
 - 1.2 Actual scenario 19
 - 1.2.1 Air Pollution..... 19
 - 1.2.2 Greenhouse effect 26
 - 1.3 FPT Industrial 29
 - 1.3.1 XC13 engine 30
 - 1.4 System engineering discipline 32
 - 1.5 XC13 PCU study case 38
 - 1.5.1 PCU system..... 38
 - 1.5.2 System engineering applied to the XC13 PCU system..... 50
- 2. Engine frictions 55
 - 2.1 Pumping work..... 57
 - 2.2 Mechanical frictions 59
 - 2.2.1 Piston rings..... 59
 - 2.2.2 Piston skirt 66
 - 2.2.4 Small eye..... 67

2.3 Accessories	68
3. Thermal analysis of the piston	69
4. GT Power model for friction prediction.....	78
3.1 Piston rings and piston lands	80
3.2 Liner.....	84
3.3 Piston skirt.....	85
3.3 Working points	87
3.4 Results	90
3.4.1 XC13 Frictions.....	91
3.4.2 PCU friction at maximum power	94
3.4.3 Comparison between Alternative A and Alternative B of piston rings	102
5. Blow-by phenomenon	105
6. GT Power model for blow-by prediction	106
5.1 Results	109
7. Conclusions	121
7.1 Recommendations and future works	123
References	124

List of Figures

Figure 1. Air pollutants classification	20
Figure 2. Special report on energy and air pollution from IEA, WEO 2016	21
Figure 3. Special report on Energy and Air Pollution from IEA, WEO 2016, with focus on NO _x emissions	21
Figure 4. Special report on Energy and Air Pollution from IEA, WEO 2016 with focus on PM emissions	22
Figure 5. PM _{2.5} outdoor concentrations according to special report on Energy and Air Pollution from IEA, WEO 2016.....	22
Figure 6. Recommended levels from WHO 2022 report	23
Figure 7. Locations of settlements with data on PM _{2.5} concentration during the period 2010-2019.....	23
Figure 8. Locations of settlements with data on PM ₁₀ concentration during the period 2010-2019.....	23
Figure 9. Locations of settlements with data on NO ₂ concentration during the period 2010-2019	24
Figure 10. PM ₁₀ , PM _{2.5} and NO ₂ by region and settlement size from WHO 2022 report.....	24
Figure 11. Evolution of Euro regulation for heavy-duty applications during years	25
Figure 12. Evolution of NO _x and PM emission limit according to the matching Euro regulation	26
Figure 13. Composition of exhaust gas (untreated emission) from gasoline engines during stoichiometric operation.....	27
Figure 14. Greenhouse effect	27

Figure 15. Greenhouse gases concentration over years	28
Figure 16. FPT logo from 2019.....	30
Figure 17. C13 (left) and XC13 (right) engines from FPT Industrial	31
Figure 18. V-chart	32
Figure 19. Example of FMEA.....	36
Figure 20. Example of the P-diagram of the PCU system	38
Figure 21. Example of piston rings mounted on a piston.....	39
Figure 22. Examples of piston ring cross sections	40
Figure 23. Forces acting on a piston ring	41
Figure 24. Aluminum piston with a ring carrier in the first groove	42
Figure 25. DIN ISO 6621	44
Figure 26. Rectangular ring.....	44
Figure 27. Rectangular ring with taper - faced running face	45
Figure 28. Piston ring with top internal bevel or internal step.....	45
Figure 29. Stable and unstable pre-twist	46
Figure 30. Piston ring with bottom internal bevel or internal step.....	47
Figure 31. Keystone ring.....	48
Figure 32. First piston ring with barrel-shaped surface	48
Figure 33. Napier ring with taper-faced running face	49
Figure 34. Spring-loaded oil control ring.....	49
Figure 35. Ovality and superposition, double oval (left), tri-oval (right)	50

Figure 36. p-V diagram and imep	56
Figure 37. Full-load torque, bmep, bsfc and power versus speed for a typical TC truck diesel engine	57
Figure 38. 4-stroke engine thermodynamic cycle	57
Figure 39. 4-stroke NA and TC engine thermodynamic cycle	58
Figure 40. Piston ring diagram	60
Figure 41. Schematic for the boundary conditions	62
Figure 42. Forces acting on a piston ring	63
Figure 43. Algorithm for solving force equilibrium equation.....	64
Figure 44. Bore distortion	65
Figure 45. Support area and lubricant gap	66
Figure 46. XC13 small eye.....	68
Figure 47. Friction coefficient behavior	68
Figure 48. Views of the FE model used on Hypermesh.....	69
Figure 49. Elements of convective heat exchange surface of Piston Top and Cooling gallery	70
Figure 50. Elements of convective (left) and conductive (right) heat exchange surface of Piston hub and Wrist pin	71
Figure 51. Elements of convective heat exchange surface of Internal Piston (left) and Piston lands (right)	71
Figure 52. Elements of conductive heat exchange surface of Internal Piston Groove-Rings (left) and Rings-Liner (right).....	71
Figure 53. Temperatures results from the static thermal analysis.....	72

Figure 54. Piston rings temperatures results from the static thermal analysis	73
Figure 55. Mechanical constraints	74
Figure 56. Maximum pressure of 98 bar applied on the top of the piston	74
Figure 57. Displacements of the piston due to thermo-structural load	75
Figure 58. Amplified deformed shape of the piston.....	76
Figure 59. Known diameters of the piston from technical drawings	77
Figure 60. GT Power friction model	79
Figure 61. GT Power TDC angle convention	80
Figure 62. GT Power piston ring convention.....	81
Figure 63. Pressures in the rings	81
Figure 64. Section of the first piston ring. Technical drawing on the left and GT Power implementation on the right	82
Figure 65. Section of the second piston ring. Technical drawing on the left and GT Power implementation on the right	82
Figure 66. Section of the third piston ring. Technical drawing on the left and GT Power implementation on the right	83
Figure 67. Quantities to define the ring geometry in GT Power.....	83
Figure 68. Liner temperature.....	84
Figure 69. Hot bore distortion.....	85
Figure 70. Convention for skirt axial profile and ovality on GT Power	86
Figure 71. Ring axial profile in cold condition	86
Figure 72. Ring axial profile in hot condition.....	87

Figure 73. Pressures at full load	89
Figure 74. Torque and Power curve at full load.....	90
Figure 75. Friction of the crank mechanism	92
Figure 76. Brake power with respect to total friction power	94
Figure 77. PCU friction.....	95
Figure 78. 1 st ring friction power loss (left) and oil film thickness (right)	96
Figure 79. 2 nd ring friction power loss (left) and oil film thickness (right).....	96
Figure 80. 3 rd ring friction power loss (left) and oil film thickness (right)	97
Figure 81. Piston velocity.....	97
Figure 82. Lateral force trend.....	98
Figure 83. Skirt friction power loss.....	99
Figure 84. Minimum skirt oil film thickness.....	99
Figure 85. Minimum oil film thickness.....	100
Figure 86. Maximum oil film pressure.....	100
Figure 87. Axial (left) and Lateral (right) force acting on the small eye	101
Figure 88. Total power loss in the small eye.....	101
Figure 89. Friction contribution of the first ring on the VECTO points	103
Figure 90. Friction contribution of the second ring on the VECTO points	103
Figure 91. Blow-by mechanism	105
Figure 92. GT Power model for blowby prediction	107
Figure 93. Ring pack subassembly.....	108

Figure 94. GT Power reference for volumes around piston rings	109
Figure 95. Volume between first and second ring	110
Figure 96. First ring displacement relative to groove	111
Figure 97. Second ring displacement relative to groove	111
Figure 98. Bottom and Top volume of the first ring	112
Figure 99. Bottom and Top volume of the second ring	112
Figure 100. Volume behind first (Top) and second ring (Bottom)	113
Figure 101. Pressures on first ring's lands.....	113
Figure 102. Pressures on second ring's lands	114
Figure 103. Pressure below first ring	114
Figure 104. First ring end gap during the cycle	115
Figure 105. Second ring end gap during the cycle	115
Figure 106. First ring volumetric flow rate through the end gap	117
Figure 107. Second ring volumetric flow rate through the end gap.....	117
Figure 108. Top land volumetric flow rate of the second ring.....	118
Figure 109. Bottom land volumetric flow rate of the second ring	118
Figure 110. Test bench results.....	119

List of Tables

Table 1. General characteristics of the XC13	31
Table 2. V-chart items	33
Table 3. Example of a pugh matrix	35
Table 4. Risk level definition	37
Table 5. Engineering target of the PCU system	51
Table 6. Statement of requirement	52
Table 7. Alternative A for piston rings	53
Table 8. Alternative B for piston rings.....	54
Table 9. Piston temperatures from static thermal analysis.....	72
Table 10. Piston rings temperatures from static thermal analysis.....	73
Table 11. Properties of the piston material	75
Table 12. Expanded diameter of the piston.....	77
Table 13. VECTO points.....	88
Table 14. System targets to evaluate through GT Power results	91
Table 15. Engine frictions	91
Table 16. Brake power and total friction power at full load at different engine speeds	93
Table 17. PCU frictions.....	94
Table 18. Friction power of first and second ring for the two alternatives of piston rings....	102
Table 19. CO2 penalties on VECTO points	104

Table 20. Targets investigated through the blowby model in GT Power 109

Table 21. Blow-by results 119

Nomenclature

Chapter 2

η_m mechanical efficiency

P_b brake power [kW]

P_{ig} gross indicated power [kW]

P_f total friction power [kW]

P_{mf} mechanical friction power [kW]

P_{acc} accessories power [kW]

P_{pump} pumping power [kW]

mep mean effective pressure [bar]

V_d engine displacement [L]

i number of cylinders

n engine speed [rpm]

f_{mep} total friction mean effective pressure [bar]

mf_{mep} mechanical friction mean effective pressure [bar]

$amep$	accessory mean effective pressure [bar]
pmp	pumping mean effective pressure [bar]
bmp	brake mean effective pressure [bar]
$imep$	indicated mean effective pressure [bar]
$bsfc$	brake specific fuel consumption
\dot{m}_f	fuel mass flow rate [kg/h]
W_i	indicated work
h_{min}	minimum oil film thickness on piston ring [μm]
$h(x, \theta)$	oil film thickness on piston ring at the generic liner and ring height [μm]
η	oil viscosity [cps]
U	piston speed [m/s]
ω	engine speed [rad/s]
θ	crank angle [$^\circ$]
$p(x)$	pressure along external surface of the piston ring [Pa]
p_{up}	pressure above the ring [Pa]

p_{down}	pressure below the ring [Pa]
$2a$	ring thickness [mm]
o	position of the most external point of the ring section with respect to the ring centerline [mm]
$F_f(\theta)$	friction force [N]
A_n^{max}	piston ring conformability [μm]
F_r	tangential force of the ring [N]
R	nominal operating ring radius of the piston ring [mm]
E	Young's module of the piston ring material [MPa]
I	moment of inertia of the ring cross section [kgm^2]
n	number of lobes of the deformed liner

Chapter 3

K	conductive heat coefficient [W/mmK]
A	thermal expansion heat coefficient [1/K]
$R_{p0,2}$	yield stress [MPa]
c_p	specific heat coefficient [J/kgK]

ρ	material's density [g/cm ³]
E	Young's module of the piston ring material [MPa]
ν	Poisson ratio
T_{melt}	material's melting point [°C]
$MOFT$	normalized position of the most external part of the piston ring with respect to the ring thickness
T_m	position of the most external part of the piston ring from the bottom face of it [mm]
T	piston ring axial thickness [mm]
$h(z, \theta, t)$	oil film thickness between the piston skirt and liner [μm]
C_0	nominal radial clearance between the piston skirt and the liner [mm]
ΔR_{SP}	the skirt profile [mm]
ΔR_B	local bore distortion [mm]
$\Delta h_{\epsilon\phi}$	radial movement of the piston due to secondary motions [mm]
P_b	brake power [kW]
T	engine torque [Nm]

ω engine speed [rad/s]

\dot{m}_f fuel mass flow rate [kg/h]

$bsfc$ brake specific fuel consumption

Chapter 6

V_{top} volume above the piston ring [mm³]

V_{grv} volume behind the piston ring [mm³]

V_{bot} volume below the piston ring [mm³]

$V_{bot,first\ ring}$ volume below the first piston ring considering the additional volume [mm³]

$V_{top,second\ ring}$ volume above the second piston ring considering the additional volume [mm³]

1. Introduction

The thesis work was carried out with FPT Industrial in Turin and focuses on the Power Cell Unit (PCU) of the XC13, a 12.9 L natural gas inline 6-cylinder engine for heavy-duty applications. The PCU, consisting of the piston, piston pin, piston rings, and cylinder liner, was developed as complete modules by the supplier. The work approach followed System Engineering guidelines to integrate theoretical knowledge with work dynamics.

Due to strict environmental regulations and the fact that internal combustion engines (ICEs) are the primary energy source for transportation, vehicle manufacturers are motivated to improve ICE efficiency. Mechanical power loss is an attractive area of study and research to increase ICE productivity. Most of the mechanical power loss in an engine can be attributed to its main tribological components such as the PCU system, connecting rod big-end, and crankshaft main bearings.

The thesis aims to develop two models in GT Power: one to predict friction and another to study blow-by flow rate. These models were used to verify the PCU system's project target and compare different piston ring alternatives proposed by the supplier to find the best trade-off between ring stability and friction and their impact on CO₂ emissions during homologation test cycles.

1.1 Organization of the thesis

The thesis is structured into seven chapters, briefly introduced as follows:

- CHAPTER 1 - *Introduction*: Provides an overview of the thesis's main topics and goals, with a reference to the current scenario in terms of ICE emission regulations, also explaining the system engineering approach used to verify system targets.
- CHAPTER 2 - *Engine Friction*: An overview of factors influencing engine friction from a theoretical point of view, with a focus on mechanical friction and the parts accounted by the GT Power model.

- CHAPTER 3 - *Thermal analysis of the piston*: In this chapter is described the static and thermo-structural analysis done in the program Hypermesh, by means the temperature and the deformed diameters of the piston in hot conditions have been extrapolated.
- CHAPTER 4 - *GT Power Model for Engine Friction Prediction*: Explains the GT Power model used to calculate friction and the engine working points considered. An overview of the results is provided.
- CHAPTER 5 - *Blow-by phenomenon*: Introduction to the phenomenon of the blow-by from a theoretical point of view.
- CHAPTER 6 - *GT Power Model for Blow-by Prediction*: Explains the GT Power model used to calculate blow-by and compares it with experimental results. An overview of the results is provided along with matching considerations.
- CHAPTER 7 - *Conclusion*: The final part of this study presents the conclusions arising from the research and suggestions for further development of possible topics.

1.2 Actual scenario

Before to enter into the detail of the thesis it is important to provide a general overview of what is currently happening in the world regarding exhaust gas emission regulations for internal combustion engines. In this historical period, emissions and environmental pollution have been widely discussed and critical measures have already been decided for the future of ICEs. The thesis focuses on an engine for heavy-duty applications, so it is important to understand the corresponding regulations and potential future scenarios and challenges. Two main types of regulations have been developed, referring respectively to pollutant emissions and greenhouse effect. These will be discussed in more detail in the following paragraphs.

1.2.1 Air Pollution

The combustion of hydrocarbon fuels removes O_2 from the atmosphere and releases equivalent amounts of H_2O and CO_2 , along with trace amounts of numerous other compounds including hydrocarbons (HC), carbon monoxide (CO), nitrogen oxides (NO_x), reduced nitrogen, sulfur gases (SO_x), and particles.

Pollution is defined as the introduction by humans into the environment of substances or energy liable to cause hazards to human health, harm to living resources and ecological systems,

damage to structures or amenities, or interference with legitimate uses of the environment. Air pollutants can be either gaseous or particulate in form.

First, it is necessary to define the main air pollutants and how they are classified. The main classification is between primary and secondary pollutants. Primary pollutants are those emitted directly as a result of human activity or natural processes, while secondary pollutants are created from primary pollutants reacting with sunlight and components in the atmosphere. Figure 1 can be referred to for the species of pollutants emitted by engines.

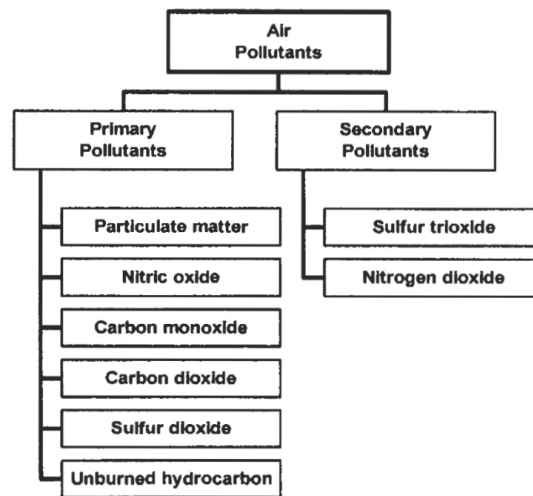


Figure 1. Air pollutants classification

In the world the main sectors that contributes to air pollution are:

- 1) Power generation
- 2) Industry
- 3) Transport
- 4) Buildings
- 5) Fuel supply
- 6) Non-energy

The contribution of all these sectors with respect to the different pollutant species is shown in Figure 2.

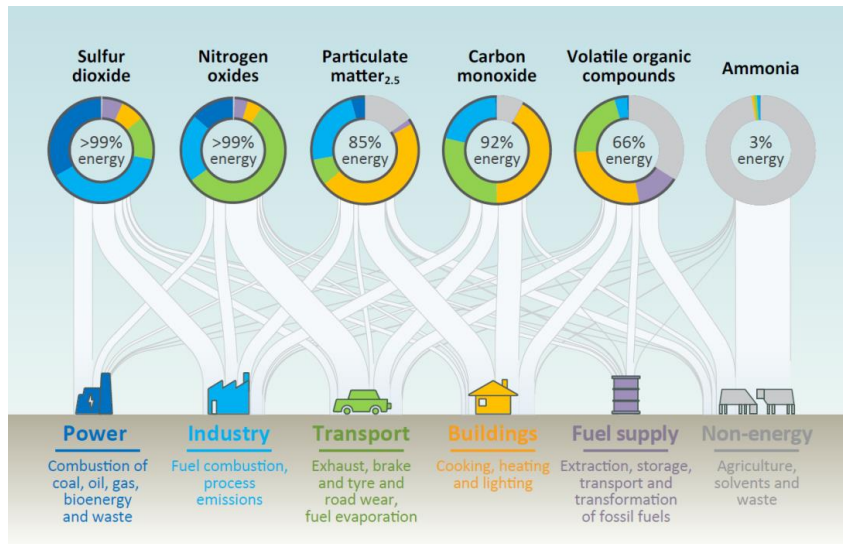


Figure 2. Special report on energy and air pollution from IEA, WEO 2016

Globally, transport is a major contributor to air pollution in terms of NO_x emissions as shown also in Figure 3.

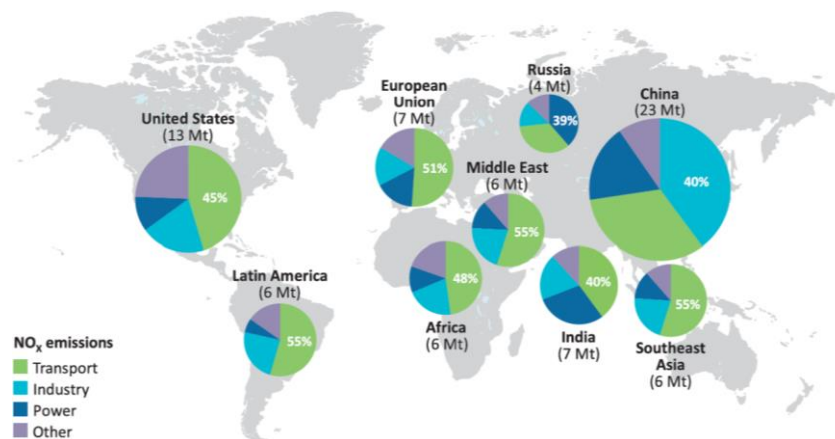


Figure 3. Special report on Energy and Air Pollution from IEA, WEO 2016, with focus on NO_x emissions

On the other hand, focusing on other pollutants, the contribution from transport is significantly reduced. For example, for particulate matter, Figure 4 provides a global overview.

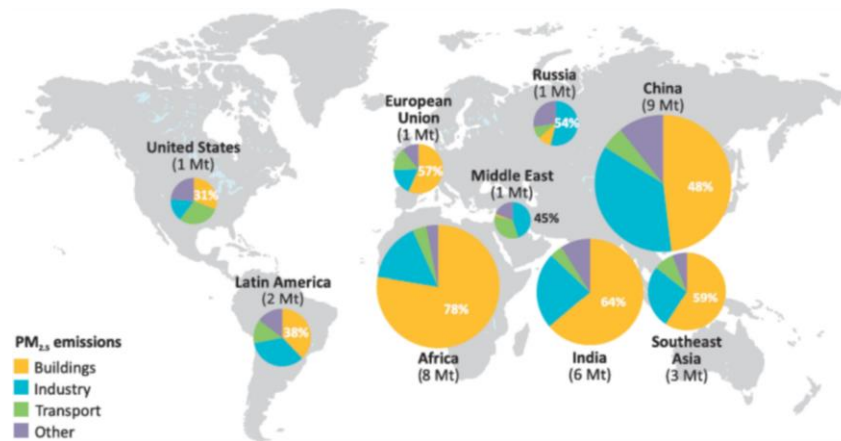


Figure 4. Special report on Energy and Air Pollution from IEA, WEO 2016 with focus on PM emissions

Today, populations around the world live with air quality that consistently fails to meet the World Health Organization’s (WHO) annual mean concentration standards for PM. Nearly 80% of the population living in urban areas that monitor air quality are breathing air that does not comply with WHO air quality guidelines, as shown in Figure 5. [1]

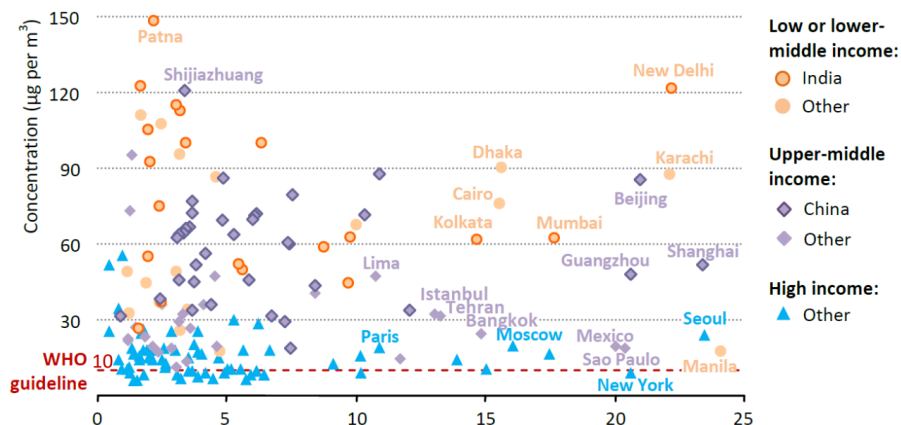


Figure 5. PM_{2.5} outdoor concentrations according to special report on Energy and Air Pollution from IEA, WEO 2016

On the other hand, it is possible to focus on the report released in 2022 by the WHO regarding the ambient air quality database. There are published the measurements of air quality and, specifically, the annual mean concentrations of particulate matter with a diameter $\leq 2,5 \mu m$ (PM_{2.5}) and $\leq 10 \mu m$ (PM₁₀) and NO₂. The actual recommended levels and interim targets (in $\mu g/m^3$) for annual averaging time of PM and NO₂ concentrations according to the health community, medical societies, and patient organizations are listed in Figure 6.

Pollutant	Interim target				AQG (2021)	AQG (2005)
	1	2	3	4		
PM _{2.5}	35	25	15	10	5	10
PM ₁₀	70	50	30	20	15	20
NO ₂	40	30	20		25	40

AQG: WHO air quality guidelines.

Figure 6. Recommended levels from WHO 2022 report

All the data regarding the PM content in the air are collected thanks to human settlements in 117 countries worldwide, while for NO₂ content there are settlements in 74 countries. The position in the world of the settlements is shown in Figure 7, Figure 8 and Figure 9, respectively for PM_{2.5}, PM₁₀ and NO₂.

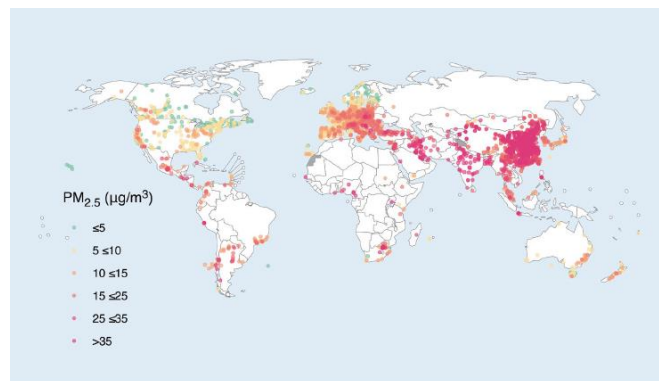


Figure 7. Locations of settlements with data on PM_{2.5} concentration during the period 2010-2019

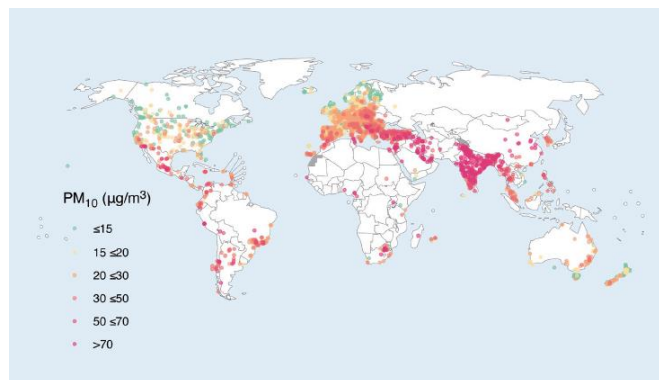


Figure 8. Locations of settlements with data on PM₁₀ concentration during the period 2010-2019

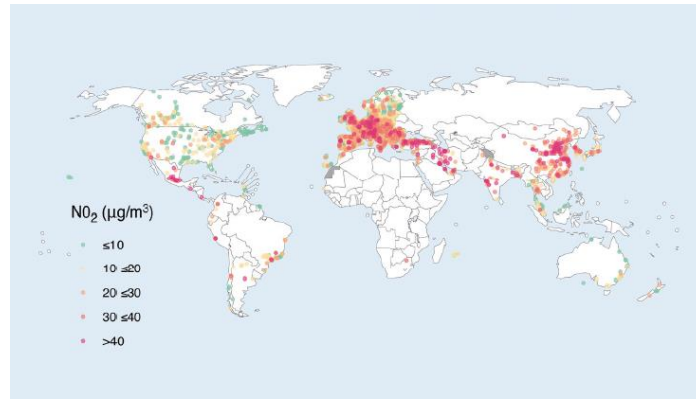


Figure 9. Locations of settlements with data on NO₂ concentration during the period 2010-2019

For the results is possible to refer to Figure 10, where are listed the part of the world in which settlements are present with the number of them (in the lower part) and the pollutants concentration registered (in the upper part).

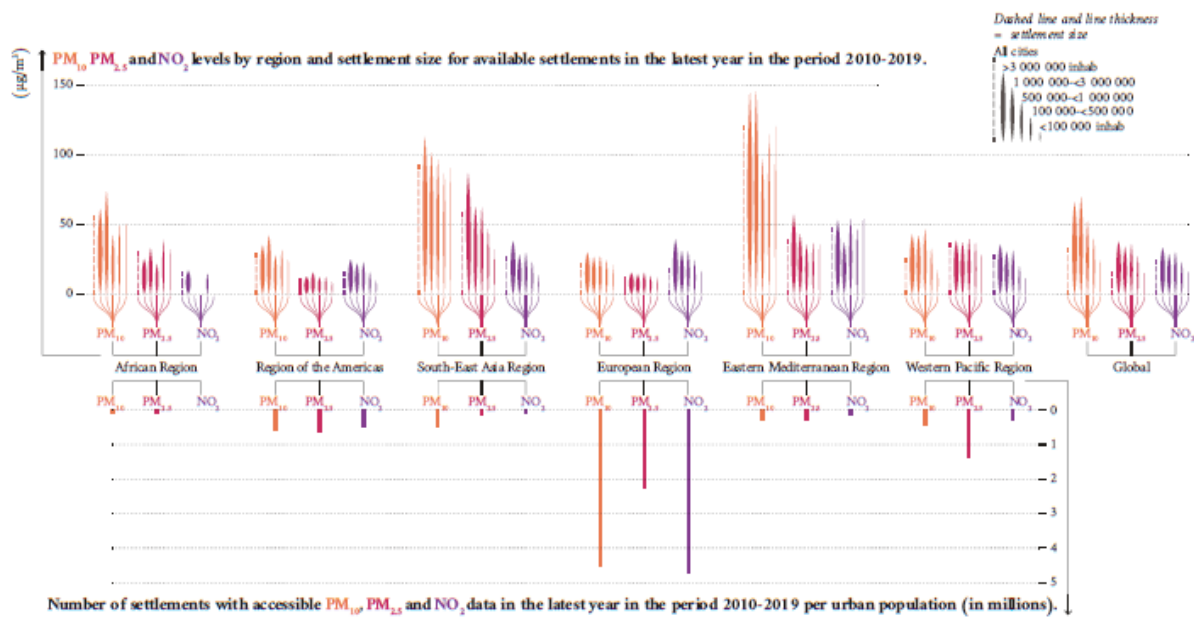


Figure 10. PM₁₀, PM_{2.5} and NO₂ by region and settlement size from WHO 2022 report

It is evidenced here that the largest number of settlements is in the European region and, referring to the standards defined in Figure 6, it is possible to see that the air quality guidelines are not respected in any part of the world. The highest levels of PM₁₀ are in the Eastern Mediterranean and South-East Asia regions, partly due to the fact that they received large quantities of desert dust particles. Similar patterns are evidenced for PM_{2.5} and NO₂, although for the latter pollutant a higher concentration than the global average is registered in the Eastern

Mediterranean Region, while all other regions had lower, homogeneous levels. The lowest levels of PM and NO₂ were observed in Europe and the Americas, respectively. While PM₁₀ levels varied widely by region, NO₂ levels appeared to be more homogeneous, probably due to the local nature of NO₂ sources and its reactive chemical nature.

With regard to exposure levels in human settlements of different sizes, NO₂ concentration tended to increase with settlement size, which might reflect larger emissions from traffic, whereas the highest PM concentrations were found in settlements that varied in size from 500,000 to 3 million inhabitants.

In conclusion, nowadays all engines are equipped with an After-treatment system (ATS) that can reduce engine-out emissions at the tailpipe by about 90%. So, what is most critical nowadays are CO₂ emissions that contribute to Earth’s warming. This will be discussed in the next paragraph.

Euro regulations

The focus of this paragraph will be on regulations related to heavy duty application due to the topic of the thesis. Since 1992, the EU has introduced increasingly stricter limits on heavy-duty vehicle emissions through a series of ‘Euro’ standards for the approval of the engine emissions. Euro I, II and III led to improvements in engine emissions, but catalytic emission control technologies were only effectively required with the introduction of Euro IV and V in 2005 and 2008. The latest and most stringent standard currently in place is Euro VI since 2013. Since the introduction of the Euro standards, nitrogen oxides (NO_x) limits for heavy-duty engines have been reduced by 95 %, and those of particulates (PM) by 97 %

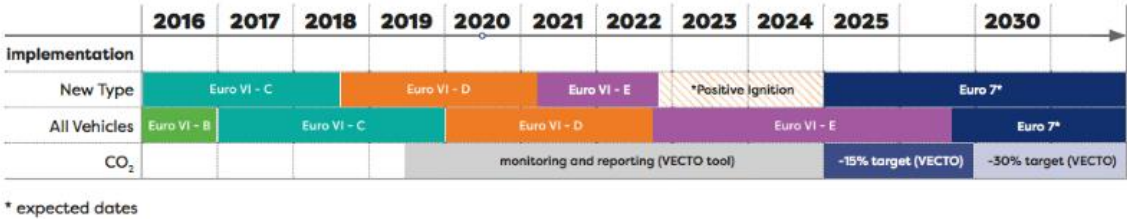


Figure 11. Evolution of Euro regulation for heavy-duty applications during years

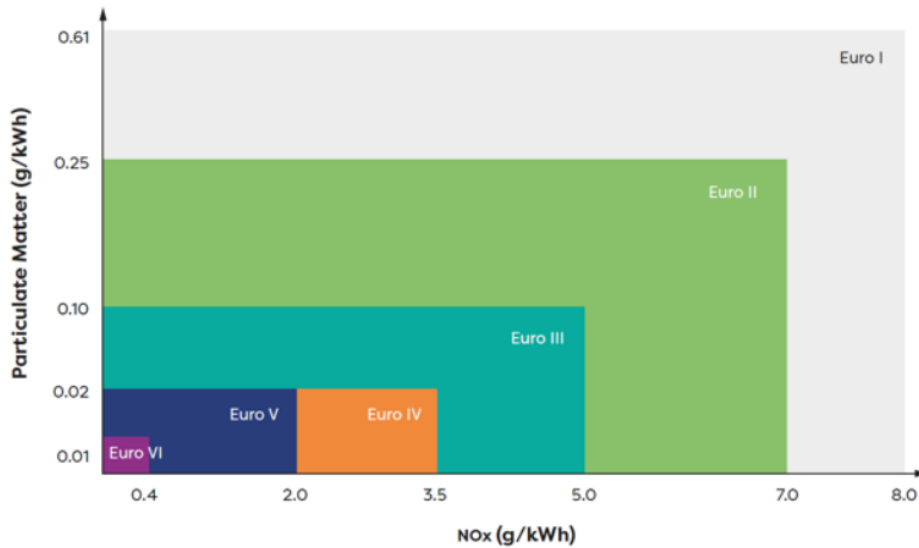


Figure 12. Evolution of NOx and PM emission limit according to the matching Euro regulation

The Euro regulations for heavy-duty applications refer to the emission standards for heavy-duty vehicles in the European Union. The current standard is Euro VI, which has applied to all new diesel and gas engines since 2013. The testing is performed on engines alone rather than complete vehicles, and limit values are expressed in terms of grams per kilowatt-hour (g/kWh). [2]

1.2.2 Greenhouse effect

Under complete combustion, the hydrocarbons in the chemical bonds of the fuel are transformed into carbon dioxide (CO_2), which makes up approximately 14% of the exhaust gas (considering gasoline or diesel oil as fuel) as shown in Figure 13. Carbon dioxide is a natural component of atmospheric air, and CO_2 related to combustion processes is not classified as a pollutant. However, CO_2 related to human activities is one of the substances responsible for altering Earth's natural greenhouse effect and therefore responsible for global climate change.

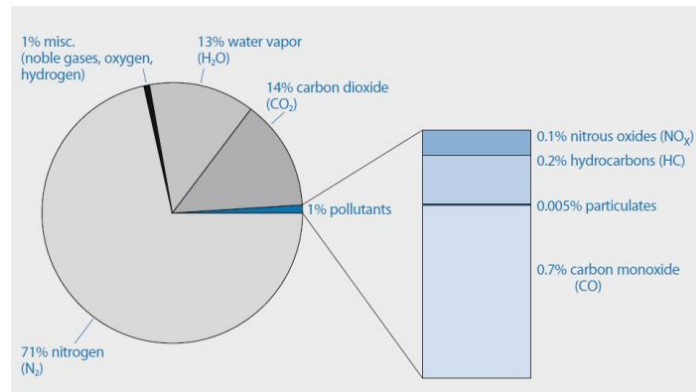


Figure 13. Composition of exhaust gas (untreated emission) from gasoline engines during stoichiometric operation

Short-wave solar radiation penetrates Earth's atmosphere and continues to the ground, where it is absorbed. This process promotes warming in the ground, which then radiates long-wave heat or infrared energy. A portion of this radiation is reflected by the atmosphere, causing Earth to warm. Without this natural greenhouse effect, Earth would be an inhospitable planet with an average temperature of -18°C . Greenhouse gases within the atmosphere raise average temperatures to approximately $+15^{\circ}\text{C}$.

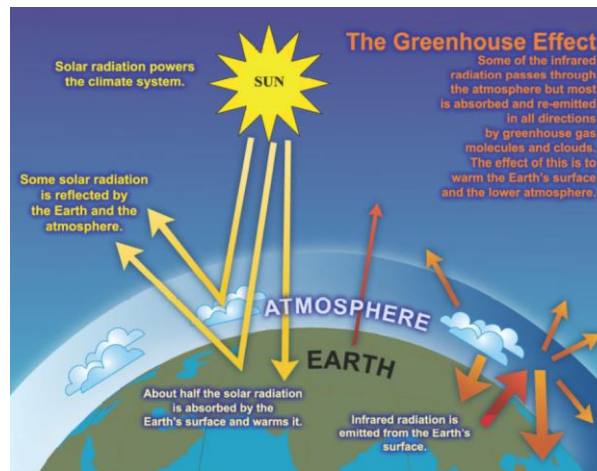


Figure 14. Greenhouse effect

Human activities result in emissions of four principal greenhouse gases: carbon dioxide (CO₂), methane (CH₄), nitrous oxide (N₂O), and halocarbons. These gases accumulate in the atmosphere, causing concentrations to increase over time. A significant increase has been faced in the industrial era, as shown in Figure 15. [1]

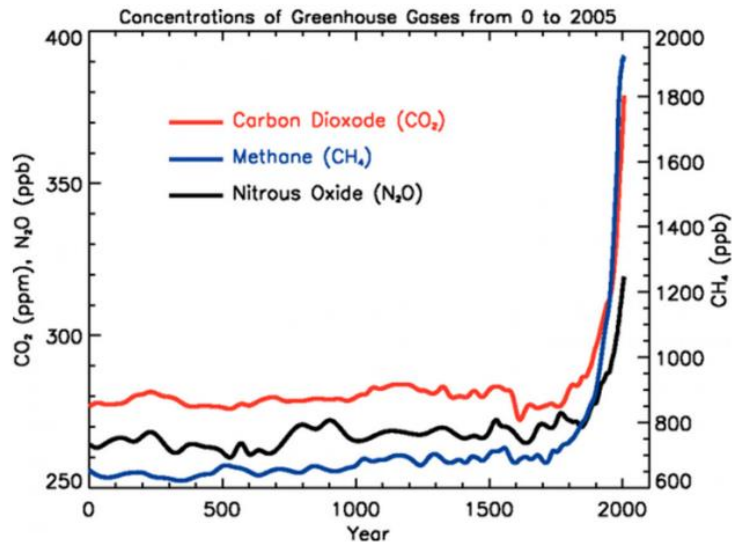


Figure 15. Greenhouse gases concentration over years

Focusing now on engine emissions, it is possible to say that the amount of converted carbon dioxide in the exhaust is a direct index of fuel consumption. Thus, the only way to reduce carbon dioxide emissions is to reduce fuel consumption. From this aspect, the target of the XC13 project in reducing fuel consumption by 10.5% compared to the previous engine is very important.

Moreover, from a driver's perspective, it is also economically convenient. In fact, considering that the XC13 is an engine for heavy-duty applications, it is possible to make a consideration of saved money corresponding to a reduction in fuel consumption referring to a typical mission of a Heavy-Duty vehicle. According to the EU Eco Innovations Technical Guidelines, Transport & Environment, the typical traveled distance is 150 000 *km/year* with a fuel consumption of around 2,6 *km/l*. So, considering the actual cost of the natural gas (CNG) in Italy of 0,8 €/l the reduction of 10,5 % on fuel consumption (corresponding to 2,9 *km/l*) will generate a saving of: [3]

$$Fuel_{year} = \frac{150\,000\ km}{2,6\ \frac{km}{l}} = 57692,3\ \frac{l}{year}$$

$$Fuel_{year,-10,5\%} = \frac{150\,000\ km}{2,9\ \frac{km}{l}} = 51724,1\ \frac{l}{year}$$

$$Saved\ fuel_{year} = Fuel_{year} - Fuel_{year,-10,5\%} = 5968,2 \frac{l}{year}$$

$$Saved\ money_{year} = 0,8 \frac{\text{€}}{l} \cdot Saved\ money_{year} = 4775 \frac{\text{€}}{year}$$

So, it means that in 10 years the owner of the vehicle will save about 48 000 €, that is a significant amount of money that would justify, eventually, a higher cost of the vehicle.

Finally, to understand the current regulations about greenhouse gases is possible to refer to the official website of the European Union in the section of Road transport. VECTO is the new simulation tool that has been developed by the European Commission and is used for determining CO₂ emissions and Fuel Consumption from Heavy Duty Vehicles (trucks, buses and coaches) with a Gross Vehicle Weight (GVW) above 3500 kg. Since 1 January 2019, the tool is mandatory for new trucks under certain vehicle categories in application to the certification legislation under type approval.

CO₂ emissions and fuel consumption data determined with VECTO, together with other related parameters, must be monitored and reported to the Commission by Member States and manufactures, and made publicly available for each of those new trucks.

Five different mission profiles for trucks and five different mission profiles for buses and coaches have been developed and implemented in the tool to better reflect the current European fleet.

The inputs for VECTO are characteristic parameters to determine the power consumption of every relevant vehicle component. Among others, the parameters for rolling resistance, air drag, masses and inertias, gearbox friction, auxiliary power and engine performance are input values to simulate fuel consumption and CO₂ emissions on standardized driving cycles. [4]

1.3 FPT Industrial

FPT Industrial is an Italian company founded on January 1, 2011, and now part of the IVECO Group. Its goal is to design, produce, and sell propulsion systems for industrial vehicles for on-road, off-road, marine, and power generation applications.



Figure 16. FPT logo from 2019

The company produce 6 main engine families:

- **R22:** Turbocharged In-line 3-cylinders 2.2 L
- **F1:** Turbocharged In-line 4-cylinders 3 L
- **F5:** Turbocharged In-line 4-cylinders 3.2 - 3.6 L
- **NEF:** Turbocharged In-line 4-cylinder 3.9 (N40) - 4.5 (N45) L / Turbocharged In-line 6-cylinder 5.9 (N60) - 6.7 (N67) L
- **CURSOR:** Turbocharged In-line 6-cylinders 8.7 (C9) - 12.9 (C13) - 15.9 (C16) L
- **VECTOR:** Turbocharged V8 engine (90° V angle) 20.1 L

For each family, FPT can adapt the engines and manage the production process according to the application and client requests. Each engine can be adapted for all four applications mentioned above and with different fuels such as natural gas or diesel. The only engine parts directly produced by FPT are the “5-C”:

- 1) Crankshaft
- 2) Camshaft
- 3) Cylinder head
- 4) Cylinder block
- 5) Conrod

All other parts are supplied by suppliers and assembled by the company.

1.3.1 XC13 engine

The thesis work focuses on the CURSOR family in the development of the new natural gas XC13 engine, whose design began in 2021 as an enhancement of the C13 with the primary goal of CO₂ reduction. The C13 offers high-performance light/medium/heavy-duty versions ranging from 330-825 HP and combines very high power and torque density levels with low fuel

consumption to minimize environmental impact. Its dimensions are 1058 (height) x 1465 (length) x 1000 (width) mm.

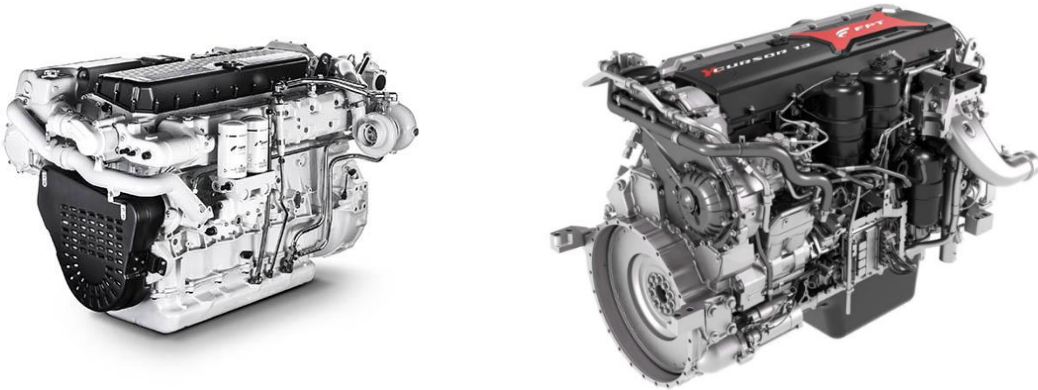


Figure 17. C13 (left) and XC13 (right) engines from FPT Industrial

The main features of the XC13 in terms of dimensions and performances are listed in Table 1.

Characteristic	Value	Unit of measurement
Number of cylinders	6	-
Engine displacement	12,9	L
Bore	135	mm
Stroke	150	mm
Compression ratio	12	-
Crank offset	20	mm
Conrod length	231	mm
Max power	404	kW
Max power speed	1900	rpm
Oil	0W16	-

Table 1. General characteristics of the XC13

1.4 System engineering discipline

The discipline of system engineering originated in the software field and later expanded to the automotive field. Its main pillar is requirement management, which involves listing all targets and ensuring that the corresponding system meets them at every level.

The system engineer role was introduced at FPT six years ago, which brought to the definition of three different levels:

1. Powertrain
2. Engine system
3. Components

Each level is strongly connected with the systems above and below it. The higher the level, the more general is the targets. At different levels, targets become more detailed in a cascading manner. The main goal is to ultimately achieve the main target defined at the highest level. The approach used is based on the V-chart.

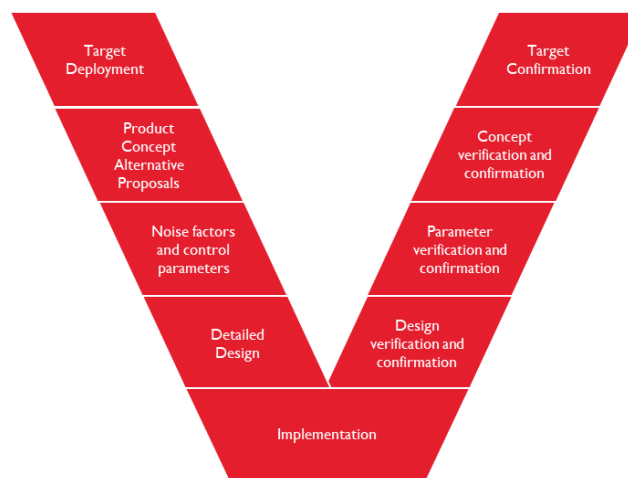


Figure 18. V-chart

For each step a proper tool is used to obtain an output that successively can be used as an input for another step. It is possible to summarize as follow each V-step:

Item	Input	Output	Tool
Target Deployment	Project Targets (Core Functional Objectives and Additional Objectives), Lesson Learned	System Drivers	Dashboard
Product Concept Alternative Proposals	System Drivers Possible concepts	Recommended concept	Pugh Matrix
Noise factors and control parameters	Recommended concept	Main noise factors and control parameters	P – Diagram, SFMEA
Detailed Design	Control parameters	Technical Enablers and component specification	SFMEA, System preliminary virtual validation, Design guidelines, Dashboard
Verification and confirmation (design, parameters and concept)	Component detailed design	Status and critical points of component and system validation	Dashboard, Component and system validation plan
Target Confirmation	Project target	Status and critical points of project target validation	Project Scorecard

Table 2. V-chart items

Before delving into the details of each item, it is important to clarify the evolution of a new project. Several steps can be identified:

- *Demo phase*: Preliminary study based on existing engines.
- *Alpha phase*: Similar to the Demo phase but with some prototype components.
- *Beta phase*: Final component and system design, but still produced using prototype processes (also known as Soft Tools), such as sand casting instead of die casting.
- *Gamma phase*: Like the Beta phase, but all parts are made using industrial processes and the final product is representative of the production process. In this phase, several tests must be performed to verify the robustness of both the design and industrial production, as some material properties may change due to different manufacturing processes.

If one of these phases fails, production will start with a lower level of maturity, highlighting the crucial role of the initial phases.

At this point, it is possible to examine the different items of the V-chart in more detail. It is important to note that for each step on the left side of the V, there should be a corresponding verification step on the right side to ensure process effectiveness and optimization.

Target Deployment

According to the Dashboard, which is a matrix where a reference person is assigned to each engine system, all targets are defined. For a new engine development, the main product targets are:

- *Performance*: Power and torque.
- *CO₂*: Reduction target in the reference homologative cycle compared to the actual state-of-art.
- *Emissions*: According to current emission regulations.
- *NVH*: According to current NVH regulations.
- *Size/Packaging*: Requirements based on available space in vehicle engine compartment.
- *Maintenance*: Interval at which specific engine parts requires maintenance (usually in terms of km).
- *Durability*: Durability guaranteed by the company for the product.
- *Start ability*: Ensuring engine start in critical situation.
- *Serviceability installation*: Guaranteeing service operations.

Once product targets are defined, an engineering target is implemented to allow adaptation of the same product for another client with similar requests in the future. For each target, a system driver is defined as a way to achieve it (e.g., minimize mechanical friction, minimize wear, minimize load, guarantee bearing lifetime). It should be noted that all targets are defined based on the system engineer's experience and this step represents one of the most challenging.

Product concept and alternative proposal

Considering the system drivers defined in the first step, an analysis of alternative concepts for achieving targets is performed using a Pugh Matrix. For each concept, it is determined whether or not it can achieve its corresponding target. Table 3 can be referred to as an example.

Item	System drivers HW	Main system target	Concept 1	Concept 2	Concept 3
Fuel consumption	Minimize mechanical friction	First ring tangential force ≤ 30 N	Green	Green	Yellow
NVH	Minimize piston slap	Cylinder offset \geq 10 mm	Yellow	Red	Red

Table 3. Example of a pugh matrix

For each concept, it is determined whether the target is achievable (green), not achievable (red), or if action is required (yellow). Base criteria that are mandatory to satisfy (killer targets) and driver criteria that are not mandatory can also be defined. In the latter case, the selection of the concept can be evaluated even if not all targets are met. Finally, for a specific system target is possible to add eventual solution to achieve it.

Main risk analysis & Noise factors and control parameters

Once the concept has been decided from the previous step, all control parameters that can be acted upon and noise effects are defined. Noise refers to parameters that cannot be controlled but influence system behavior. To perform this step with proper feasibility, two tools can be used:

- 1) Failure Modes and Effects Analysis (FMEA)
- 2) P-diagram

Since only a preliminary design phase is present, only a Software FMEA (SFMEA) can be implemented. This methodology is a “bottom-up” analysis technique that examines how each component could fail, how failure propagates through the system, and whether it can lead to a hazard. FMEA begins by looking for potential system problems while the project is still in the design phase. Each component in the system is examined and all ways it can fail are listed. Each possible failure is traced through the system to see its effects and whether it can result in a hazardous state. The likelihood of failure and the severity of system failure are considered. A widely used FMEA procedure for hardware involves the following steps:

- 1) Definition of the system to be analyzed.

- 2) Construction of functional block diagrams.
- 3) Identification of all potential item and interface failure modes.
- 4) Evaluation of each failure mode in terms of the worst potential consequences.
- 5) Identification of failure detection methods.
- 6) Identification of corrective design or other action to eliminate/control failure.
- 7) Identification of the impacts of corrective change.
- 8) Document the analysis and summarize the problems which could not be corrected.

In the case of a SFMEA the methods of a standard (hardware) FMEA are used but substituting software components with hardware components in each case.

To have an example of a FMEA is possible to refer to Figure 19.

System	Component	DFMEA	SYSE COMMENT	IFMEA	SYSE COMMENT
AIR HANDLING	Air Filter		Notes:		Notes:
AIR HANDLING	Intake Compressor Ducts		Notes:		Notes:
AIR HANDLING	Turbocharger	YES (Supplier re	Notes DFMEA from supplier has to be included both actuator and TC	YES (FPT resp.)	Notes:
AIR HANDLING	Outlet Compressor Ducts		Notes:		Notes:
AIR HANDLING	Intercooler (air to air)		Notes:		Notes:
AIR HANDLING	pop-off	YES (Supplier re	Notes:	YES (FPT resp.)	Notes:
AIR HANDLING	Throttle Valve (TVA)	YES (Supplier re	Notes:	YES (FPT resp.)	Notes:
AIR HANDLING	Intake Manifold	YES (FPT resp.)	Notes: Point of attention on injector installation	YES (FPT resp.)	Notes:
					Notes: Interface with head same as diesel engine. Include IFMEA of exhaust manifold-head and exhaust manifold - turbine gaskets
AIR HANDLING	Exhaust Manifold	YES (FPT resp.)	Notes:	YES (FPT resp.)	Notes:
AIR HANDLING	Head - Exhaust manifold gasket	YES (Supplier re	Notes:	NO	Notes: To be included in exhaust manifold
AIR HANDLING	EGR Cooler+Reed valve	YES (Supplier re	Notes:	YES (FPT resp.)	Notes:
AIR HANDLING	EGR Valve	YES (Supplier re	Notes:	YES (FPT resp.)	Notes:
AIR HANDLING	EGR Piping Hot Side	YES (Supplier re	Notes:	YES (FPT resp.)	Notes:
AIR HANDLING	EGR Piping Cold Side	YES (FPT resp.)	Notes:	YES (FPT resp.)	Notes:
AIR HANDLING	Exhaust manifold - Turbine gasket	YES (Supplier re	Notes:	NO	Notes: To be included in exhaust manifold

Figure 19. Example of FMEA

For each system item, an issue description or lesson learned from previous projects with corresponding potential failure mode and effect on the customer is considered. A value from 1 to 3 is assigned to both severity and occurrence of each issue. Multiplying these two scores as shown in Table 4 allows defining a risk level.

SEVERITY	Vehicle /durability test stop with such long time to replace components / fix issue to skip / nullify validation Homologation impact or delay Component redesign anyway necessary	3	3	6	9
	Limited vehicle / durability test stop without impact on deliverable No relevant impact on calibration Redesign of component	2	2	4	6
	Minor impact without vehicle/bench stop or calibration Minor adjustment on design	1	1	2	3
			1	2	3
			High maturity / experience High confidence level of preventive actions on failure mode	Medium maturity / experience Medium confidence level of preventive actions on failure mode	Low maturity / experience Low confidence level of preventive actions on failure mode
OCCURRENCE					

Table 4. Risk level definition

Finally, a recommended action for each issue is proposed to either solve it or analyze/study it through a specific test bench procedure or numerical calculation.

On the other hand, the P-diagram defines control parameters that can be acted upon to achieve a specific target and noise factors that cannot be controlled but influence the target. In order to understand properly how it works Figure 20 can be taken as a reference.

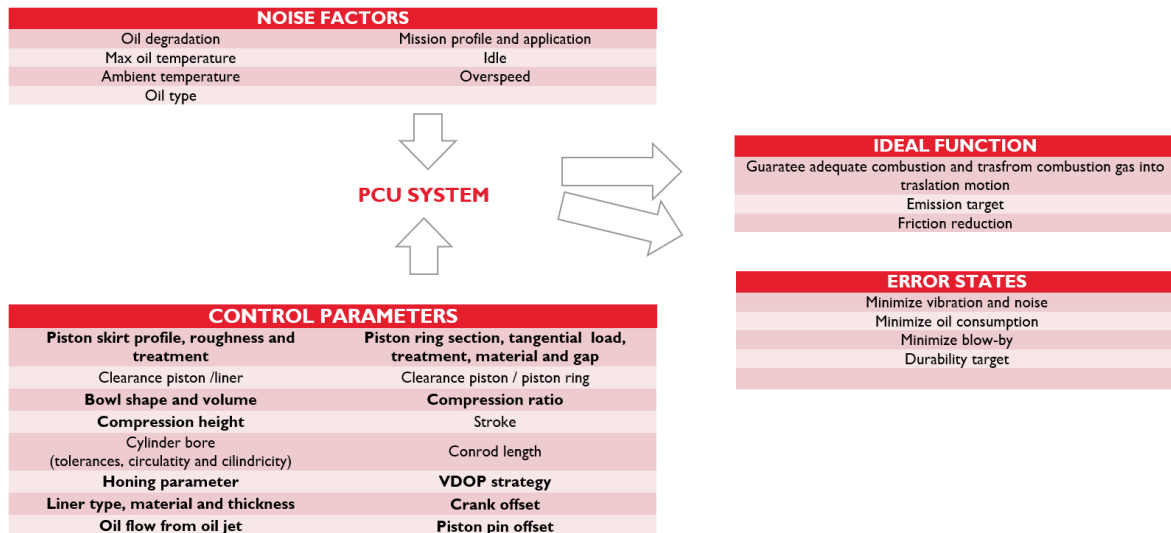


Figure 20. Example of the P-diagram of the PCU system

Verification and confirmation (design, parameters and concept)

This step lists all activities to be performed in terms of design, virtual validation, and testing to verify and confirm each target established in the previous step. The final result of each activity can be positive, critical, or identified gap (in that case an action is required).

A dedicated time plan must be programmed during this phase, taking into account the duration of each test to be performed. This aspect is particularly sensitive with respect to duration-type test benches that can last up to 3000 hours.

1.5 XC13 PCU study case

Now that a theoretical description of the different steps involved in the project development has been introduced, it is possible to examine the thesis's case study in detail: the PCU system of the XC13 engine. As a first step, is necessary to define in what consist the PCU system and for this is possible to refer to the next paragraph.

1.5.1 PCU system

The PCU system, as already mentioned, is made up of piston rings, piston skirt, cylinder liner, and small eye of the connecting rod. In this paragraph, a description of each part is provided.

Piston rings

Usually, engines pistons are equipped with three piston rings mounted on dedicated grooves. Each one has a different task:

- 1st piston ring: Compression of combustion air or gas mixture (today's rings can manage until to 260 bar of pressure)
- 2nd piston ring: Support of the remaining gas pressure due to blow-by past the 1st piston ring, scraping of oil from the liner and transfer of generated heat to the cylinder surface
- 3rd piston ring: Oil scraping function from the cylinder liner



Figure 21. Example of piston rings mounted on a piston

During the design of a piston ring some aspects must be considered:

- 1) Scuffing: Partial seizure process leading to severe wear, poor sealing, increased oil consumption and increased blow-by level.
- 2) Ring flutter: Occurrence of radial and axial vibrations. The gas pressure acting radially on the piston ring in the groove root drops off and the piston ring is no longer tightly guided.
- 3) Ring sticking: At excessive piston temperatures, the oil in the ring grooves cokes up, so that the piston rings get stuck.
- 4) High oil consumption: Determining factors are conformability of the piston rings, and deformation and honing of the cylinder bore.
- 5) Friction: The piston rings have a large part in the friction of the piston group.

The basic shape of a piston ring is a thin walled, axially short circular cylinder. To generate the necessary contact pressure against the cylinder wall, the piston rings are in the shape of an open circular spring. The spring force acting radially in the installed state is greatly amplified by the gas pressure behind the piston ring. When the piston is installed in the cylinder, the piston rings are compressed at their ends to their gap clearance. The force with which a piston ring presses against the cylinder wall depends mainly on the difference in diameters of the pre-stressed piston ring and the cylinder. This tangential force is designed in such a way that the piston ring meets the requirements arising from the combustion process and operating conditions. When the piston ring is installed in the cylinder, a tangential force is created that in turn generates the contact pressure. The radial distribution of the contact pressure depends on the shape of the ring cross section.

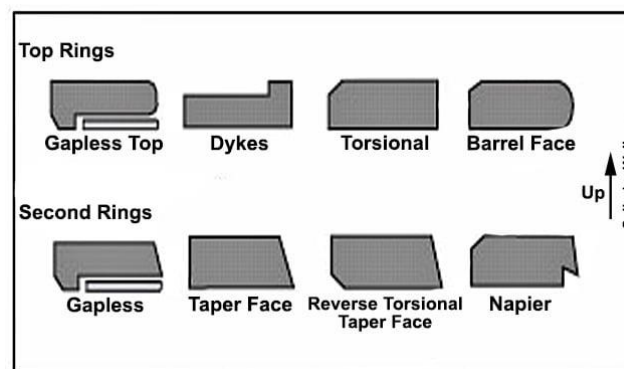


Figure 22. Examples of piston ring cross sections

The radial pressure applied by the piston ring to the cylinder bore is small in comparison to the gas pressure applied via the ring groove in the piston to the inner side of the piston ring. Despite every effort, the piston ring cannot form a perfect seal. Leakage occurs at the ring gap, at the side faces, and at the contact faces to the cylinder.

In general, the material used for piston rings are mainly untempered or tempered gray cast iron with nodular graphite, tempered steel or stainless steel. To improve running-in characteristics, reduce wear and prevent scuffing, special measures are taken by coating and reinforcing the running surfaces.

Piston rings are highly stressed mechanically, thermally, tribologically, and corrosively. They faced gas temperatures of up to 2600 °C and combustion pressure of up to 260 bar. About 25-60 % of the heat absorbed by the piston is transferred to the cylinder wall by the piston rings.

The limit of the temperature load on the first piston ring is reached when the oil in the first piston ring groove starts to carbonize due to excessive temperature. The movement of the first piston ring, which is a requirement for its reliable function, is thereby limited. It can no longer maintain its proper contact to the cylinder surface, and ring sticking occurs. Effective piston cooling is essential, as it significantly helps to reduce the thermal loads of the piston rings. Depending on the type of piston cooling, the heat flowing into the piston rings can be reduced to less than one-third.

During one revolution of the crankshaft, the piston moves from the top (TDC) to the bottom (BDC) and back to the top dead center. It travels twice the stroke distance. During this motion, it is accelerated and decelerated and due to its inertia, the piston ring moves in the ring groove relative to the piston. Due to frictional forces at the cylinder surface, it tends to tilt as it moves as shown in Figure 23. Upon impact, it can exert high forces on the side faces of the ring groove. In diesel engines, this effect is increased further by the high gas pressure.

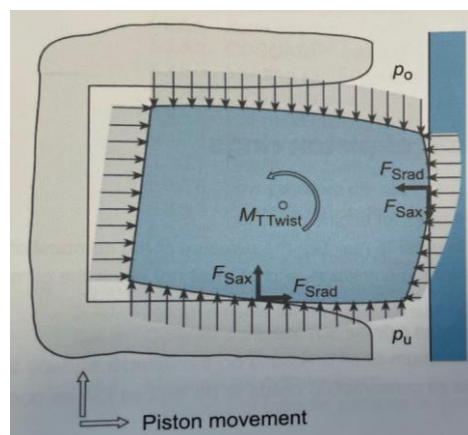


Figure 23. Forces acting on a piston ring

Wear of the groove side faces degrades the function of the piston rings, until it causes ring scoring, ring fracture and, as a result, piston seizure. The introduction of aluminum pistons for diesel engines used in commercial vehicles at the beginning of the 1930s nearly failed due to this type of damage. For this reason, Dr. Ernst Mahle created an effective solution with the ring carrier as a groove protector.



Figure 24. Aluminum piston with a ring carrier in the first groove

Moreover, combustion gases contain corrosive components, the worst of which is sulfur dioxide (SO_2). It promotes corrosive wear of the cylinder surface, mainly in the region of the TDC.

The motion of the ring pack generates friction and thus mechanical losses. Between 10 to 20% of the total engine friction loss is caused by the ring pack. Friction is determined mainly by the following factors:

- Surface pressure (tangential load and gas pressure)
- Ring width
- Coefficients of friction of the contact surface (coating)
- Running face shape (barrel shape)
- Surface condition of the counterpart (cylinder surface)

Reduction of friction losses can be achieved primarily by minimizing surface pressure, so reducing the tangential load and ring width.

In recent years, the width of the piston rings has been drastically reduced and they also show better operating behavior in terms of friction, ring flutter and blow-by. Precise machining of the ring groove, however, is made more difficult. For extreme ratios of radial piston ring width to axial piston ring width, the piston rings become unstable. [5]

Types of piston rings

The first piston ring is closest to the combustion chamber. This means that it is exposed to the highest mechanical and thermal loads. To ensure good temperature resistance, nodular cast iron

or steel materials are used as the base material in these piston rings. They are also coated or specially treated, in order to reduce friction and wear. Piston rings are allowed to cause only minimal wear on the cylinder bore.

The second piston ring has a double function, depending on its type: it must seal against gas pressure while scraping oil off the cylinder wall; at the same time, sufficient lubrication of the first piston ring must be ensured. The second piston ring features a reinforced design with regard to its scraping effect, based on its additional function as an oil control ring. Its effectiveness is based on the contact pressure, the shape of the scraping surface (land) and method of removal of scraped oil. This requires good conformability, i.e. the ability to adapt as smoothly as possible to the continuously changing cylinder deformation while maintaining the required contact pressure against the cylinder wall. Friction and wear need to be minimized, of course.

The various tasks of the piston rings can no longer be met by a single ring type. Thus, it became necessary to classify the piston ring types in use today. This classification is made by the normative DIN ISO 6621, as shown in the Figure 25.

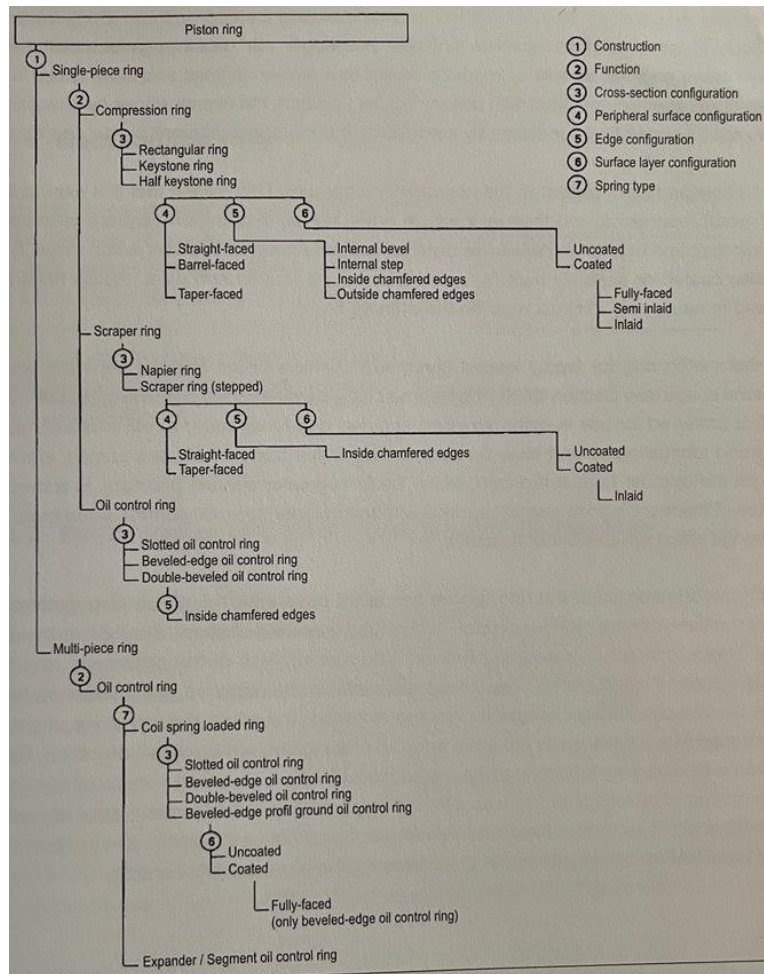


Figure 25. DIN ISO 6621

Referring to DIN ISO 6621, the type of rings listed can be defined as follow:

Rectangular ring

Its task is to seal against the gas pressure in the combustion chamber. Rectangular rings are used for normal operating conditions, primarily as first piston rings in gasoline engines.

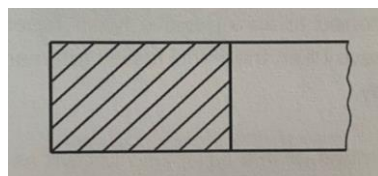


Figure 26. Rectangular ring

Rectangular ring with taper – faced running face

A slight taper (conicity) to the running face of the piston ring increases its effectiveness. Contact between the piston ring and the cylinder wall is reduced to a narrow line. This line contact increases the contact pressure of the piston ring against the cylinder bore and ensures that contact is maintained with the bore, even if the cylinder is deformed. It also provides a downward scraping effect, which supports the oil control function of the oil control rings. This type of ring is typically employed as a second piston ring.

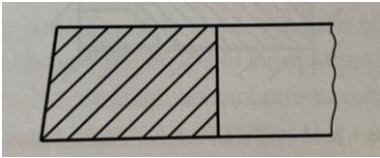


Figure 27. Rectangular ring with taper - faced running face

Piston ring with top internal bevel or internal step

Due to a chamfer on the inner side of the piston ring, the forces of the piston ring are modified such that its cross-section tips about its axis, due to compression during installation of the piston in the cylinder. This twist provides a line contact of the oil scraping edge of the ring against the cylinder surface, as well as between the lower inner edge of the piston ring side face and the piston groove side face. The latter reduces the passage of combustion gases as well as engine oil. When the internal bevel is at the top, it is referred to as a positive twist. Taper-face rings are also designed with a positive twist. They have been tried and tested for years and allow control of oil passage and reduction of blow-by. Piston rings of this type are used both as first and as second piston rings.

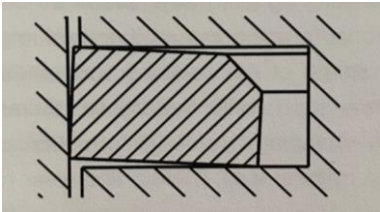


Figure 28. Piston ring with top internal bevel or internal step

Very important to take into account is the pre-twist. As sad it is crucial from a point of view of the gas passage, even if, some considerations have to take into account.

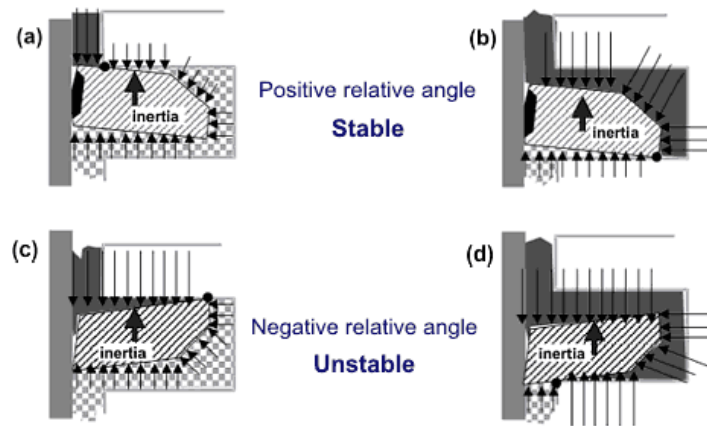


Figure 29. Stable and unstable pre-twist

The main purpose of the beveled edge is to allow compression gases to sneak behind the ring, that actually it is the job of the combustion pressure and ring groove side clearance, which is the rings' specific amount of space between the top face of the ring and the ring land. This gap is what allows the gases behind the ring to push it out against the cylinder walls. According to the piston ring edge that is beveled is possible to say that:

The top compression ring is most commonly cut on the top inside edge, which then creates positive (upward) twist as compression pushes down on the piston, giving it a look similar to a Belleville washer. This torsion then pushes the lower inside edge of the ring down into the ring groove to create a tight seal. (Schematics (a) and (b) of Figure 29).

The second compression ring bevel is commonly found on the bottom inside edge to create negative (downward) twist. Unless a Napier style ring is used, which would then have a bevel in the same position as the top ring or on the bottom outside edge, creating positive twist.

Since the top compression ring is effective at preventing most of the cylinder pressure from reaching the second ring, the integrity of the seal created is left to the rings natural twist since it doesn't have the assistance of compression like the top ring. The outer tapered edge is designed to assist with residual oil removal. As the piston travels downward, the tapered bottom edge is dragged against the cylinder wall, removing the excess oil pulled up by the vacuum created on the intake stroke. [5]

Piston ring with bottom internal bevel or internal step

Moving the internal bevel to the bottom provides a negative twist. These piston rings with bottom internal bevel make contact at the bottom with the cylinder and at the top inside with the groove side face. Such piston rings are preferably installed in the second ring groove and are part of the group of oil control rings. With regard to oil control, contact of the lower part of the ring face against the cylinder surface is desired. Oil control rings with greater taper are therefore used to compensate for the twist. The negatively twisted piston ring creates a good seal at the bottom against the cylinder surface is desired. Oil control rings with greater taper are therefore used to compensate for the twist. The negatively twisted piston ring creates a good seal at the bottom against the cylinder surface, due to its linear contact, and prevents oil from entering the ring groove. On the other hand, piston rings with positive twist have a tendency to control blow-by more efficiently. Since the passage of oil and blow-by gases cannot be equally well controlled with a single type of piston ring, a compromise must be made, based on the circumstances. The superior oil control of the negative twist in the second piston ring comes at the cost of slightly higher blow-by rates. The high gas pressure under full load deforms both types of twisted piston rings in such a way that they are nearly flat at the bottom contact to the groove side face. Under partial load, the piston ring deformation is not as severe, making the behavior of the rings more effective.

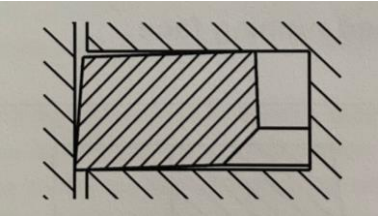


Figure 30. Piston ring with bottom internal bevel or internal step

Keystone ring

They are divided into single- and double-sided types. On a single-sided keystone ring, only one side has a taper-faced design, while on a double-sided keystone ring both sides do. These piston ring geometries reduce oil carbon build-up in the ring groove. The radial motion of the piston ring in the ring groove keeps it clear of oil carbon. Keystone rings of both types are used as first piston ring.

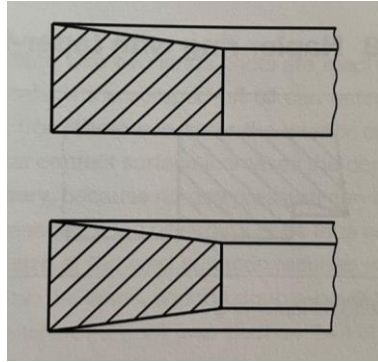


Figure 31. Keystone ring

First piston ring with barrel-shaped surface

Practical experience demonstrated that the sealing behavior of the first piston ring improved over time, when the sharp square corners had been worn off. This wear state was then anticipated, first by chamfering, then with a barrel-shaped running face. With the barrel shape, better hydrodynamic lubricating conditions are achieved, and the axially shorter contact surface at the cylinder surface improves sealing. In addition, the negative effects of cylinder deformations during engine operation can be better compensated. Piston rings of this type are used as first piston rings.

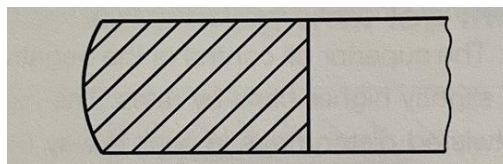


Figure 32. First piston ring with barrel-shaped surface

Napier ring with taper-faced running face

Due to a taper-faced running surface, the run-in time of this oil control ring is shortened and its oil-scraping effect is amplified. This type of design is used as a second piston ring.

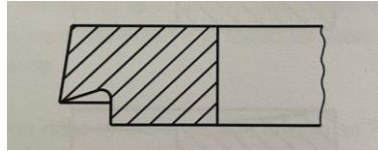


Figure 33. Napier ring with taper-faced running face

Spring-loaded oil control ring

To improve conformability and increase contact pressure, oil control rings are preloaded with a cylindrical spring (coil spring) on the inside of the ring. The ends of the spring are butted against each other. As with springless piston rings, beveled-edge oil control rings with coil spring and double-beveled oil control ring with spring are used. In most modern gasoline engines, three-piece oil control rings are used, primarily for cost reasons. One of the most important characteristics of oil control rings is the specific surface pressure. Generally, the greater the specific surface pressure, the lower the lubricating oil consumption. In order to reduce lubricating oil consumption during engine run-in, the two-part lands of the piston rings are angled at the running face. After a certain period of operation, the angled profiles wear down and take on a cylindrical shape. Spring-loaded oil control rings are used in the third ring groove.

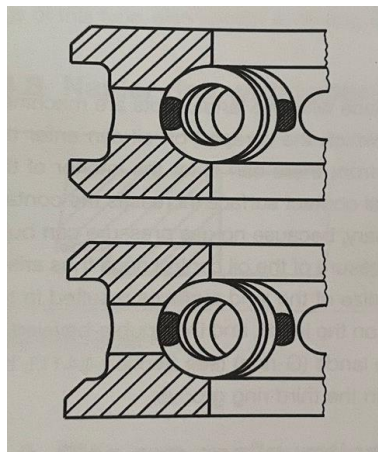


Figure 34. Spring-loaded oil control ring

Piston skirt

The piston profile deviates from the ideal circular cylinder in the axial direction (conicity, barrel shape) and in the circumferential direction (ovality). Piston typically has a slightly smaller diameter in the piston pin axis than in the thrust-antithrust axis (the difference is the diametric ovality). The skirt ovality creates space for thermal expansion in the piston pin axis direction.

In addition to normal ovality, ovalities with superposition are also possible, such as double or tri-ovality. For double ovality, in the form of a positive (double oval plus) or negative (double oval minus) superposition, the local piston diameter is greater or less than for normal ovality. The positive superposition widens the wear pattern relative to normal ovality, and the negative makes it narrower. Tri-ovality in the form of positive superposition widens the wear pattern, which is limited because of a significantly reduced local piston diameter starting at about 35° from the thrust-antithrust axis.

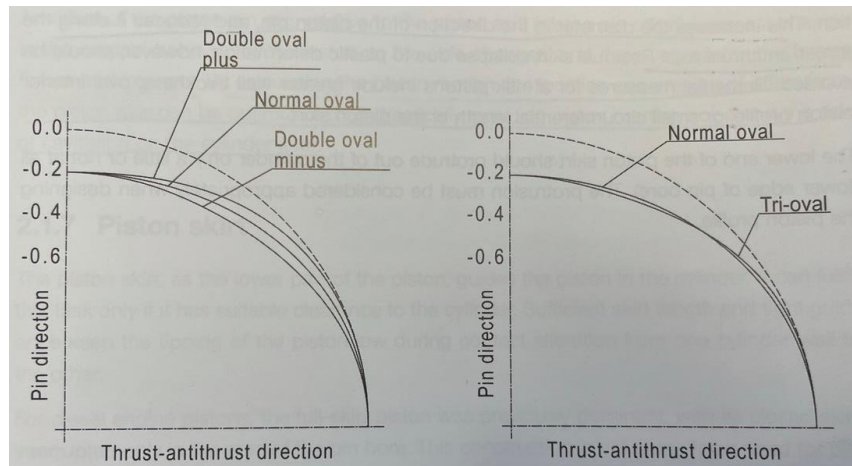


Figure 35. Ovality and superposition, double oval (left), tri-oval (right)

The resulting running surfaces in the thrust and antithrust direction should not be too narrow, so that the specific pressures between piston and cylinder remain low. In order to prevent hard contact and the risk of galling, the support area should not, however, extend out to the box walls.

The piston is tapered slightly at the upper and lower skirt ends, in order to promote the formation of the wedge of lubricating oil that acts as a support element. The greater taper in the area of the ring belt compensates for the great thermal expansion due to high temperatures in this area and for the deformation due to gas force. It also prevents the piston ring belt from impacting the cylinder owing to secondary piston motion. For noise-sensitive gasoline engines, in particular, there should be no contact between the ring belt and the cylinder. [5]

1.5.2 System engineering applied to the XC13 PCU system

The Target Deployment is considered referring to Table 5, which lists all engineering targets for the system.

Item	Product Target	System drivers
Performance	480 Hp (353 kW) @1900 rpm/ 2200 Nm @1100 rpm	PCP: 140 bar (+12% vs current production) CR: 12:1 Bowl
Fuel consumption	-10,5% vs current production	Low friction figures: Liner / rings friction Piston / liner friction Conrod length maximization with minimization of compression height Minimize need of oil flow for cooling Maximize the combustion thermal efficiency (adiabatic expansion)
NVH	Aligned to current production C13 Natural Gas	Minimize noise
Durability	>1 milion of km on European application GVV 44t	Stability of oil consumption and blow by trough life Scuffing resistance Avoid cavitation
Interval service	90 000 km on LH mission	Minimize oil consumption
Breaking performance	Europe: -260 kW@2350 rpm	Allow exhaust valve reopening at TDC with adequate clearance (pocket)

Table 5. Engineering target of the PCU system

Referring to Table 6 for the Statement of Requirement, a value is assigned to each item to ensure the achievement of the engineering target with the corresponding enabler, which explains what can be done to achieve the target.

Item	System Target	Enabler
Performance	Compression ratio: 12:1	Bowl shape and volume
Fuel consumption	Mechanical friction < 0,75 kW @max power	

Emission	Oil consumption <20g/h at full load 3rd ring conformability: 150 mm	3rd ring conformability Liner honing
	Reverse gas flow: 50,4 g/h at idle	Second land volume 2nd ring radial clearance
NVH	Piston rocking angle: target according to supplier	Piston pin offset Piston skirt profile, roughness, and treatment Clearance piston - liner
	Crown-bore minimum running clearance < 50µm	
Durability	Skirt contact pressure: target according to supplier	Piston skirt profile, roughness and treatment Clearance piston / liner
	Piston temperature: target according to supplier	Oil flow requirement Oil gallery design
	Fatigue safety factor: 1	Piston material and design
	Pin / piston contact pressure: target according to supplier Fatigue safety factor pin bore >1	Pin diameter and length
	Piston – valve clearance > 0 mm with 5° shift	Valve pocket
	Closed gap hot at BDC > 0,05 mm	Closed gap: 0,35 – 0,40 mm
	Liner cavitation: target according to supplier (piston secondary motion)	Skirt profile
	Oil consumption < 20 g/h at full load 3rd ring conformability: 150 mm	Piston ring section, tangential load, treatment, material and gap Honing parameter Liner type, material and thickness
Interval service	Blow-by < 150 l/min at full load	Piston ring section, tangential load, treatment, material and gap Clearance piston / piston ring
	Compression ratio: 12:1	Bowl shape and volume
Breaking performance		

Table 6. Statement of requirement

In the case of the PCU system, different piston ring solutions have been provided by the supplier, so a comparison between them is necessary. To determine the best one, several aspects are considered such as blow-by, oil consumption, and friction with the goal of finding the best trade-off between these three main aspects while also reducing costs. The alternatives presented are shown in Table 7 and Table 8.

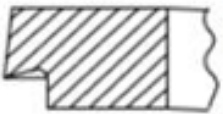
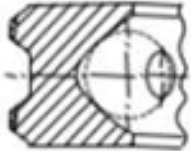
Groove	Ring picture	Ring characteristics
1		Dimensions: 135 x 2,5 mm
		Rad. Wall: 5,0 mm
		Closed gap: 0,35 – 0,40 mm
		Ft = 25,7 N
		Material: Cast iron
2		Dimensions: 135 x 2,5 mm
		Rad. Wall: 5,0 mm
		Closed gap: 0,65 – 0,80 mm
		Ft = 18,1 N
		Material: Cast iron
3		Dimensions: 135 x 3 mm
		Rad. Wall: 4,05 mm
		Ft = 50,5 N
		Material: Cast iron

Table 7. Alternative A for piston rings

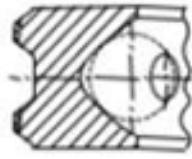
Groove	Ring picture	Ring characteristics
1		Dimensions: 135 x 3 mm
		Rad. Wall: 5,4 mm
		Closed gap: 0,35 – 0,45 mm
		Ft = 38,8 N
		Material: Cast iron
2		Dimensions: 135 x 2,5 mm
		Rad. Wall: 5,4 mm
		Closed gap: 0,65 – 0,80 mm
		Ft = 28,3 N
		Material: Cast iron
3		Dimensions: 135 x 3 mm
		Rad. Wall: 4,05 mm
		Ft = 50,5 N
		Material: Cast iron

Table 8. Alternative B for piston rings

Table 7 shows the *alternative A* presented by the supplier, while Table 8 shows *alternative B* with the first two rings as those of the C13 engine, while the third remains the same. As can be seen from the tables above, the main difference is that in the *alternative B*, the tangential force of the first and second rings is higher. Furthermore, for the two alternatives, different piston design should be considered due the different thickness and radial dimension of the first ring.

2. Engine frictions

Engine frictions is composed of three main components:

- 1) Pumping work
- 2) Mechanical frictions
- 3) Accessories

All of these contribute to reducing the work transferred to the piston, making it possible to define a mechanical efficiency as follows:

$$\eta_m = \frac{P_b}{P_{ig}} = 1 - \frac{P_f}{P_{ig}}$$

Where P_b is the brake power (useful power), P_{ig} is the gross indicated power and P_f is the friction power. The brake power can be defined as:

$$P_b = P_{ig} - P_f$$

While the friction power is the sum of the three contributions:

$$P_f = P_{mf} + P_{acc} + P_{pump}$$

Where P_{mf} is the mechanical friction loss, P_{acc} is the loss related to accessories and P_{pump} is the loss due to the pumping. It is important to keep in mind that pumping power is also considered in friction losses because, in the definition of mechanical friction, gross indicated power has been considered. Instead, if net indicated power is taken into account, pumping power can be neglected. Once the different powers involved have been defined, it is possible to consider a nomenclature based on mean effective pressure (mep) to normalize values with respect to engine size:

$$mep = \frac{W}{V_d} = \frac{P}{i \frac{n}{m} V_d}$$

Where W is the work per cycle, P the power per cycle, i the number of cylinders, n the engine speed, m is 2 for 4-stroke or 1 for 2-stroke engines and V_d the engine displacement. According to the power considered it is possible to define:

$$fmep = mf_{mep} + amep + pmep$$

$$bmep = imep - fmep$$

Considering the mep is useful because it is possible to refer to the thermodynamic cycle in the p-V diagram and compare the thermodynamic cycle with $imep$:

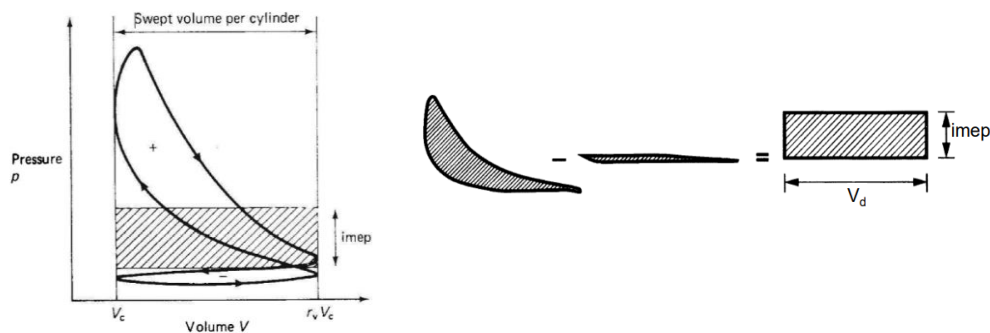


Figure 36. p-V diagram and imep

In order to understand the importance of the mechanical efficiency on the fuel consumption it is possible to refer to the brake specific fuel consumption that is an effective measure of the fuel consumption in $\frac{g}{kWh}$:

$$bsfc = \frac{\dot{m}_f}{P_b}$$

Looking at the equations above it is possible to evidence that if the same useful power (P_b) want to be produced with a lower fuel consumption ($bsfc$) it is possible to act on the mechanical efficiency. To notice that to a specific amount of fuel correspond an indicated power P_i . [6]

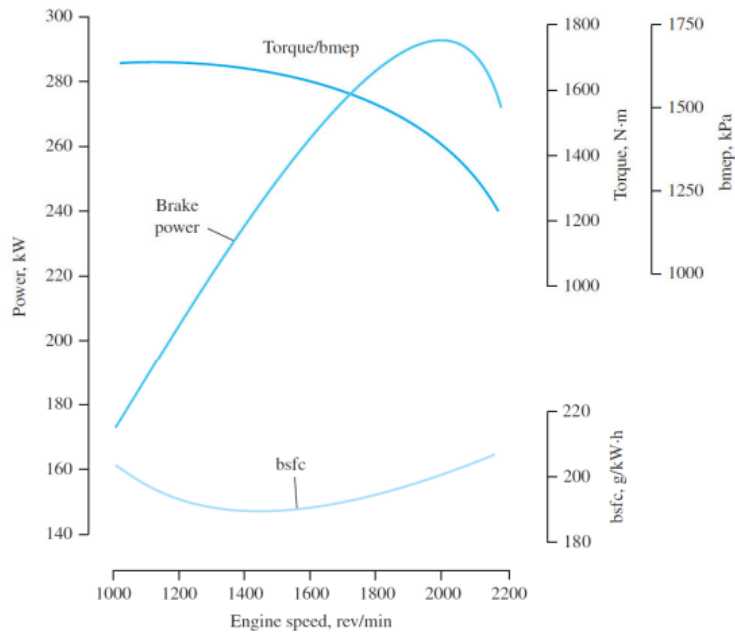


Figure 37. Full-load torque, bmep, bsfc and power versus speed for a typical TC truck diesel engine

2.1 Pumping work

Considering a 4 – stroke engine analyzing the thermodynamic cycle it is possible to refer to an indicated work per cycle per cylinder:

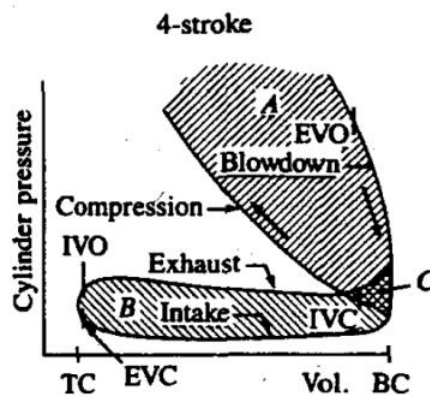


Figure 38. 4-stroke engine thermodynamic cycle

The indicated work can be obtained by integrating the curve (to obtain the area enclosed) on the diagram:

$$W_i = \oint p dV$$

Two different indicated work can be defined:

- **Gross indicated work per cycle W_{ig}** : work delivered to the piston over the compression and expansion strokes only (area A + C, for NA engines)
- **Net indicated work per cycle W_{in}** : work delivered to the piston over the entire 4-stroke cycle (area (A+C) – (B+C), for NA engines)

Then for a naturally aspirated engine (intake pressure < exhaust pressure) it is possible to define the area B + C as the pumping work (work transferred between the piston and the cylinder gases during the inlet and exhaust strokes). Pumping work transfer to the in-cylinder gases reduces the work transferred to the crankshaft and constitutes one component of engine friction. On the other hand, if a turbocharged engine is considered (intake pressure > exhaust pressure) the pumping work can be considered as a positive contribution.

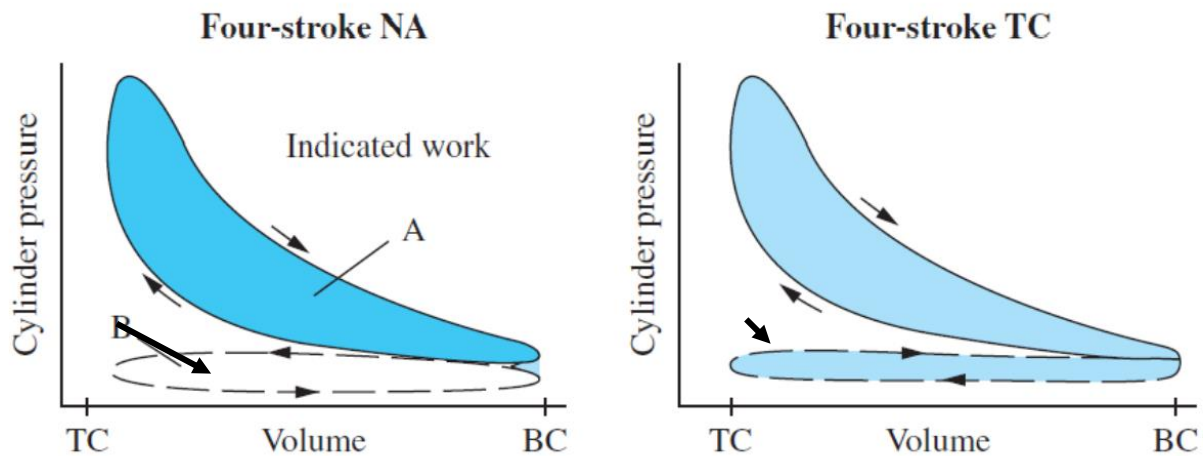


Figure 39. 4-stroke NA and TC engine thermodynamic cycle

Looking at the Figure 39 is possible to evidence the reason why in the TC engine pumping work has a positive contribution. Referring to the direction of the arrows and considering that the indicated work is an integral on the curve, a clockwise path (TC cycle) will give a positive value. Finally, is important to highlight that if the EGR is implemented the contribution of the pumping work will be again negative, because to permit an EGR flowrate the intake pressure should be lower with respect to the exhaust pressure. [6]

2.2 Mechanical frictions

In an internal combustion engine, the parts that contribute mainly to the mechanical frictions are:

- Piston skirt
- Piston rings
- Piston pin
- Bearings
- Valvetrain

In the following paragraphs a description of the phenomenon correlated with the friction of the piston skirt, piston rings and bearings has been provided due to the fact that these parts among the PCU system, whose frictions will be studied by means of a GT Power model in the next chapter.

2.2.1 Piston rings

Piston rings tribology

The friction related to the piston rings is highly dependent on their tribology. During the operating conditions they can experience three different lubrication conditions that are:

- **Hydrodynamic lubrication:** at mid-phase of the engine stroke. Here the oil film is sufficiently thick to sustain loads and asperity contacts are negligible
- **Boundary lubrication:** at critical position (TDC or BDC) where the velocity of the piston tends to be zero. Here the oil film is thin, and the load is supported mainly or completely by asperity contacts
- **Mixed lubrication:** nearby to critical positions. It is a transition phase between hydrodynamic and boundary lubrication, so here the load is sustained by both lubricant film and asperity contacts. It takes place usually when there is high load, low speed and/or low viscosity due to high temperature

From a more practical point of view, in order to evaluate the friction of piston rings, it is necessary to start by calculating the oil film thickness between the rings and liner. This can be expressed as a function of time (crank angle) and ring face profile.

$$h(x, \theta) = h_{min} + \frac{c}{\left(\frac{b}{2} + o\right)^2} (x - o)^2 = h_{min} + B(x - o)^2$$

with:

$$B = \frac{c}{\left(\frac{b}{2} + o\right)^2}$$

For the quantities in the equation is possible to refer to the Figure 40:

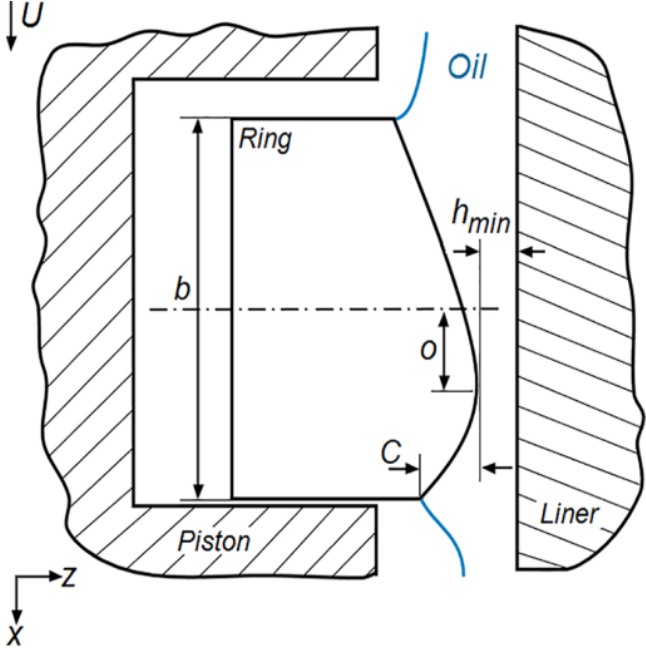


Figure 40. Piston ring diagram

Then, it is possible now to apply the 1D Reynolds Equation considering uniform circumferential oil film thickness:

$$\frac{\partial}{\partial x} \left(h^3 \frac{\partial p}{\partial x} \right) = -6\eta U \frac{\partial h}{\partial x} + 12\eta \frac{\partial h}{\partial t}$$

Where η is the oil viscosity, U the piston speed and p the pressure on the external surface of the ring (between ring and liner). Integrating two times the equation with respect to the position x it is possible to obtain the pressure:

$$p(x) = -6\eta UI_0(x) + 12\eta\omega \frac{\partial h}{\partial \theta} I_1(x) + C_1 I_2(x) + C_2$$

Where the different constant are defined as:

$$I_0(x) = \int \frac{1}{h^2(x, \theta)} dx = \frac{1}{2h_{min}\sqrt{Bh_{min}}} \tan^{-1} \left((x - o) \sqrt{\frac{B}{h_{min}}} \right) + \frac{(x - o)}{2h_{min}(h_{min} + B(x - o)^2)}$$

$$I_1(x) = \int \frac{x}{h^3(x, \theta)} dx = \frac{3o}{8h_{min}^2\sqrt{Bh_{min}}} \tan^{-1} \left((x - o) \sqrt{\frac{B}{h_{min}}} \right) + \frac{3o(x - o)}{8h_{min}^2(h_{min} + B(x - o)^2)} +$$

$$+ \frac{o(x - o)}{4h_{min}(h_{min} + B(x - o)^2)^2} + \frac{1}{4B(h_{min} + B(x - o)^2)^2}$$

$$I_2(x) = \int \frac{1}{h^3(x, \theta)} dx = \frac{3o}{8h_{min}^2\sqrt{Bh_{min}}} \tan^{-1} \left((x - o) \sqrt{\frac{B}{h_{min}}} \right) + \frac{(x - o)(5h_{min} + 3B(x - o)^2)}{8h_{min}^2(h_{min} + B(x - o)^2)^2}$$

At this point it is possible to define the boundary conditions to calculate the integrating constant C_1 and C_2

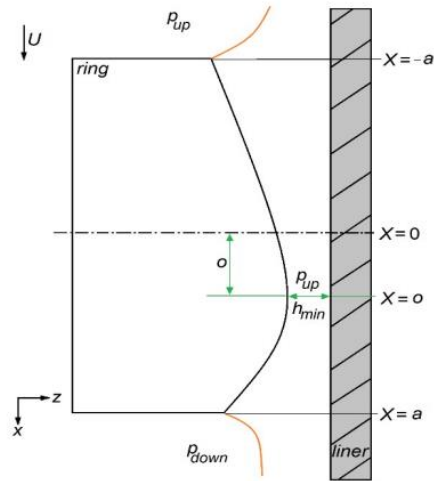


Figure 41. Schematic for the boundary conditions

- Downward stroke:

$$p = p_{down} \quad x = a$$

$$p = p_{up} \quad x = 0$$

- Upward stroke:

$$p = p_{up} \quad x = -a$$

$$p = p_{down} \quad x = 0$$

Then it is possible to consider the force balance equilibrium equation in both downward and upward stroke:

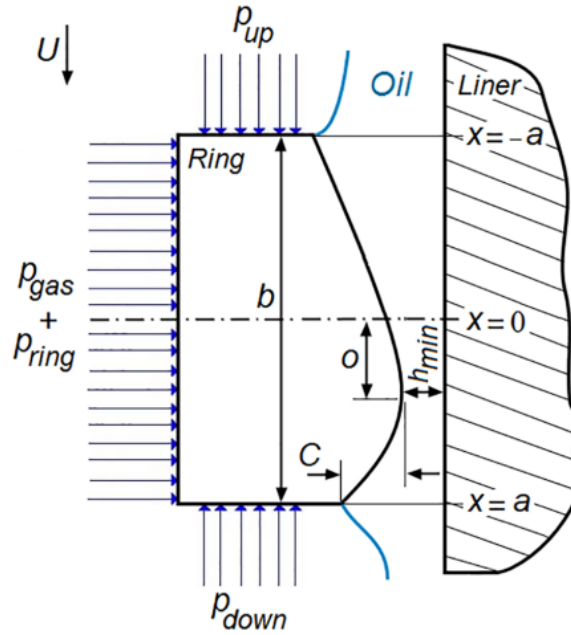


Figure 42. Forces acting on a piston ring

- Downward stroke:

$$\int_0^a p(x)dx + (a + o)p_{up} = b \left(\frac{2T}{bD} + p_{gas} \right)$$

- Upward stroke:

$$\int_{-a}^o p(x)dx + (a - o)p_{down} = b \left(\frac{2T}{bD} + p_{gas} \right)$$

Where T is the ring tension force and p_{gas} the pressure acting on the rear of the ring that depends on the boundary pressures:

$$p_{gas} = p_{up} \quad \text{if } p_{up} > p_{down}$$

$$p_{gas} = p_{down} \quad \text{if } p_{up} < p_{down}$$

Algorithm for solving force equilibrium equation to calculate instantaneous minimum oil film thickness h_{min} as a function of crank angle is shown in Figure 43:

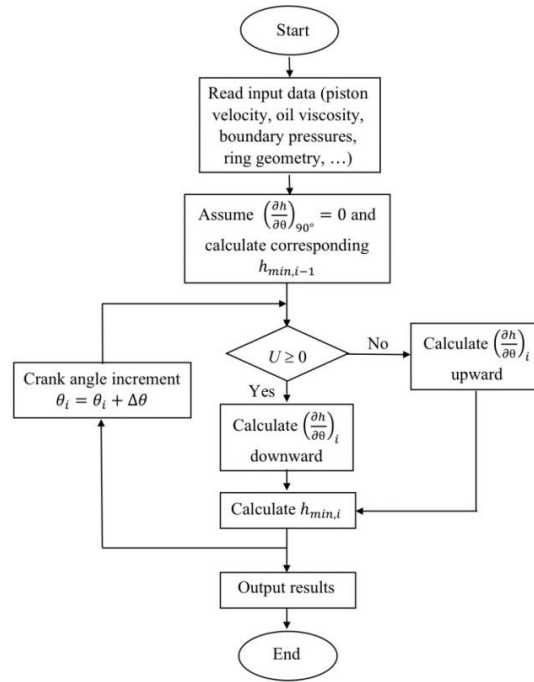


Figure 43. Algorithm for solving force equilibrium equation

After the calculation of instantaneous minimum oil film thickness h_{min} , the nominal oil film thickness $h(x, \theta)$ can be updated and used to evaluate friction force and then corresponding friction power loss: [7]

- Hydrodynamic lubrication:

$$F_f(\theta) = \int \left(\frac{\eta U}{h(x, \theta)} + \frac{h(x, \theta)}{2} \frac{dp}{dx} \right) dA$$

- Boundary lubrication:

$$F_f(\theta) = \mu \left(\pi D F_{ring, gas}(\theta) \right) \text{sign}(-U)$$

Piston rings conformability

Piston rings must adapt themselves to the deformed liner and therefore their geometry must be such as to allow them to flex easily to ‘follow’ the deformed shape of the liner. This capability of the rings is called conformability. The first conformability criterion was developed by Müller (1970) by finding an approximate solution of the equilibrium of the piston ring within a distorted liner:

$$A_n^{max} = \frac{F_r R^3}{EI(n^2 - 1)^2}$$

With $R = D/2$, the nominal operating ring radius, n number of lobes of the deformed liner, I moment of inertia of the ring cross section, E Young's modulus of the ring material and F_r the tangential force of the ring. If the limit A_n^{max} is exceeded the piston ring starts to lose its correct contact with the liner.

A new curved beam finite element has been presented in literature [8] and specifically developed to couple the piston ring structural deformation with the liner distortion. To describe the deformed shape of the liner transversal section the Fourier series can be used:

$$y(\alpha) = A_0 + \sum_{k=1}^n A_k \sin(k\alpha + \Phi_k)$$

Where α is the position along the liner circumference, A_k and Φ_k the magnitude and the phase of the k -th distortion order.

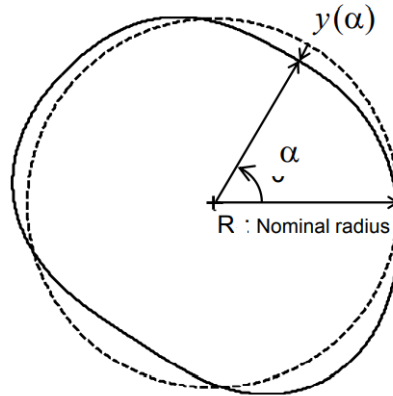


Figure 44. Bore distortion

As 0-th order of distortion corresponds to a uniform expansion of the liner radius and 1-st order of distortion corresponds to a rigid displacement of the liner axis (without modifying its radius). 0-th and 1-st order of distortion can be neglected. The shape of the k -th order of distortion will contain k lobes equally distributed around the liner circumference.

2.2.2 Piston skirt

One major parameter that influences piston friction is the installation clearance. An appropriate installation clearance can significantly reduce the typical thermal warping between piston and cylinder in warm operating conditions. Excess clearance is counterproductive, because it can lead to greater secondary motion and wedging of the piston in the cylinder. Under these circumstances, the hydrodynamic lubricating film can be penetrated, and mixed friction can arise. Too large installation clearance can also have a negative acoustic effect. The lower thermal expansion coefficients of steel pistons in comparison with aluminum pistons can result in frictional advantages.

For low friction power loss values, the local tapering of the piston profile toward the piston axis (mantle curve decrease values) and the ovality are designed in such a way that the contact pressures in the desired support area are uniform. As a rule, this can limit the disturbance of the hydrodynamic lubrication behavior by the change in the direction of movement of the piston to the points where the piston reverses direction (top and bottom dead center). This is where mixed friction conditions arise in the support area.

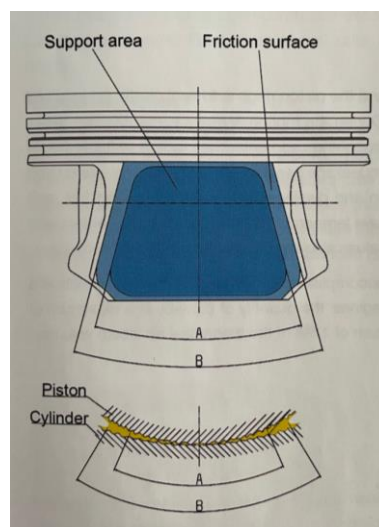


Figure 45. Support area and lubricant gap

Besides the skirt profile, the surface of the skirt running surface also has a great influence on the sliding behavior of the piston. Excessive skirt roughness increases friction power losses. In addition to friction forces on the piston skirt, the lubrication of the skirt also plays a decisive role in the proper functioning of the piston in the cylinder. Certain minimum surface roughness values of the piston skirt and the honed cylinder surface:

- Enhance running-in characteristics.
- Prevent abrasive wear.
- Contribute to the formation of a hydrodynamic lubricating film between the piston skirt and the cylinder wall.
- Prevent the piston from seizing, i.e., local fusing between the piston and the cylinder due to a lack of clearance or lubricating oil.

If the skirt roughness is too great, friction power losses are increased, while if the skirt roughness is too low, then the piston may not run in as well. A good compromise between these requirements yields piston skirt surface roughness levels in the range $R_a = 1,5 - 5 \mu m$.

Protective coatings for the running surface have a positive effect on friction losses in the boundary lubrication conditions, increase wear resistance, and improve resistance to seizing. [5]

2.2.4 Small eye

The small eye of the connecting rod can be thought as a thin pipe drilled perpendicular to the axis of the wrist pin housing (to allow the lubricant oil adduction). In medium stressed engines the small eye has parallel sides, while in high stressed engine like in the XC13 case, the expansion phase generates high forces on the surface between the connecting rod and the wrist pin, on the contrary the inertial forces are lower and then the opposite contact surface can be smaller. In this case, the small eye is shaped with converging sides, reducing the overall length of the pin, then the reciprocating masses and hence the stress on the connecting rod.

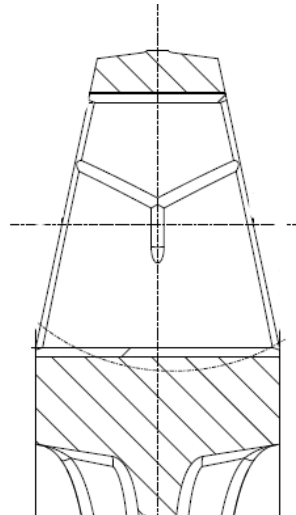


Figure 46. XC13 small eye

The small eye can be considered as a bushing, so is possible to make some consideration regarding the friction generation. The behavior of the friction coefficient follows the Stribeck curve shown in Figure 47. [9]

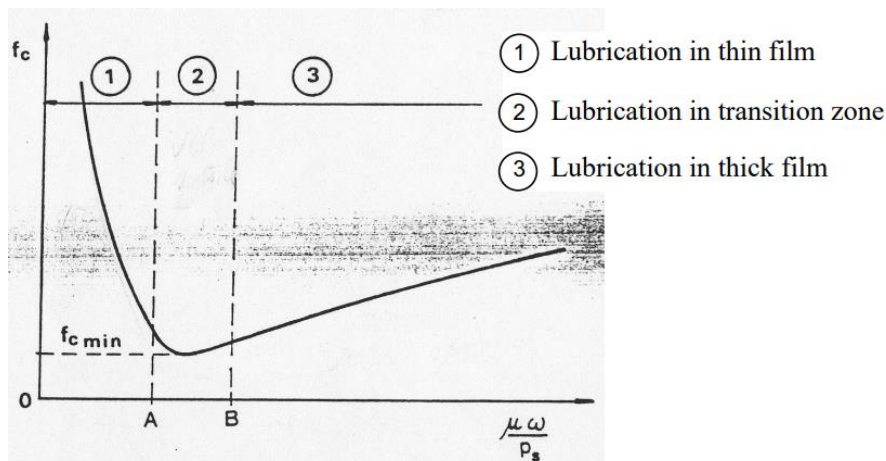


Figure 47. Friction coefficient behavior

2.3 Accessories

It is possible to distinguish between several contributions to mechanical loss due to accessories. Typically, only 2% of a vehicle's total power output goes towards powering accessories. Some accessories are connected directly to the engine through gears or belts and usually require large

amounts of power. There is also a contribution due to the electrical power absorption from windows, seats, door locks, steering, air conditioning, and so on.

Obviously, the contribution of accessories to engine friction can vary depending on factors such as the type and number of accessories in use, as well as the design of the vehicle's engine and electrical system. However, it is important to note that even small contributions from accessories can add up over time, leading to increased fuel consumption and reduced engine efficiency. [6]

3. Thermal analysis of the piston

In the GT Power model used for both friction and blow-by prediction a hot working condition is taken into account. For this reason, a thermal static analysis and then a thermo-structural analysis have been done through the program *Hypermesh* to implement both the right temperatures of the piston and the rings and the deformed diameters of the piston.

In the FE modeling half piston with the liner, piston rings and wrist pin have been considered as shown in Figure 48:

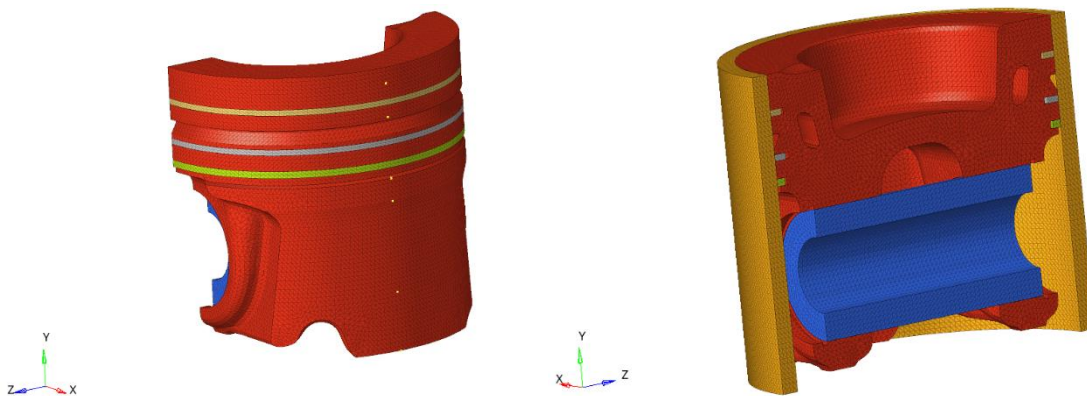


Figure 48. Views of the FE model used on Hypermesh

Regarding the definition of the surfaces involved in the heat exchange:

- 1) Piston top: the upper part of the piston faced the temperature in the combustion chamber, so a convective heat exchange is modeled with respect to a mean temperature of the

substrate layer of around 300 °C in agreement with the temperature in the combustion chamber.

- 2) Cooling gallery: Thanks to dedicated nozzles, oil at a temperature of 105 °C with a flow rate of 4,7 l/min passed through the cooling gallery, so it exchanges heat by means of convection.
- 3) Piston lands: piston lands are not directly in touch with the liner and exchange heat thanks to a mix of oil and gases, so also for them a convection surface is modeled with respect to a reference temperature of 130 °C that is the mean temperature of the liner.
- 4) Piston grooves: piston grooves transfer heat both through conduction by means of the contact with the piston rings and through convection in the volume behind the rings, even for that case this effect has been neglected.
- 5) Internal piston: The inner part of the piston exchange heat by means of convection due to the presence of air and oil sprayed by the nozzles. Here a reference temperature of 105 °C is considered, that consists of the oil temperature.
- 6) Piston hub: Due to the connection between the wrist pin and the piston hub a conductive heat exchange is defined. Moreover, in the central part of the wrist a convective heat exchange surface is defined trying to simulate the presence of the connecting rod.
- 7) Skirt: Because of the presence of the oil layer a mixed convective / conductive heat exchange is present on the piston skirt, even if in the model only the convective exchange is modeled for simplicity.

In the figures below is possible to see the elements of the model involved in the heat exchange:

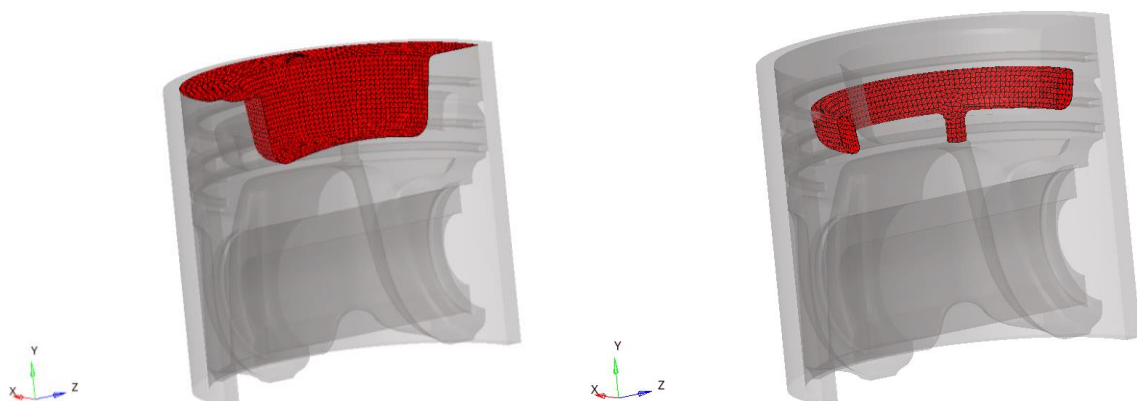


Figure 49. Elements of convective heat exchange surface of Piston Top and Cooling gallery

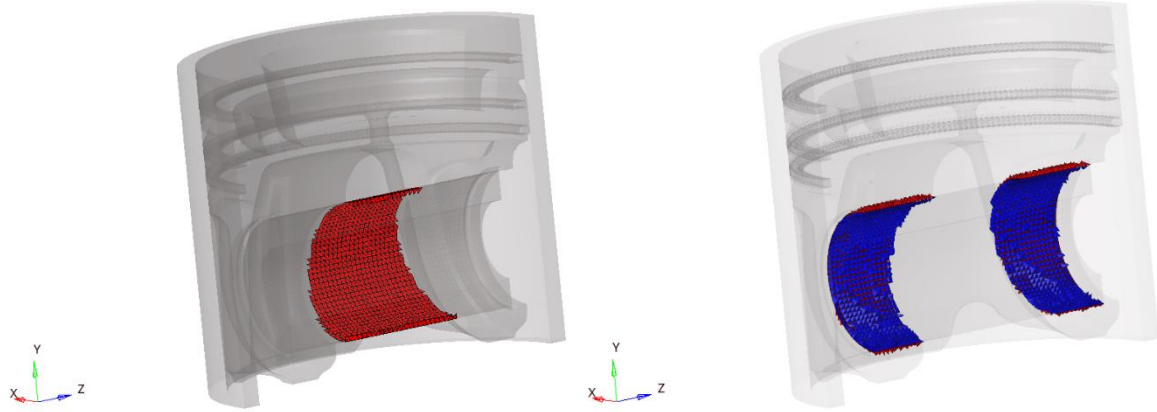


Figure 50. Elements of convective (left) and conductive (right) heat exchange surface of Piston hub and Wrist pin

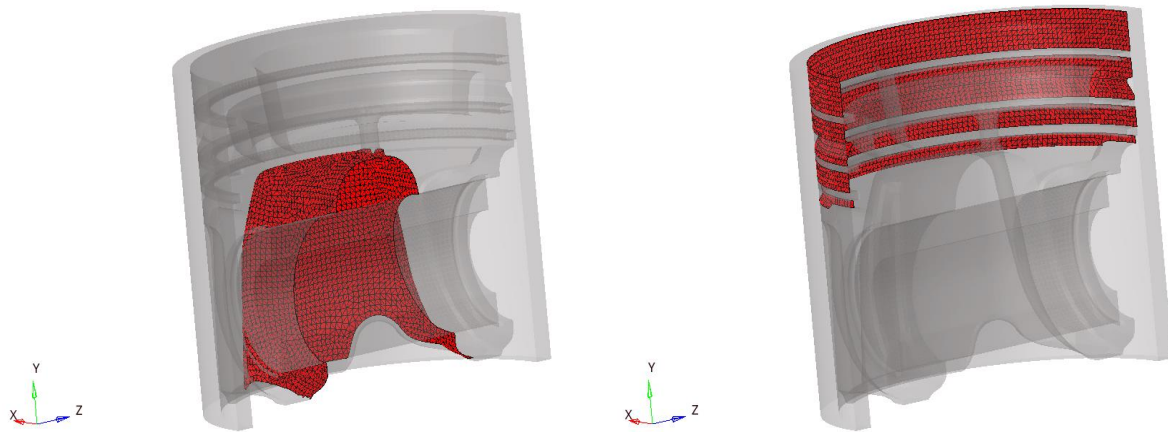


Figure 51. Elements of convective heat exchange surface of Internal Piston (left) and Piston lands (right)

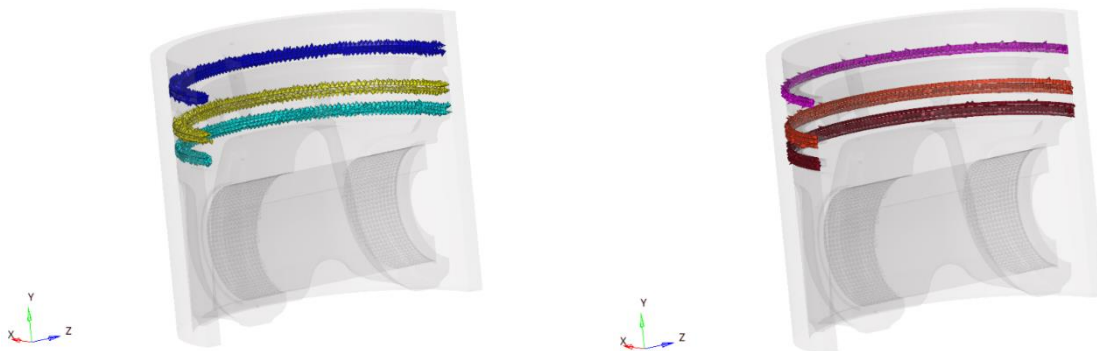


Figure 52. Elements of conductive heat exchange surface of Internal Piston Groove-Rings (left) and Rings-Liner (right)

Once defined all the surfaces of heat exchange the heat exchange coefficient has been set. For conductive surfaces the coefficient $K \left[\frac{W}{mK} \right]$ depends on the material, and it is fixed, while for convection a tuning has to be performed. Starting from values from literature according to the

type of fluid involved and to the level of turbulence initial values of convective heat exchange coefficient $H \left[\frac{W}{m^2K} \right]$ are chosen. Thanks to data from the supplier that provides the temperature reached in different parts of the piston, a correct tuning has been performed, taking into account also heat fluxes and ensuring that the global balance tends towards a null value. The results are shown in Figure 53.

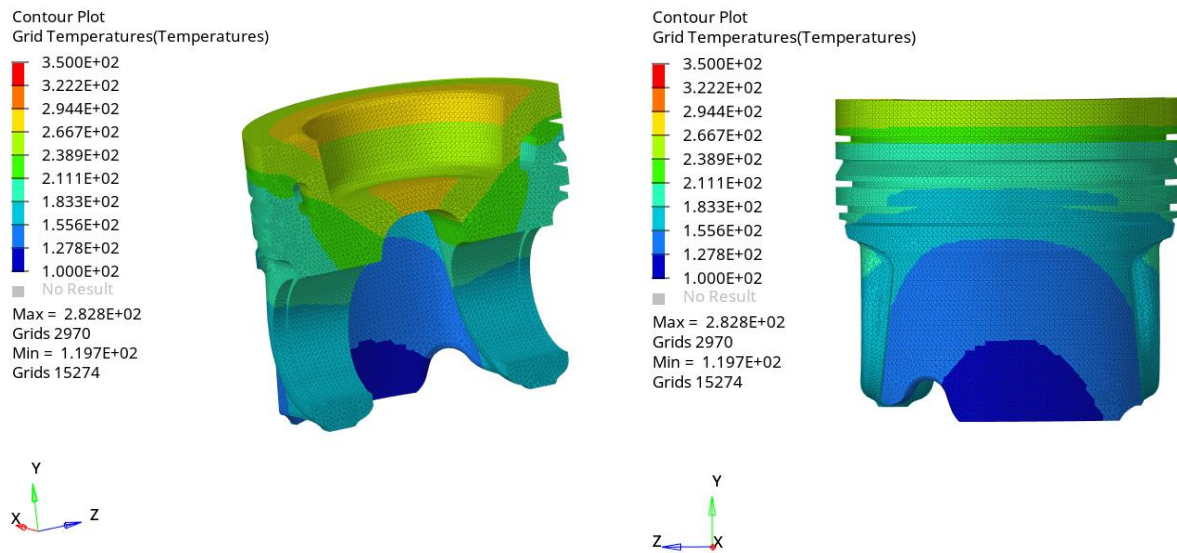


Figure 53. Temperatures results from the static thermal analysis

The temperatures reached in the piston are listed in the Table 9 and for each part of it three measurements have been done in order to have a mean value.

Piston part	Temperature 1 [°C]	Temperature 2 [°C]	Temperature 3 [°C]	Mean Temperature [°C]
Piston max T	-	-	-	283
Bowl edge	279,2	280,1	278	279,1
Top land	244,9	246	246,6	245,8
1st Ring groove	228	230	229,9	229,3
2nd Ring groove	194,3	200	201,3	198,5
Skirt top	159,4	161,2	167,3	162,6
Skirt middle	133,6	146,7	145,3	141,8
Skirt bottom	120	128,6	120,9	123,1

Table 9. Piston temperatures from static thermal analysis

Instead, for the temperatures of the rings, the results obtained are the following:

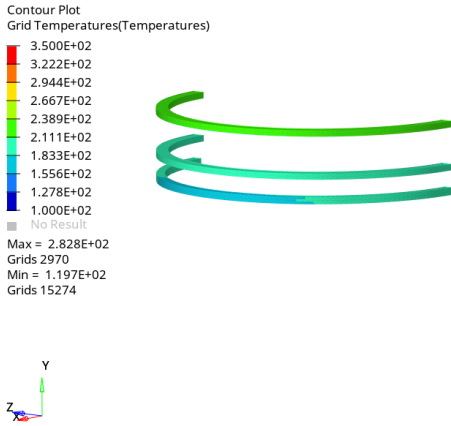


Figure 54. Piston rings temperatures results from the static thermal analysis

With the temperatures listed in Table 10:

Piston part	Temperature 1 [°C]	Temperature 2 [°C]	Temperature 3 [°C]	Mean Temperature [°C]
1st Ring	219,1	221,3	221,7	220,7
2nd Ring	188,4	194,9	195,2	192,8
3rd Ring	180,1	192	192,9	188,3

Table 10. Piston rings temperatures from static thermal analysis

Once the static thermal analysis was completed, a thermo-structural analysis was also implemented to take into account the deformation of the piston in hot conditions. This step is important because, since bore distortion in hot conditions is considered, it is necessary to also implement the deformation of the piston’s diameter at different heights. In the finite element (FE) model, as can be seen from Figure 48, some nodes on the external surface of the piston are highlighted and represent the height at which the diameter of the piston is known from technical drawings. For this reason, the mesh of the model was created to have a node at these points and obtain the measure of the deformed diameter at those points. To perform the analysis, in addition to the previous model used for static thermal analysis, mechanical constraints were added as shown in Figure 55.

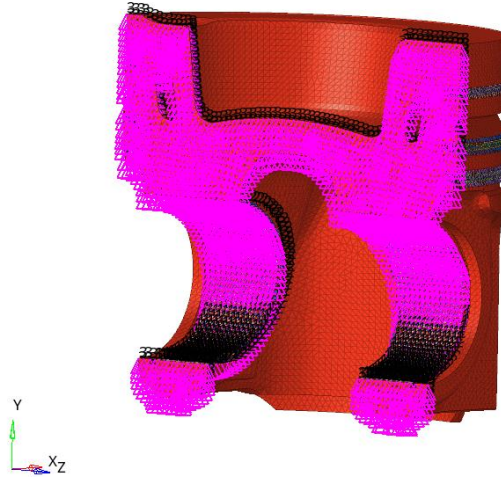


Figure 55. Mechanical constraints

The surface where the piston is cut has been constrained from translating along the z-direction, while the piston hubs have been constrained from translating along the x and y directions. In this way, all degrees of freedom, including rotation around the three axes, have been constrained. Additionally, pressure on the top surface of the piston has been implemented, but even considering the maximum pressure of 98 bar reached in the combustion chamber, its contribution to diameter deformation is negligible for the purpose of the simulation and has therefore been neglected for simplicity.

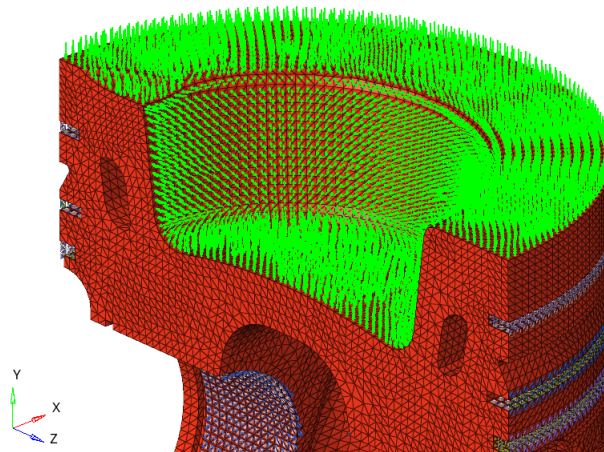


Figure 56. Maximum pressure of 98 bar applied on the top of the piston

The material of the piston is an aluminum developed by the supplier, which provides the following properties:

Material property	Value	Unity of measurement
K	0,121	$\frac{W}{mmK}$
a	$2,24 \cdot 10^{-5}$	$\frac{1}{K}$
R_{p0,2}	145	MPa
c_p	963	$\frac{J}{kgK}$
ρ	2,66	$\frac{g}{cm^3}$
ν	0,33	-
E	71	GPa
T_{melt}	574 – 582	°C

Table 11. Properties of the piston material

The results obtained are shown in Figure 57 and the expanded diameter in the characteristic points mentioned before are listed in the Table 11.

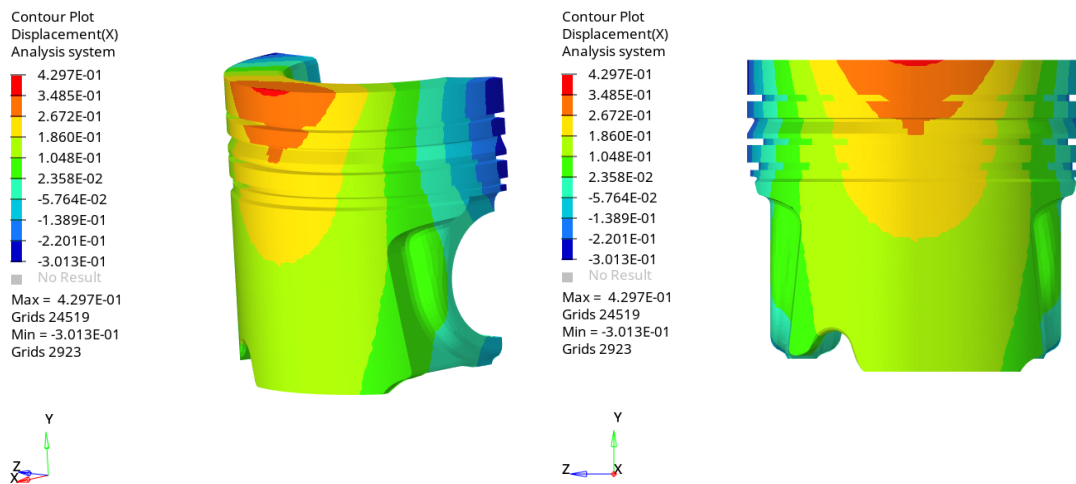


Figure 57. Displacements of the piston due to thermo-structural load

To understand the shape of the deformed piston, an amplifying factor of 50 was applied to the piston's deformation, and the result is shown in Figure 58. The results are in line with the expected behavior. In fact, for the simulation, a constant diameter is considered, but in reality, the shape of the external part of the piston is curved, as discussed in 2.2.2 *Piston skirt* to account for the greater expansion of diameters at the top of the piston due to higher temperatures involved.

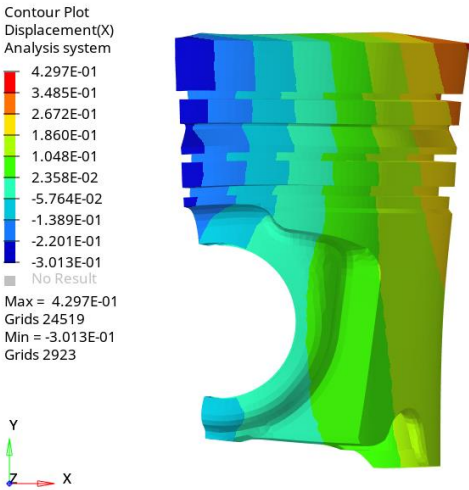


Figure 58. Amplified deformed shape of the piston

The values of the diameters are known from technical drawings at different heights of the piston and are shown in Figure 59. For each one, a node is created, as visible in Figure 48. In more detail, the diameters at those heights are defined as a radial clearance with respect to the cylinder bore, and it is possible to consider the expanded diameter as calculated in Table 12.

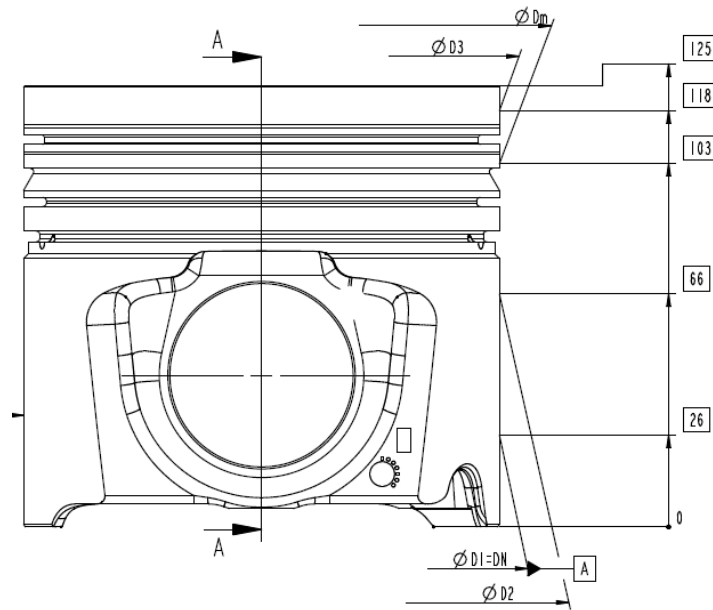


Figure 59. Known diameters of the piston from technical drawings

To calculate the expanded diameter the following equation is considered:

$$D_{expanded} = Bore - 2 \cdot Radial\ clearance + 2 \cdot Radial\ thermal\ expansion$$

Diameter	Bore diameter [mm]	Radial clearance [mm]	Radial Thermal expansion [mm]	Expanded diameter [mm]
D₃	135,01	0,425	0,332	134,81
D_m	135,01	0,260	0,241	134,96
D₂	135,01	0,097	0,063	134,93
D₁	135,01	0,040	0,028	134,97

Table 12. Expanded diameter of the piston

Once the diameters of that reference points are known through interpolation it is possible to obtain a pistons' profile in hot condition to implement in GT Power.

4. GT Power model for friction prediction

GT Power is an industry-leading engine simulation software used by all major engine manufacturers and vehicle OEMs. It is used to predict engine performance quantities such as power, torque, airflow, volumetric efficiency, fuel consumption, turbocharger performance and matching, and pumping losses, among others.

Some advantages of using GT Power include its ability to model all mechanical components involved in engine friction in detail, allowing for a thorough analysis of engine performance. GT Power also includes many advanced modeling features not found in other engine simulations, such as a full finite element solver for in-cylinder temperature and heat flux distribution, as well as complete, fully flexible, detailed in-cylinder chemical kinetics solvers.

A model is already present in the program, so the study of frictions started from it implementing new functions. The goal of the model is to predict the frictions of the XC13, as already explained in previous chapters, with a focus on the PCU system in order to verify the project targets and evaluate the friction contribution of the piston ring alternatives proposed by the supplier, understanding their impact on the VECTO test, in terms of power loss and consequently of CO₂ emissions. The single-cylinder model implemented in GT Power is shown in Figure 60.

To feed an explanation, the *Cranktrain* block in the bottom part imposes the movement of the crank mechanism at a fixed engine speed, specifying the number of cylinders, firing order, cylinder offset, and type of reference system used.

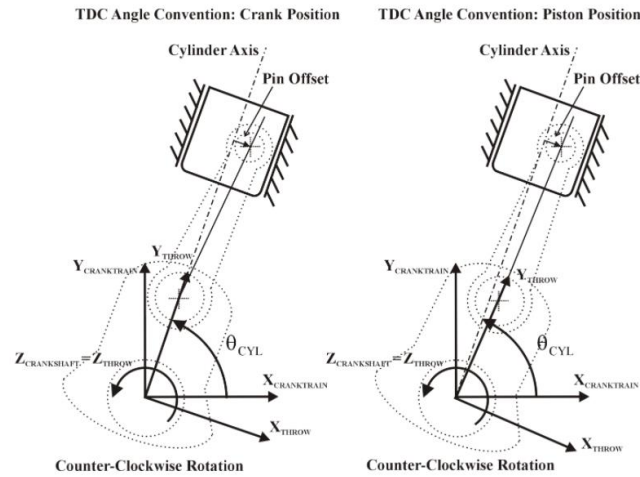


Figure 61. GT Power TDC angle convention

In that case referring to Figure 61 the *crank position* convention for the TDC angle has been chosen with a θ_{CYL} of 90° and *Pin Offset* = 0 mm.

The *BLOCK* brick is connected to the single crank through a *JournalBearing* attached to the main journals of the single crank. All the bricks of the single crank represent both the geometrical dimensions of the XC13 crankshaft, flywheel, connecting rod, and piston, as well as the dynamic properties of the different parts, such as mass and inertia, calculated using the CAD program *Creo*. All dimensions have been extrapolated from technical drawings, supplier reports, test bench results, and virtual simulation results. Particular attention has been paid to the connection between the piston and cylinder liner, considering that one of the main goals was to evaluate different alternatives for piston rings. The modeling of each part of the model will be discussed in the following paragraphs.

3.1 Piston rings and piston lands

In the *TopRing*, *ScraperRing*, and *OilRing* bricks, the geometrical dimensions of the piston rings are defined and their stiffness is computed. In particular, the program requires the free

diameter and compressed diameter at which the tangential force and end gap are known. For a better understanding, it is possible to refer to Figure 62.

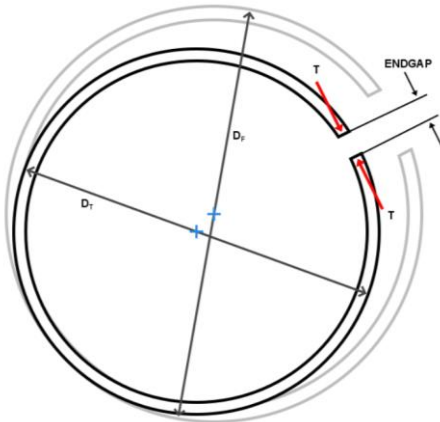


Figure 62. GT Power piston ring convention

Referring to the figure above D_F is the free diameter, D_T is the compressed diameter and T is the tangential elastic ring force. Moreover, the behavior of the rings is imposed by the connection with the piston, which imposes the movement along the cylinder and by the pressures above, behind and below the rings as shown in Figure 63:

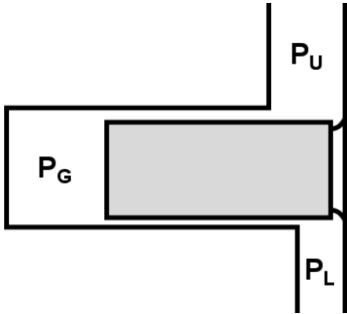


Figure 63. Pressures in the rings

The profile of the rings has been implemented thanks to technical drawings as shown in Figure 64, Figure 65, Figure 66:

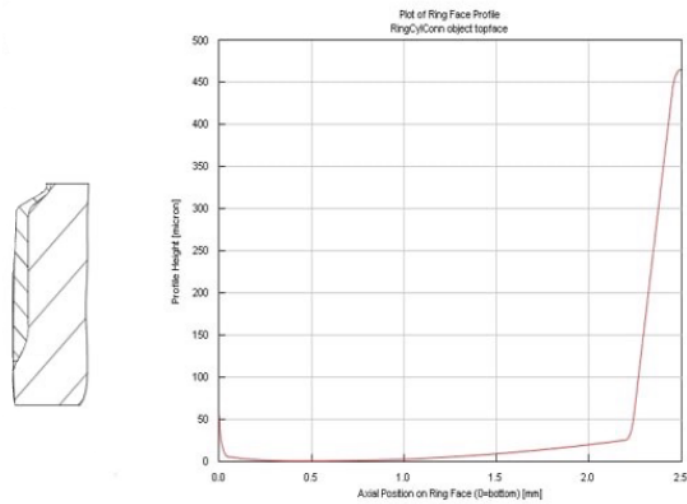


Figure 64. Section of the first piston ring. Technical drawing on the left and GT Power implementation on the right

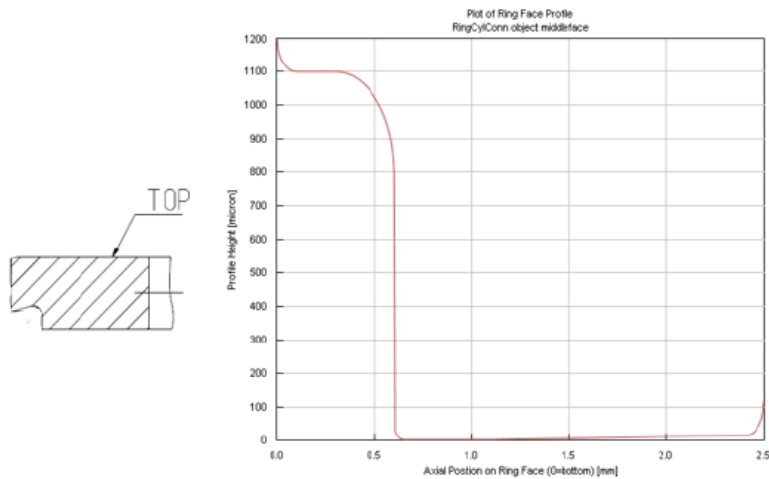


Figure 65. Section of the second piston ring. Technical drawing on the left and GT Power implementation on the right

For the first and the second ring the profile has been implemented providing the punctual profiles' height of the external surface (y axis) along the thickness (x axis) of the ring. Reference points from technical drawings has been considered and then, to make the profile smoother an interpolation has been done. Especially from Figure 65 is possible to notice that too sharp edges have been rounded to avoid the divergence of the run simulation on GT Power.

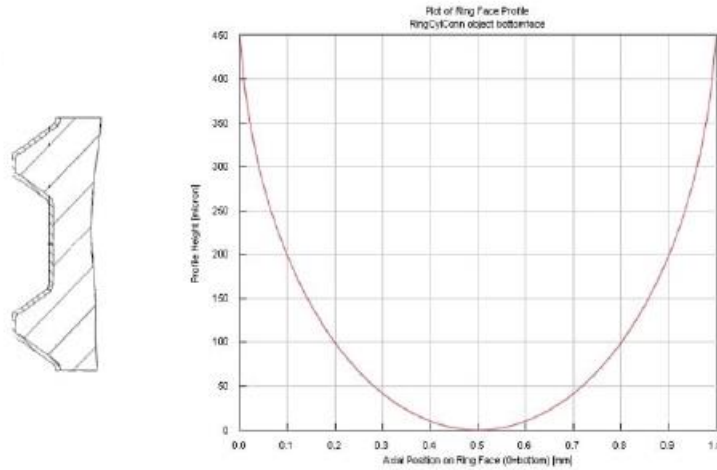


Figure 66. Section of the third piston ring. Technical drawing on the left and GT Power implementation on the right

For the third piston ring the profile on GT Power has been implemented, instead, through the dedicated tools in the program defining the thickness of the ring, the number of rails (two in that case, for this reason only one tip of the oil scraping ring is modeled) and the MOFT location, for which is possible to refer to Figure 67. To notice that also in that case with respect to the real profile the shape of the oil ring's tip is rounded in order to guarantee the convergence of the simulation.

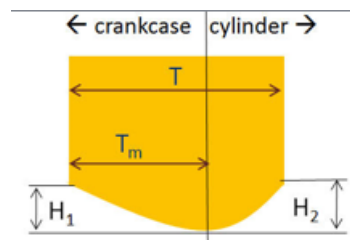


Figure 67. Quantities to define the ring geometry in GT Power

with:

$$MOFT = \frac{T_m}{T}$$

The profile of the rings is taken into account in the bricks called *topface*, *middleface* and *bottomface* of Figure 60 that model the contact between the liner and the rings and is fundamental for the oil film thickness calculation. Another important aspect is related to the temperatures of the rings and the liner. They are used by the program to calculate the viscosity

of the oil considering at each timestep a mean temperature between the one of the matching heights of the liner and the one of the piston rings asked by the program.

3.2 Liner

Regarding the temperatures of the liner, they were provided by virtual simulation from the calculation department of the team and are shown in Figure 68:

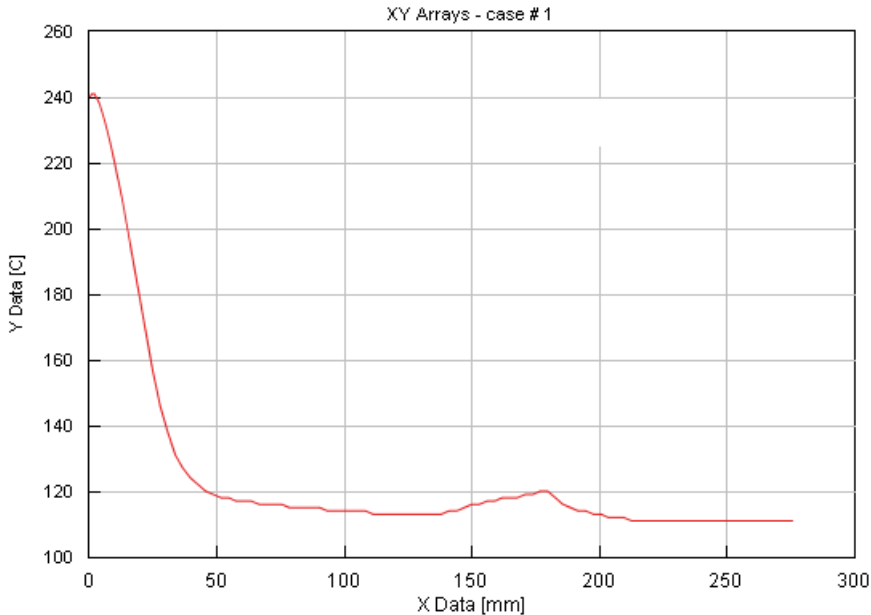


Figure 68. Liner temperature

On the y axis there is the temperature of the liner in °C, while in the x axis there is the liner height with $x = 0$ corresponding to the top of the cylinder. The total length of the liner is 276 mm. To notice that in real condition the temperature along the cylinder is not constant and vary with respect to the angle of the bore considered. Due to the fact that the range of temperature variation is in the order of maximum 15 °C for the same height along the cylinder bore and due to the fact that it is used only to calculate the oil viscosity, at each height is considered a mean value of temperature.

At this point, since the model in the program refers to a hot piston is necessary to implement also the liner distortion in hot condition to take into account a realistic operating condition. This step is also fundamental for the calculus of the ring’s conformability. The liner distortion data have been provided by the department of calculation also in this case and are the results of a FE

analysis. The distortions are representative of both the cold mechanical deformation of the liner due to the fastening of the cylinder head with the cylinder block and also of the thermal expansion due to the high temperature faced inside the cylinder. To provide a visual reference of the liner distortion is possible to refer to Figure 69, generated by GT Power:

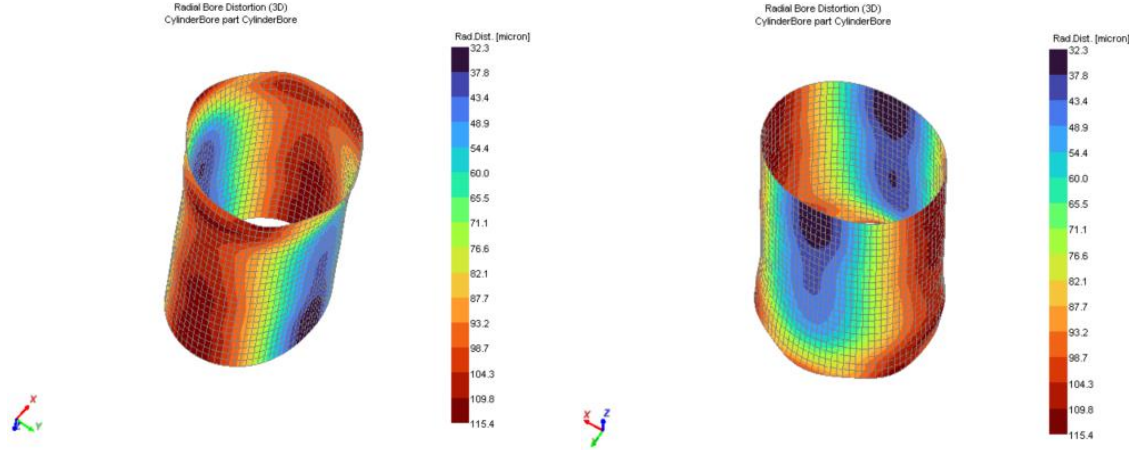


Figure 69. Hot bore distortion

Looking at the figures is possible to notice the lobe shape in the upper part that is closer to the cylinder head, while moving downward the deformed shape tends to become elliptical with the highest deformation (red parts) on the thrust and anti-thrust side of the piston. The implementation of the bore distortion is important also for friction prediction because first of all influence the oil film thickness between the piston rings, piston skirts and liner, and second, because the elastic force of the rings changed according to the operative diameters of them (a lower diameter means a higher deformation and then a higher elastic force).

3.3 Piston skirt

Another important part that influences the friction related to the PCU system is the piston skirt. For it both an axial deformation and an ovality can be defined in the program. The actual shape of the skirt is defined according to the GT Power convention showed in Figure 70.

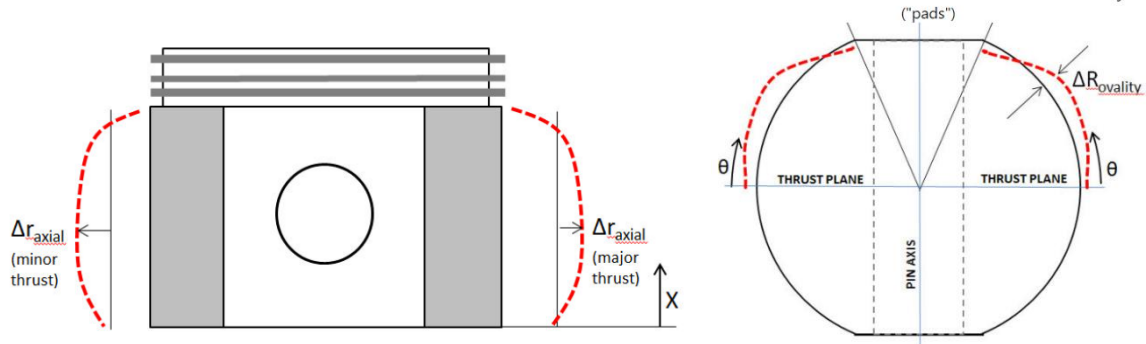


Figure 70. Convention for skirt axial profile and ovality on GT Power

For simplicity, only the axial skirt profile is considered in the model, and ovality has been neglected. From technical drawings, the real skirt axial profile in cold conditions is shown in Figure 71.

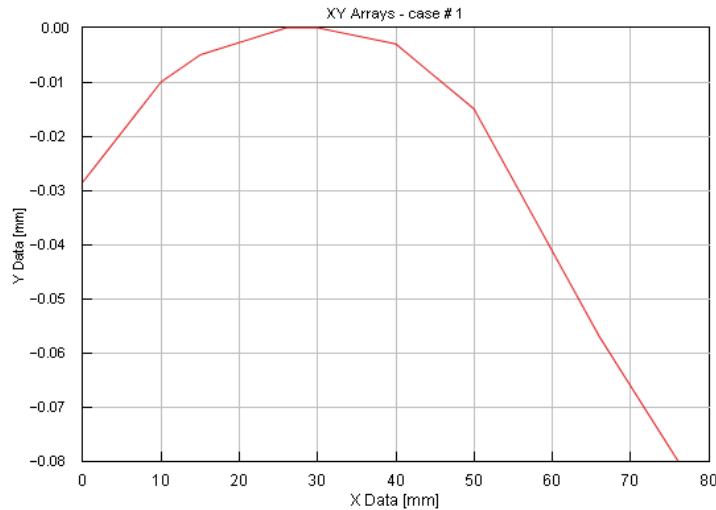


Figure 71. Ring axial profile in cold condition

The x axis refers to the skirt height with $x = 0$ the bottom part (the closest to the crankcase), while the y axis refers to the real skirt profile. GT Power calculates the oil film thickness along the piston skirt as follows:

$$h(z, \theta, t) = C_0 - \Delta R_{SP} + \Delta R_B + \Delta h_{\epsilon\phi}$$

where C_0 is the nominal radial clearance with respect to the liner that is referred to the diameter D_n referring to Figure 59 (that is the most external diameter), ΔR_{SP} is the skirt profile (the sign minus is because looking at the Figure 71 it is define with a negative value), ΔR_B is the local bore distortion implemented in the *CylinderBore* brick as explained in the 3.2 *Liner* and $\Delta h_{\epsilon\phi}$

is due to piston secondary motions calculated by GT Power. In order to be consistent with the hot working condition the real skirt axial profile has been modified with respect to the one shown in Figure 71 taking into account the deformation of the skirt calculated through the thermo-structural analysis explained in the 2.2.1 *Piston rings*. Moreover, on the skirt also a coating layer with a thickness of $15\ \mu\text{m}$ is applied so the real skirt axial profile in hot condition implemented in GT Power is shown in Figure 72:

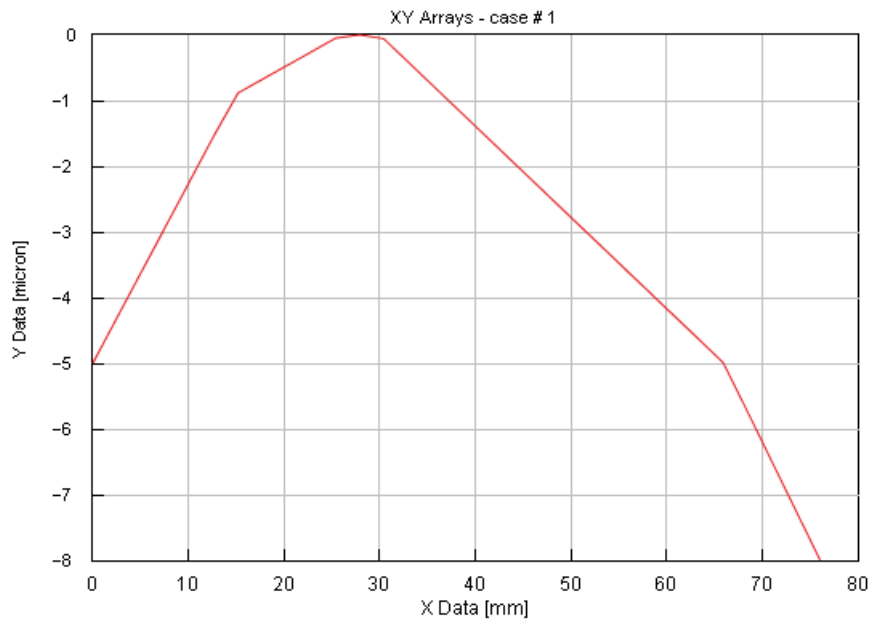


Figure 72. Ring axial profile in hot condition

From the graph is possible to notice that now the variation of the axial profile of the piston skirt in hot condition is in the order of $8\ \mu\text{m}$, while in cold condition it was around $80\ \mu\text{m}$ evidencing the influence of hot deformations of the piston.

3.3 Working points

The pressure and temperatures considered in the model are referred to a specific working point. In particular, during the homologation procedure the engine is tested in terms of CO_2 emissions through the VECTO lab cycle.

To evaluate the contribution in terms of CO_2 emission due to the engine friction of the PCU system of the XC13, but also the penalties between the different alternatives of the piston rings, on the VECTO test the operating points in Table 13 are considered.

VECTO point	Load [%]	Engine speed [rpm]
1	100	1414
2	100	1238
3	100	1078
4	85,7	1078
5	76,8	1078
6	68	1078
7	59,8	1078

Table 13. VECTO points

For each of these points, pressure and temperature data are available from bench tests for each cylinder. Since a single-cylinder model is considered in GT Power, a mean value between the 6 cylinders is taken into account for both temperature and pressure.

On the other hand, to get an idea of the pressures involved at each engine speed, it is possible to refer to the Wide-Open Throttle (WOT) condition (100% load) pressures, shown in Figure 73.

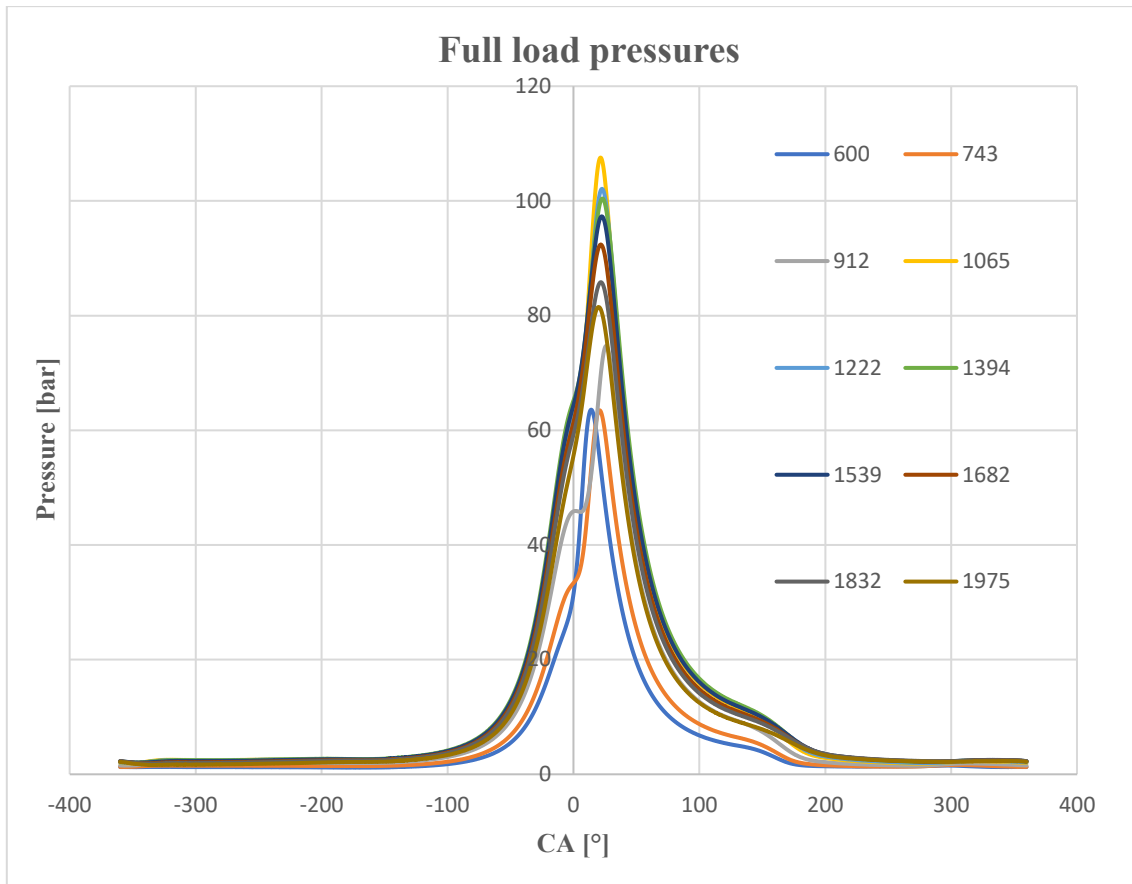


Figure 73. Pressures at full load

Looking at the picture above, the pressures at different engine speeds are plotted. From this, it is possible to understand the torque curve at full load, reaching the Maximum Braking Torque (MBT) at around 1065 rpm. It can also be evidenced looking at Figure 74 where the torque and power with respect to the engine speed is plotted.

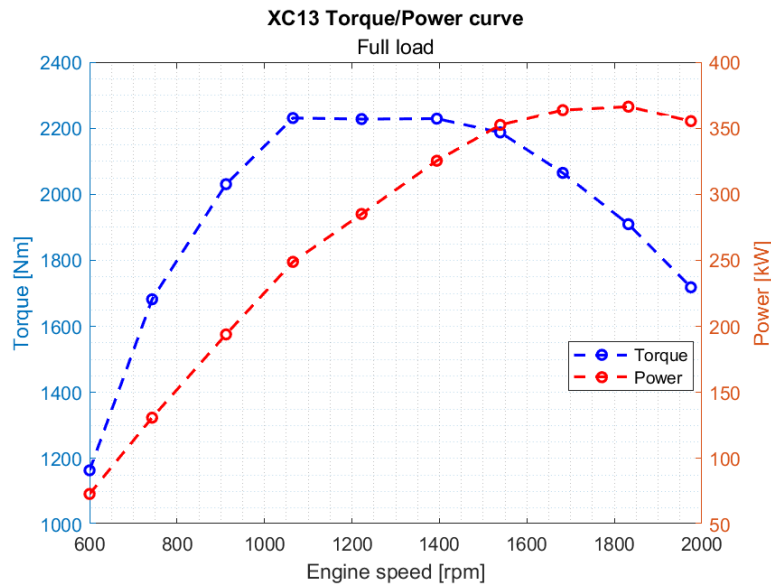


Figure 74. Torque and Power curve at full load

In the model, pressure is passed to the piston rings through gains. For the first ring, the pressure on top and behind is the same as in-cylinder pressure, while for the pressure below the first ring, above and behind the second ring, 10% of in-cylinder pressure is taken into account, as suggested by GT Power. Finally, for the pressure below the second ring and on the third ring, atmospheric pressure of 1 bar is assigned, representing the pressure in the crankcase.

3.4 Results

Once the model has been described, it is possible to analyze the results obtained and verify if the targets of the PCU system have been reached. Two types of evaluation have been considered:

1. Friction from all contributors present in the crank mechanism with the Alternative A of piston ring at full load and different engine speeds
2. PCU friction at maximum power
3. Comparison between Alternative A and Alternative B of piston rings in VECTO points

Through the results obtained is possible to verify the target listed in the Table 14.

Item	System Target
Fuel consumption	Mechanical friction < 0,75 kW @max power

Table 14. System targets to evaluate through GT Power results

3.4.1 XC13 Frictions

Before delving into the details of the XC13 targets, the engine's full load curve at different speeds was considered. While this type of analysis does not allow for the verification of any targets, it does provide insight into the main contributors to engine friction in the crank mechanism. For example, as shown in Table 5 in *1.5 XC13 PCU study case*, where the target deployment was defined, one of the targets is a 10.5% reduction in fuel consumption. Given what was discussed in previous chapters about the impact of friction on fuel consumption, this could be an interesting data point to consider.

To create a trend of overall friction, the pressures at full load at different engine speeds, as shown in Figure 73, were considered. The contribution of several parts of the crank mechanism in terms of friction was taken into account and is shown in Figure 75.

The mean friction power over the cycle due to different contributions is listed in Table 15.

Speed [rpm]	Main bearings [kW]	Conrod Big End [kW]	Conrod Small End [kW]	Piston Rings [kW]	Piston skirt [kW]
600	0,05	0,03	0,09	0,21	0,01
743	0,08	0,04	0,07	0,28	0,02
912	0,12	0,07	0,11	0,36	0,03
1065	0,17	0,09	0,18	0,44	0,04
1222	0,22	0,12	0,18	0,5	0,05
1394	0,30	0,15	0,18	0,57	0,06
1539	0,37	0,19	0,16	0,62	0,08
1682	0,43	0,22	0,12	0,66	0,09
1832	0,52	0,26	0,09	0,70	0,10
1975	0,60	0,30	0,05	0,74	0,11

Table 15. Engine frictions

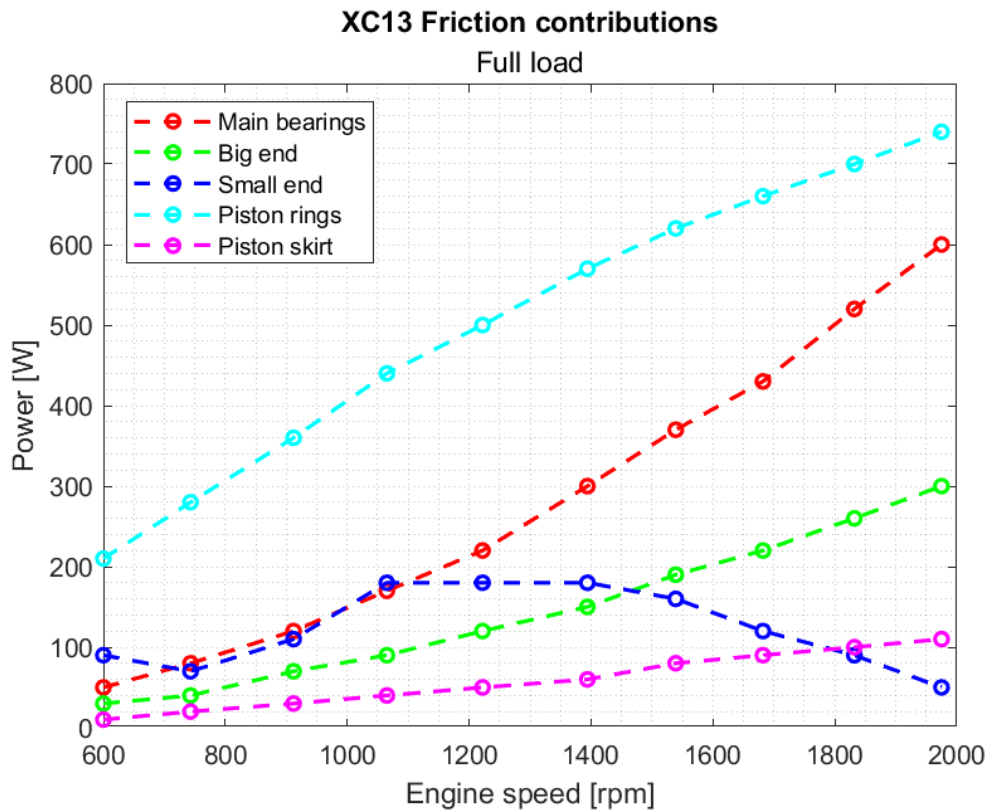


Figure 75. Friction of the crank mechanism

Looking at the Figure 75 is possible to make some considerations:

1. The highest contribution is due to the piston rings, highlighting the importance on acting on that part.
2. Every contribution tends to grow with the increase of the engine speed apart from the small end. This behavior can be justified because increasing the engine speed due to the higher pressures in the combustion chamber, also the forces acting in lateral and axial direction (referring to cylinder axis) on the small eye increase and then the characteristic pressure p_s increases. Referring to the Stribeck curve in Figure 47 the friction coefficient is inversely proportional to the pressure and then the friction power decreases with a higher velocity with respect to the increment of the engine speed.

Moreover, in addition to the absolute value of friction power is interesting to understand the weight in % with respect with the total power of the engine expressed in the matching working point expressed as:

$$P_b = T * \omega$$

Where P_b is the brake power, T is the torque expressed in Nm measured through test bench and ω is the engine speed expressed in rad/s . The values of powers are listed in Table 16. To notice that the friction power is the sum of all the contributors considered in Table 15 multiplied six times in order to take into account the contribution of all the cylinders.

Speed [rpm]	Torque [Nm]	Brake power [kW]	Friction Power [kW]	Weight of friction power [%]
600	1164,9	73,2	2,34	3,20
743	1682,3	130,9	2,94	2,25
912	2030,5	193,9	4,14	2,13
1065	2230,9	248,8	5,52	2,22
1222	2227,7	285,1	6,42	2,25
1394	2229	325,4	7,56	2,32
1539	2187,3	352,5	8,52	2,42
1682	2064,7	363,7	9,12	2,51
1832	1909,4	366,3	10,02	2,74
1975	1718,3	355,4	10,80	3,04

Table 16. Brake power and total friction power at full load at different engine speeds

As it is possible to see from Table 16 the weight of the friction with respect to the brake power is always less than 3,5 %, so in percentage it doesn't represent a too huge impact considering also that the full load characteristic has been considered, which is the worst case.

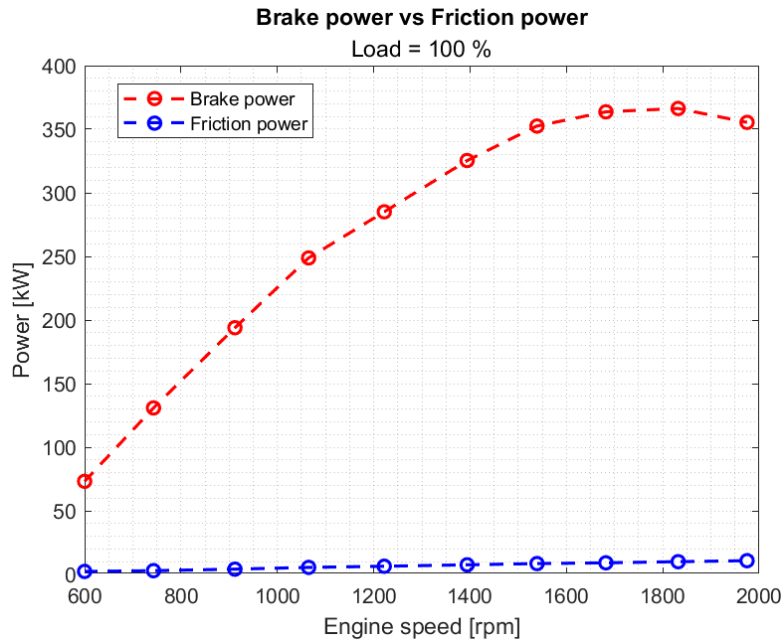


Figure 76. Brake power with respect to total friction power

3.4.2 PCU friction at maximum power

At that point to verify the target of the max friction loss of 0,7 kW per cylinder of the PCU system at max power, then at 1900 rpm in full load, a dedicated simulation on GT Power with the matching pressures in the combustion chamber is launched. The part that contributes to the PCU frictions are piston rings, piston skirt and small end bush. The results are resumed in Table 17 and plotted in .

PCU part	Friction Power [kW]
1 st Ring	0,174
2 nd Ring	0,092
3 rd Ring	0,266
Skirt	0,105
Small end	0,055

Table 17. PCU frictions

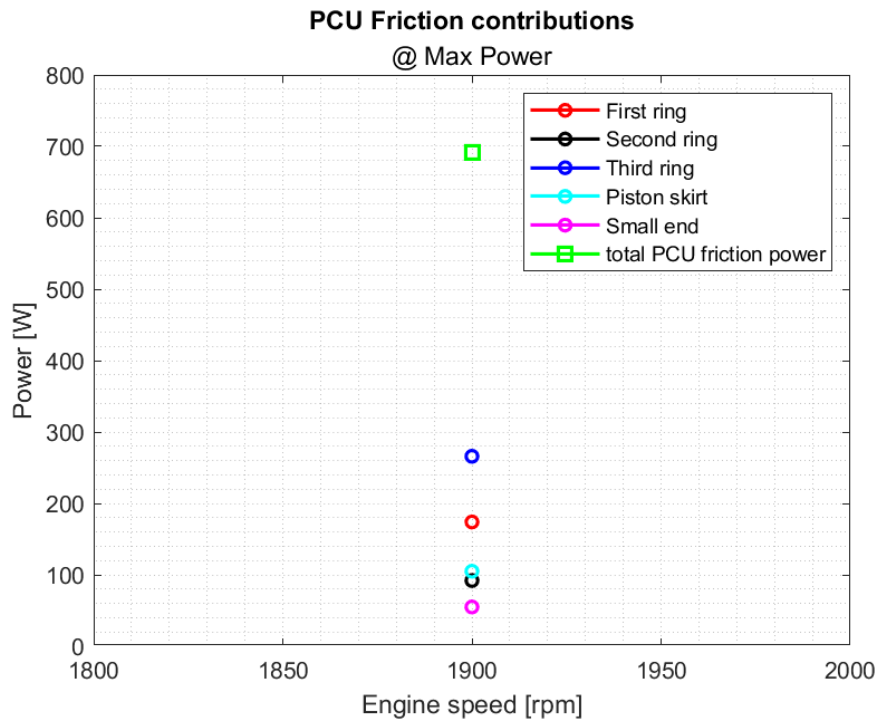


Figure 77. PCU friction

As can be seen from both the table and figure above, the target of a maximum of 0,7 kW is reached, even if it is very close to that value. On the other hand, from the results obtained at different engine speeds at full load, it is possible to understand where it is possible to act in terms of friction reduction in case more margin is necessary. To better understand what is happening, it is also possible to make other types of considerations in the program and understand what influences friction power.

As a first step, it is possible to focus on the piston rings. The program calculates friction power by integrating the instantaneous power loss over the cycle, as shown in Figure 78, Figure 79, and Figure 80 for all three rings with the matching minimum oil film thickness.

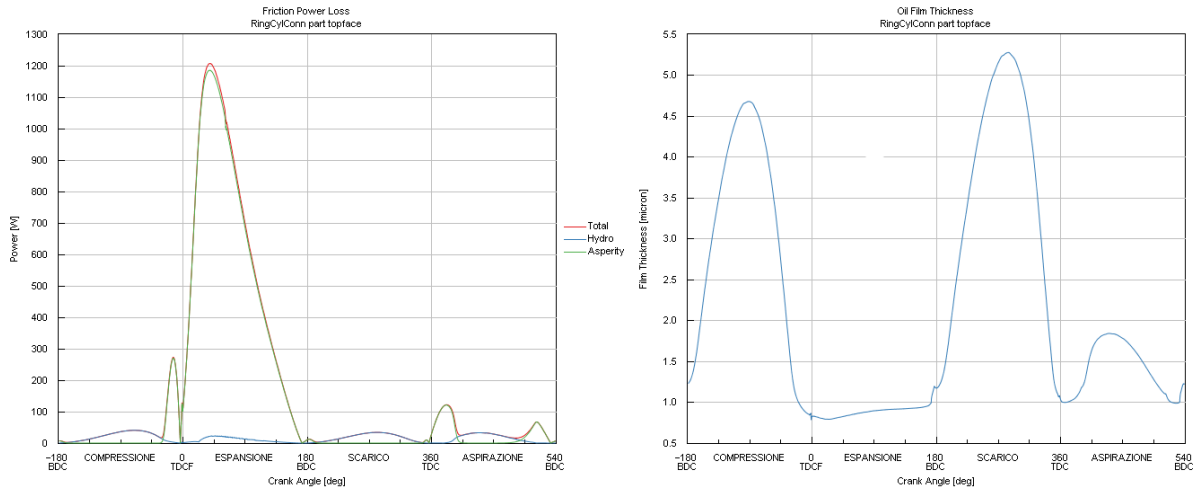


Figure 78. 1st ring friction power loss (left) and oil film thickness (right)

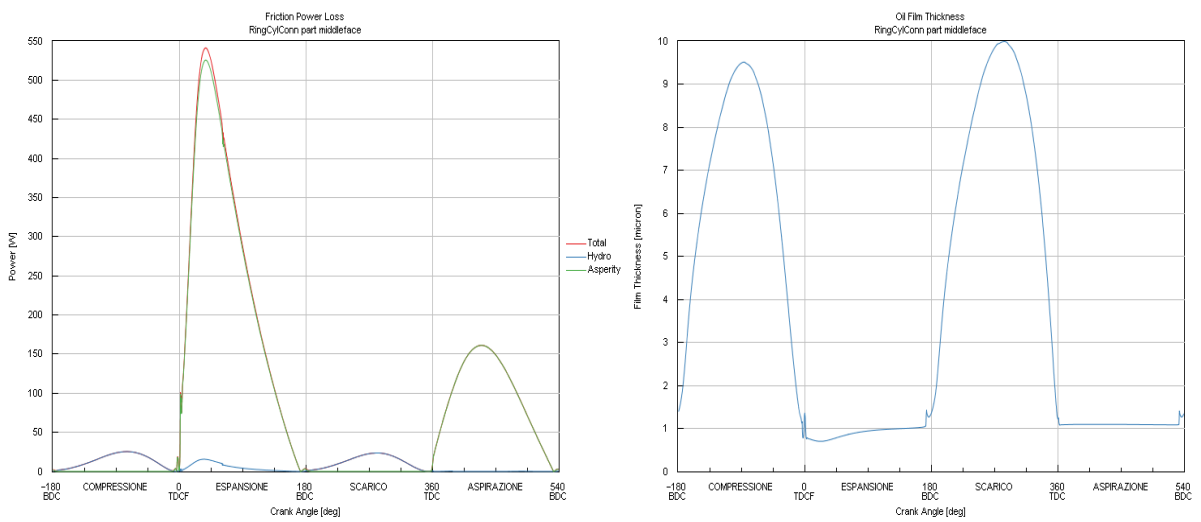


Figure 79. 2nd ring friction power loss (left) and oil film thickness (right)

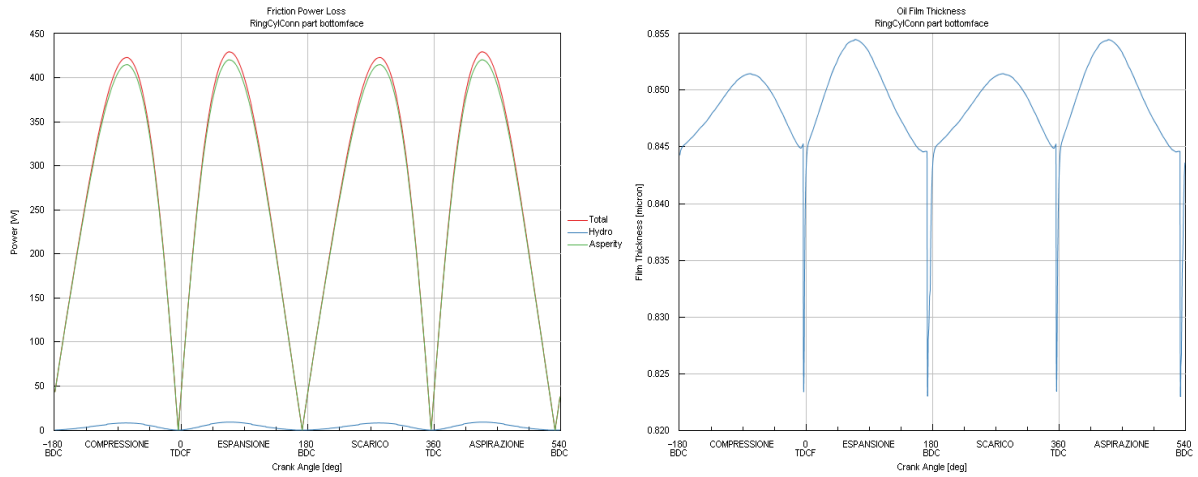


Figure 80. 3rd ring friction power loss (left) and oil film thickness (right)

As can be seen from the figures above, the total power is the sum of two contributions: Asperity and Hydrodynamic power. The first type is experienced when asperity contact between rings and liner is generated. As can be seen in both the first and second rings, this condition occurs around top and bottom dead center and is consistent with the fact that piston speed is either null or very small (in the case of proximity), as also shown in Figure 81.

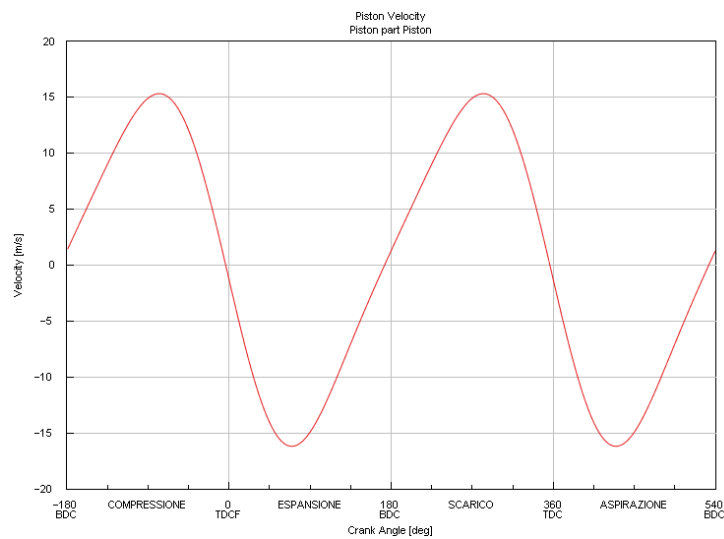


Figure 81. Piston velocity

At that point, it is possible to notice a significant growth of asperity power, which is sensibly higher than the hydrodynamic contribution. This is due to the fact that, in asperity condition, friction is governed by the friction coefficient between the liner and rings, which are both made of cast iron, while in hydrodynamic condition, friction is governed by oil viscosity. Moreover, asperity contact is also evidenced by the oil film thickness, which is lower than 1 μm when

there is asperity contact. Another important observation from both Figure 78 and Figure 79 is that the minimum oil film thickness becomes very small during the expansion stroke due to the peak of in-cylinder pressure, which tends to push the piston towards the liner with the highest values of lateral force, as also shown in Figure 82.

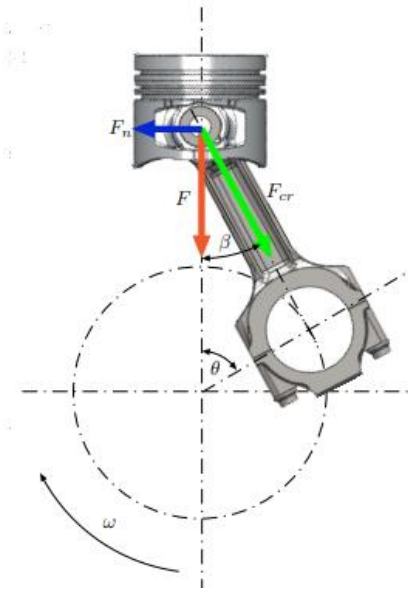
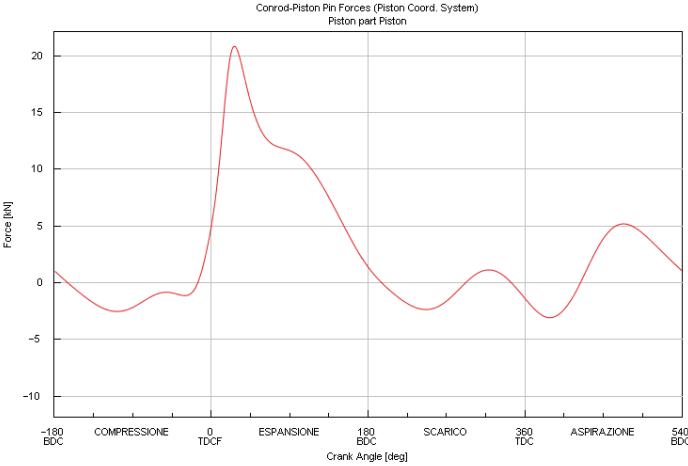


Figure 82. Lateral force trend

Instead, looking at the behavior of the third ring in Figure 80, the minimum oil film thickness remains always in a value around $0,8 \mu m$. Due to this the third ring is always in asperity condition and it is consistent with its scraping function. Also for this reason, to minimize the wear of the ring only a small tip is in contact with the liner. The fact that the third ring is always in asperity contact explain the higher value of friction power loss with respect to first and second ring.

Similar considerations can be done referring to the piston skirt. Is possible to refer to Figure 83.

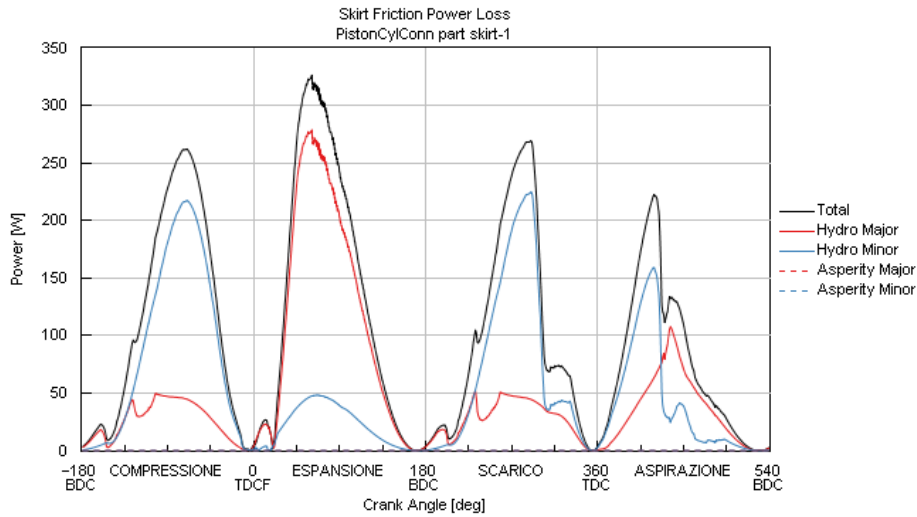


Figure 83. Skirt friction power loss

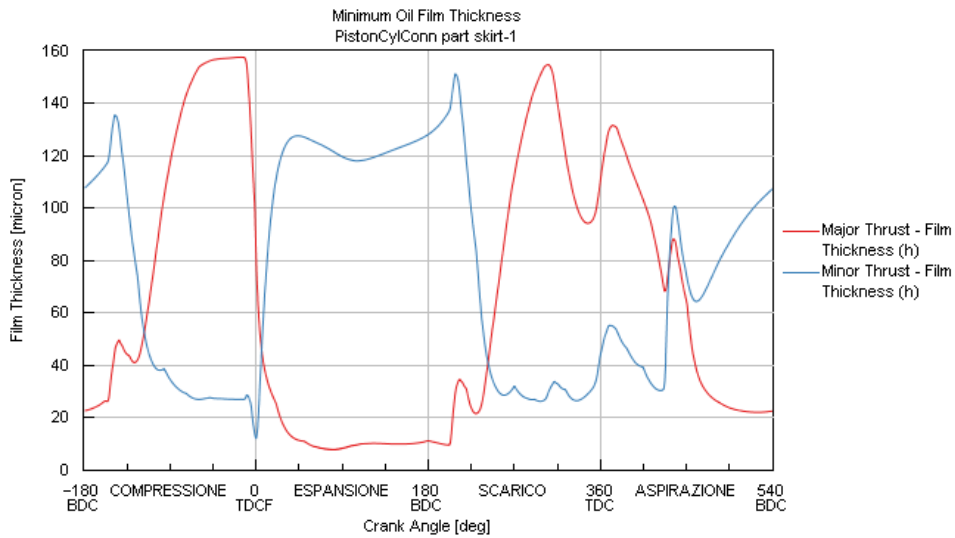


Figure 84. Minimum skirt oil film thickness

From the figures above it is possible to notice that the power loss is due to hydrodynamic condition and the asperity power is always null in both the thrust and antithrust side. This is consistent also with the minimum oil thickness where the minimum value is around $12 \mu m$ for minor and $8 \mu m$ for major thrust side. The power loss, as expected, is higher in the major with respect to the minor side due to the trend of the lateral force (the major thrust side is for definition the side where acts the first peak of the lateral force, which is the highest). Furthermore, looking at Figure 83 it is possible to evidence that the power loss trend follows

the one of the lateral piston force shown in Figure 82. Moreover, considering the axial profile of the skirt, the minimum oil film thickness is referred to the most external part of the skirt.

Finally, analyzing what happen for the last contributor on the PCU friction, is possible to say that in the small eye of the connecting rod an oil layer tends to form between the wristpin and the bush in the small eye. From Figure 85 and Figure 86 is possible to see respectively the trend of the minimum oil film thickness and the maximum oil pressure that occurs in the minimum height.

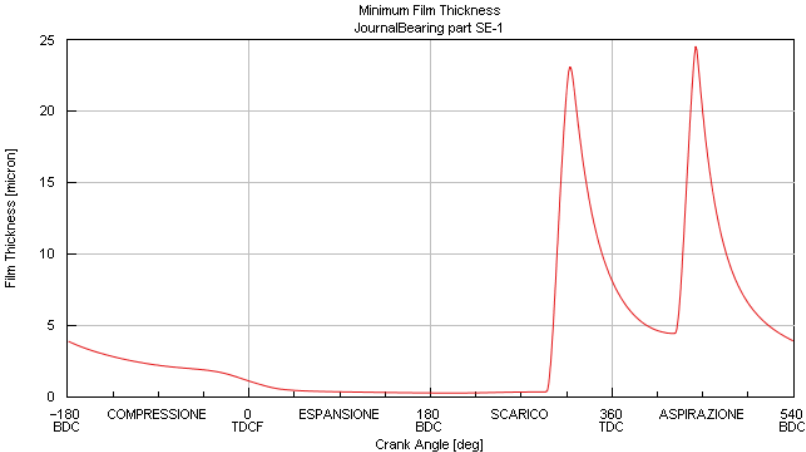


Figure 85. Minimum oil film thickness

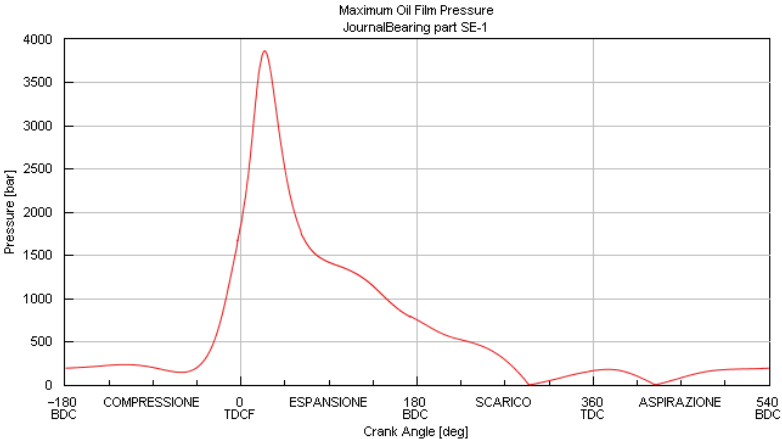


Figure 86. Maximum oil film pressure

As it is possible to notice there is a correlation between the minimum oil film thickness and the maximum oil film pressure. In fact, the two peaks of the oil film thickness close to the TDC at 360 °CA correspond to two anti-peaks of the maximum pressure at the same crank angles. The

reason of this trend can be justified looking at the forces acting on the small eye. Is possible to identify the total force applied divided into two components along x and y direction respectively referring to axial and lateral force. The trend of these two forces is shown in Figure 87.

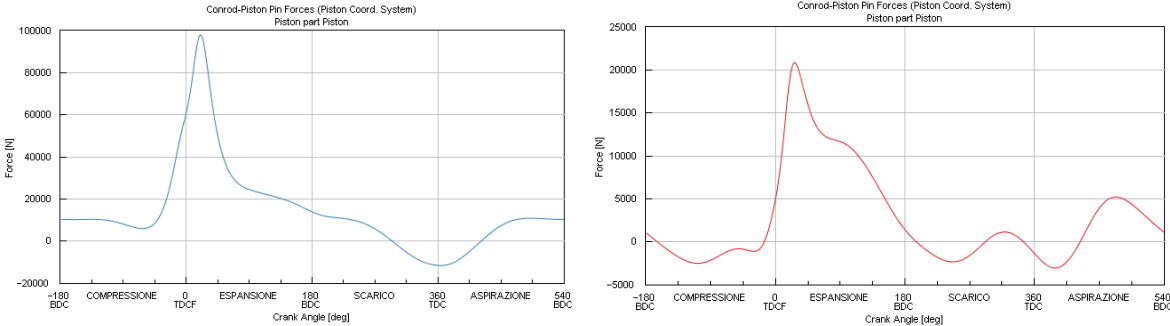


Figure 87. Axial (left) and Lateral (right) force acting on the small eye

As it is possible to notice in the lateral force there are the two anti-peaks that are then present in the total force that generates the effect described above. Moreover, still looking at the minimum oil film thickness, is possible to notice that in the expansion and exhaust stroke it is around $0,3 \mu m$, generating then asperity contact. All these effects are consistent with the total power loss trend in Figure 88.

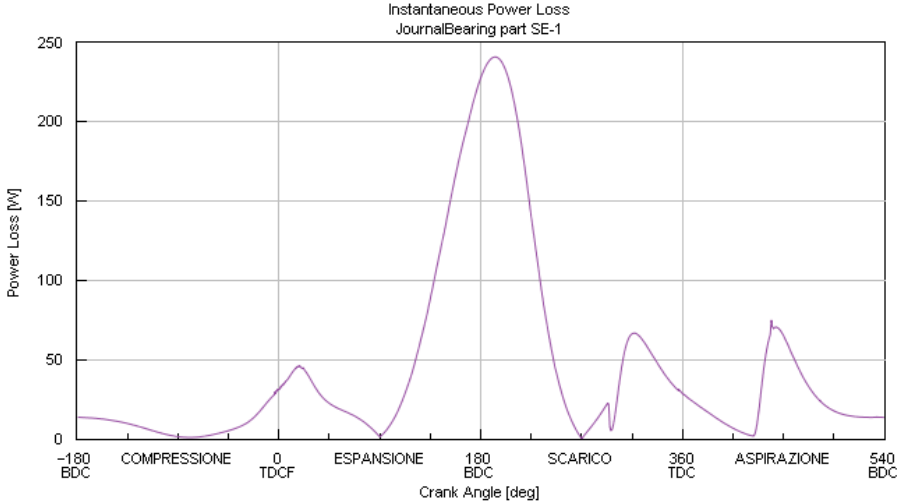


Figure 88. Total power loss in the small eye

From the figure above is possible to see the two peaks close to 360° CA due to the lateral force peaks, a peak close to 0° CA due to the peak of pressure and finally the biggest peak is due to asperity contact.

3.4.3 Comparison between Alternative A and Alternative B of piston rings

Once a general overview of the friction contribution on the single crank has been analyzed, the second task of the thesis is to investigate the loss in terms of CO₂ on the VECTO test of the two alternatives of piston rings presented by the supplier as already discussed in the *1.5 XC13 PCU study case*. Since the third ring is the same for both alternatives, is possible to take into account the sum of friction power of the first and second ring on the different VECTO point already listed in Table 13. The results are listed in Table 18.

Alternative	Ring	1	2	3	4	5	6	7
A [W]	First ring	230,3	184,7	163,9	156,2	146,5	136,8	127,4
	Second ring	15	14,3	12,3	12,1	12,1	12	11,8
B [W]	First ring	283,6	234,2	206,2	198,2	188,5	178,5	168,2
	Second ring	19,9	19,8	19,1	18,8	18,5	18,2	17,9
	Difference [W]	58,2	55	49,1	48,7	48,4	47,9	46,9

Table 18. Friction power of first and second ring for the two alternatives of piston rings

From the results collected in the table above is evidenced as expected that the Alternative B of the piston rings has a higher impact on the PCU friction and then in CO₂ emission. To have also a visual representation is possible to refer to Figure 89 and Figure 90.

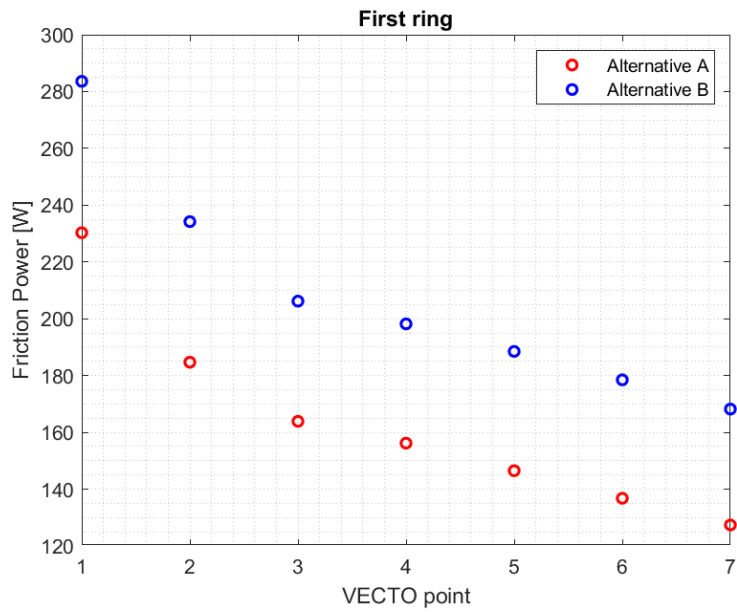


Figure 89. Friction contribution of the first ring on the VECTO points

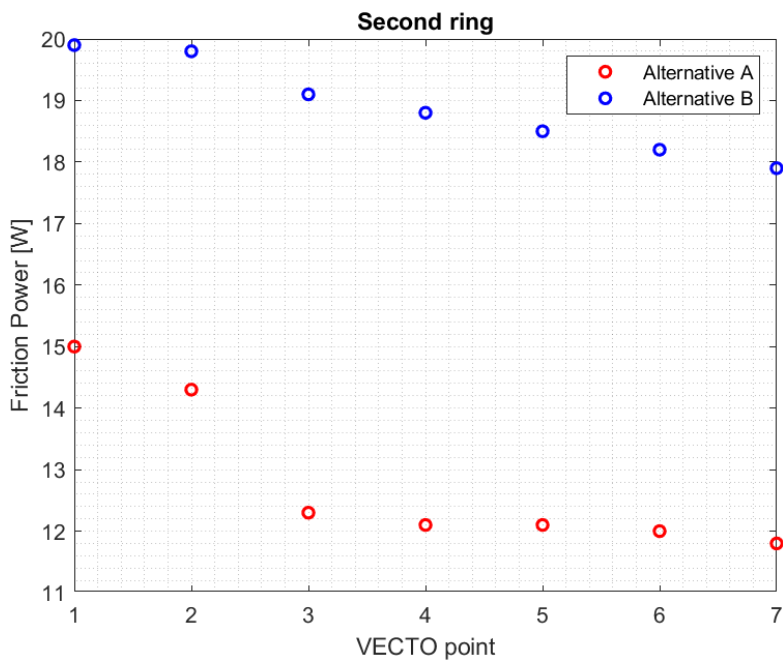


Figure 90. Friction contribution of the second ring on the VECTO points

As it is possible to see the difference between the two piston rings alternatives on the first ring is of the order of 50 W, while on the second ring around 5 W. This evidenced the importance in terms of friction reduction of the first ring.

At that point, is possible to convert the delta friction power in terms of CO₂ referring to Table 19.

VECTO point	VECTO weight	Fuel consumption [kg/h]	CO ₂ coefficient	Power increase [W]	Penalties	Weighted penalties
1	1,7 %	61,8	0,1786	349	0,10 %	0,0017%
2	8,0 %	61,8	0,1786	330	0,10 %	0,0075%
3	11,0 %	46,3	0,177	295	0,11 %	0,0100%
4	4,1 %	27,6	0,177	292	0,19 %	0,0077%
5	3,4%	23,4	0,177	290	0,22 %	0,0074%
6	3,9 %	19,1	0,177	287	0,27 %	0,0104%
7	3,1 %	15	0,177	281	0,33 %	0,0103%

Table 19. CO₂ penalties on VECTO points

The table above was already built internally in FPT and it takes into account the weight of the matching VECTO point according to the time at which the engine works at that operating condition, the fuel consumption calculated from values coming from test bench and a CO₂ coefficient that depends on the operating point. The power increase is the difference of total friction power of the two alternatives of the rings. To calculate the fuel consumption at each working point from test bench is known the $bsfc$ [$\frac{g}{kWh}$], the torque and the speed. In this way is possible to calculate the brake power and then the fuel consumption as follow:

$$\dot{m}_f = bsfc \cdot P_b$$

Considering all the penalties at each point of the VECTO listed in Table 19 is possible to define finally the weighted penalties calculated as:

$$Weighted\ penalty = VECTO\ weight \cdot Penalty$$

The sum of all the weighted penalties at each point gives the total penalty in CO₂ emission of the Alternative B with respect to Alternative A and it is equal to 0,16 %.

5. Blow-by phenomenon

Before to enter into the details of the GT Power model used to predict the blow-by of the XC13 engine and verified the matching targets is necessary to define in what consists the blow-by.

One of the primary functions of the piston and the piston rings is to seal off the pressurized combustion chamber from the crankcase. During the motion of sequence, combustion gases can escape between piston, cylinder, and piston rings and enter the crankcase (blow-by). In addition to the resulting energy loss, escaping leakage gas also poses a risk to the piston and piston ring lubrication due to contamination and displacement of the lubricating film, and due to oil carbonization as a result of excessive temperatures at the locations in contact with the combustion gases.

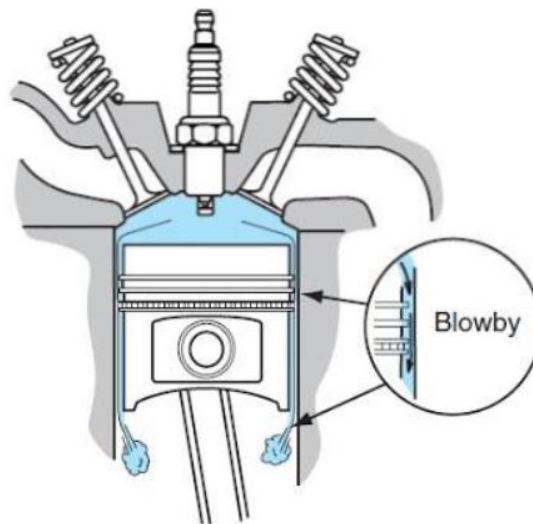


Figure 91. Blow-by mechanism

A dedicated system to manage the blow-by gases in the crankcase is used to bring back the gases at the intake. Increased blow-by values also require greater crankcase ventilation.

Sealing against gas penetration is mainly accomplished by the first piston ring, which is a compression ring. Usually for naturally aspirated engines, the quantity of blow-by is a maximum of 1 %, for turbocharged engine a maximum of 1,5 % of the theoretical air intake volume.

6. GT Power model for blow-by prediction

Starting from the model created for friction prediction to evaluate the blow-by in the single crank the blow-by compound has been added to the model for the first and second ring as shown in Figure 92.

In order to model properly this part, the subassembly *RingPack* has been created as shown in Figure 93. The idea is that the pressure in the cylinder, directly measured thanks to test bench is passed to the *TopRingBlowby* compound that calculates instantaneously the volume and pressure above, behind and below the first piston ring. For each timestep the pressure is passed to the *TopRing* brick that calculate the matching instantaneous end gap, effective bore radius, radial gap (between ring and liner) and friction force that then pass back to the blowby compound. So, a continuously updated loop is created and the friction force and blowby is calculated. This is implemented also for the second ring, while for the third ring is possible to assume the pressure close to the one on the crankcase (1 bar), so the *CrankCase* brick with the fixed temperature and pressure of the crankcase is created and is linked with the volume below the second ring through an *Orifice* brick. Furthermore, the movement is imposed thanks to the connection between the piston and the rings. Finally, also the geometry of the ring section (taken from technical drawings) and the cylinder bore distortion (taken from virtual simulation results) is implemented in order to model properly the contact between the piston rings and the liner.

**FROM CYLINDER
(FLOW)**

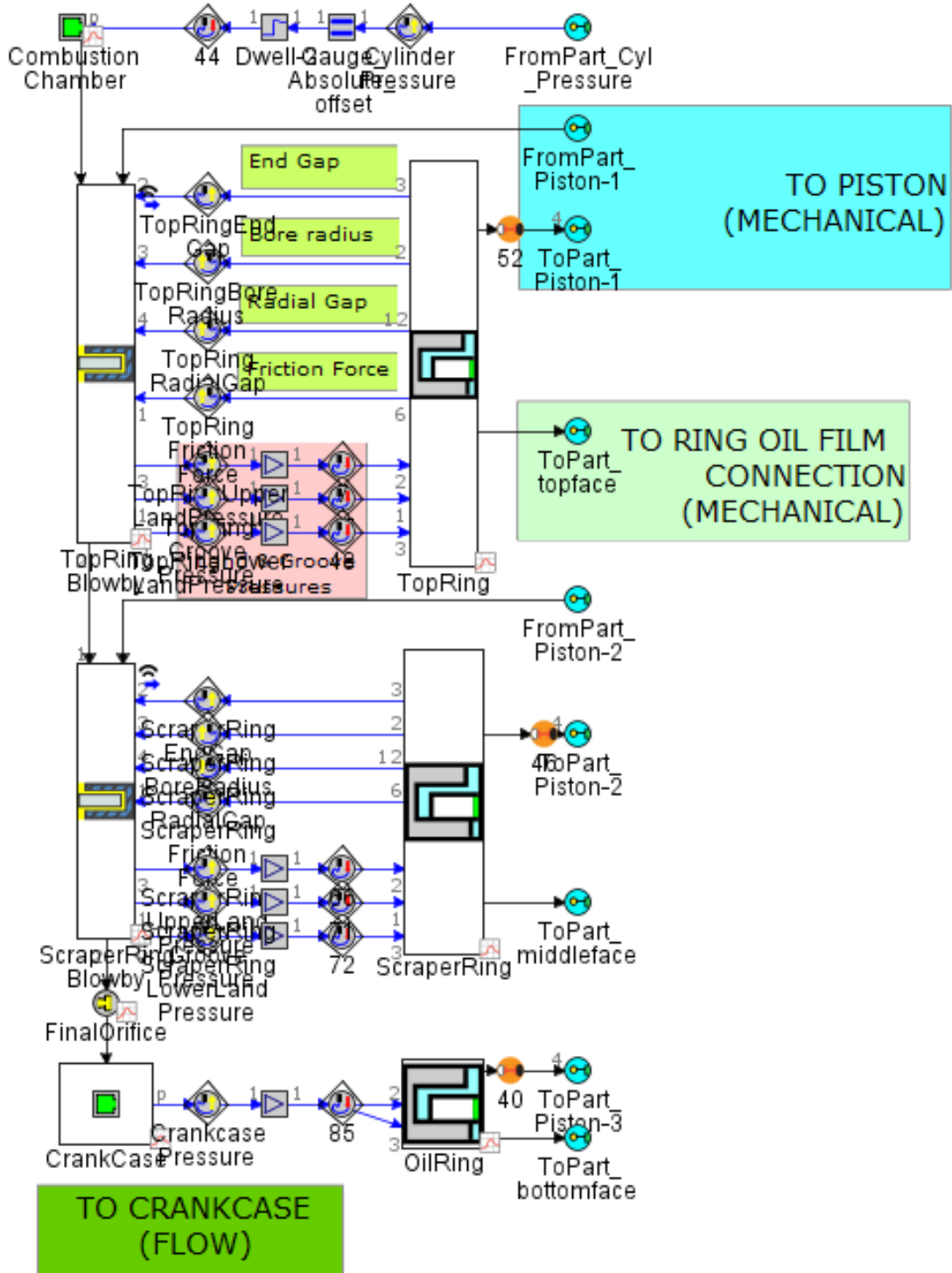


Figure 93. Ring pack subassembly

5.1 Results

With this model is possible to manage in a more precise way the behavior of the rings and then calculate the blow-by. The list of the targets investigated through this model is listed in Table 20.

Item	System Target	Enabler
Durability	Closed gap hot at BDC > 0,05 mm	Closed gap: 0,35 – 0,40 mm
Interval service	Blow-by < 150 l/min at full load	Piston ring section, tangential load, treatment, material and gap Clearance piston / piston ring

Table 20. Targets investigated through the blowby model in GT Power

In the model on GT Power is fundamental to define in a proper way the volumes around the rings because they have a key role for the blow-by. In Figure 94 it is possible to see how they are defined in the program.

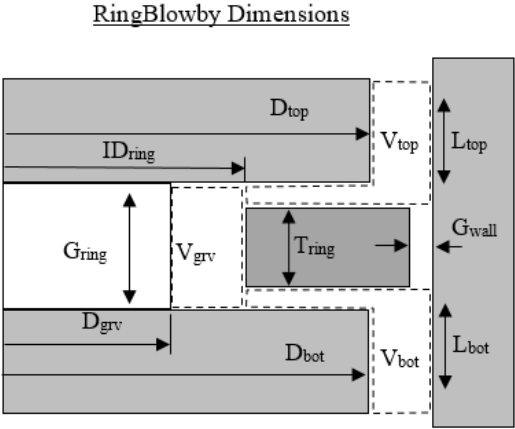


Figure 94. GT Power reference for volumes around piston rings

During the simulation these volumes are continuously updated starting from an initial value defined using the diameters of the piston expanded due to heat calculated by means of the simulation on Hypermesh explained in the previous paragraph. The formulas used to calculate the initial volumes are:

$$V_{top} = \frac{\pi}{4} \cdot (D_{bore}^2 - D_{top}^2) \cdot L_{top} + \frac{\pi}{4} \cdot (D_{top}^2 - ID_{ring}^2) \cdot \frac{G_{ring} - T_{ring}}{2}$$

$$V_{grv} = \frac{\pi}{4} \cdot (ID_{ring}^2 - D_{grv}^2) \cdot G_{ring}$$

$$V_{bot} = \frac{\pi}{4} \cdot (D_{bore}^2 - D_{bot}^2) \cdot L_{top} + \frac{\pi}{4} \cdot (D_{bot}^2 - ID_{ring}^2) \cdot \frac{G_{ring} - T_{ring}}{2}$$

Moreover, is important to take into account also the volume between the first and second ring evidenced in Figure 95 because it plays an important role for the blow-by.

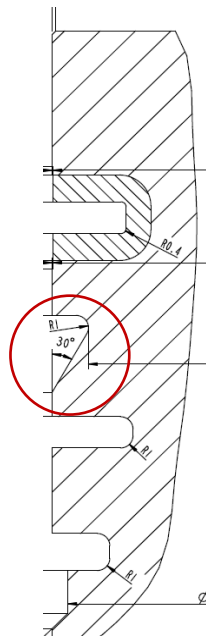


Figure 95. Volume between first and second ring

That volume is calculated thanks to the CAD program Creo and its value is 4483 mm³, which is divided between bottom volume of the first ring and top volume of the second ring such that they become:

$$V_{bot,first\ ring} = V_{bot} + 2241,5$$

$$V_{top,second\ ring} = V_{top} + 2241,5$$

According to the program the movement of the rings inside the piston grooves it is evidenced in Figure 96 and Figure 97

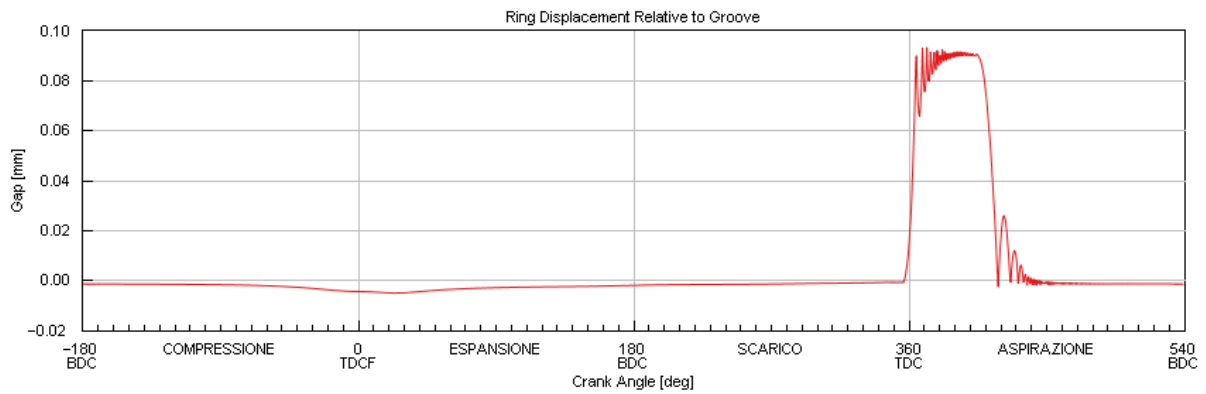


Figure 96. First ring displacement relative to groove

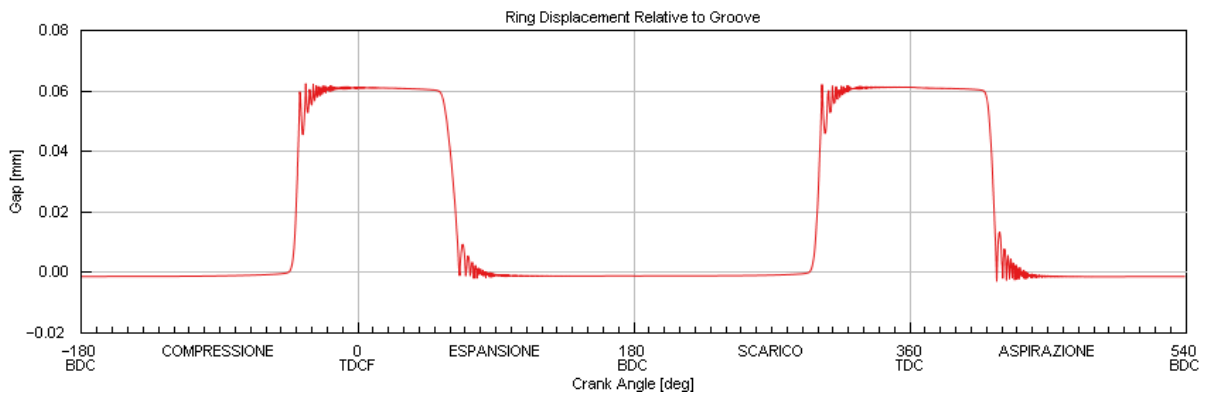


Figure 97. Second ring displacement relative to groove

As it is possible to see the first ring remains attached to the lower part of the groove for the initial part due to the high pressure on the top that push the ring downward. Then on the second revolution of the cycle when the pressure is low thanks to the inertia of the ring it tends to move upward with respect to the groove. A sensitivity has been taken into account varying the mass of the ring. The results show that for low values of ring mass the passage remains close evidencing the importance of this parameter for blow-by. On the other hand, the second ring opens twice, and it is due to the fact that the pressure in the second land is lower, so the inertia of the ring is sufficient to let it opening during also the first revolution of the cycle when the peak of pressure occur. This behavior of the rings is fundamental because in practice it means that a passage where blow-by gases can escape is created. Consequently, also the volume around the rings changes accordingly as shown in Figure 98 and Figure 99

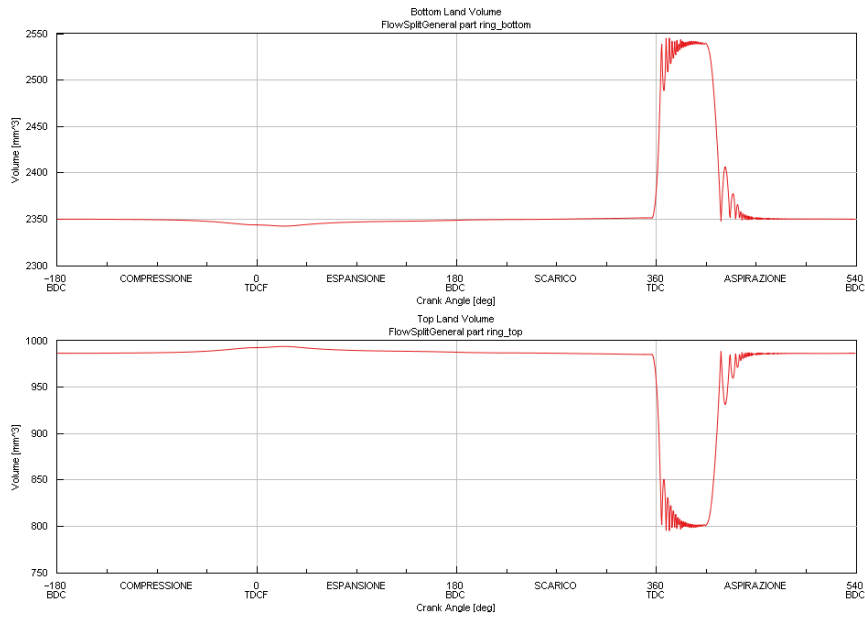


Figure 98. Bottom and Top volume of the first ring

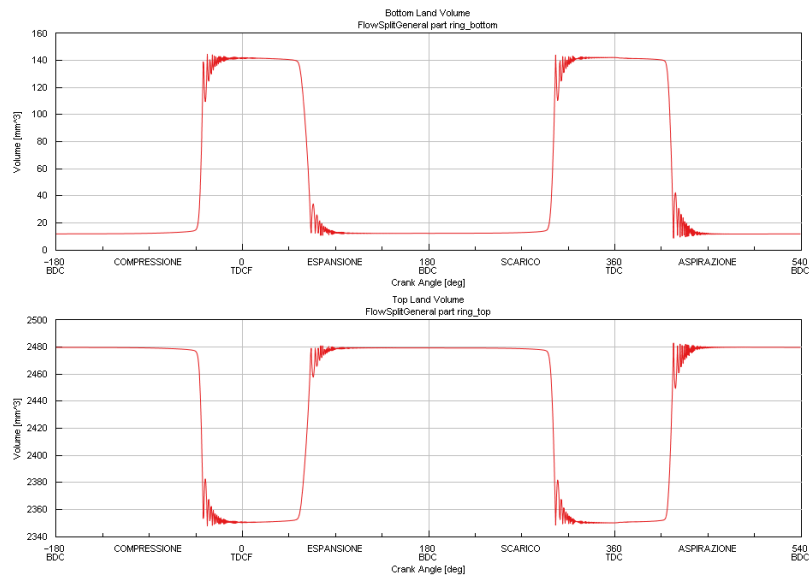


Figure 99. Bottom and Top volume of the second ring

Another interesting aspect to take into account is that looking at the volume behind both first and second ring, shown in Figure 100, is evidenced that it doesn't change, meaning that the model doesn't take into account the radial movement of the rings.

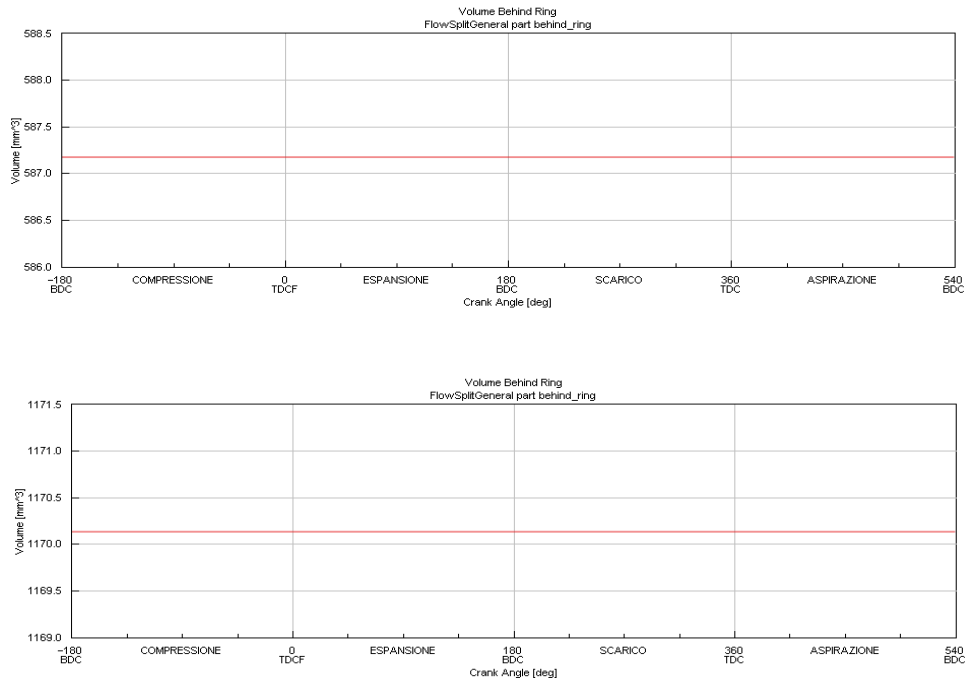


Figure 100. Volume behind first (Top) and second ring (Bottom)

Then also referring to the pressures in Figure 101 and Figure 102 is possible to evidence some relations with the ring's movement.

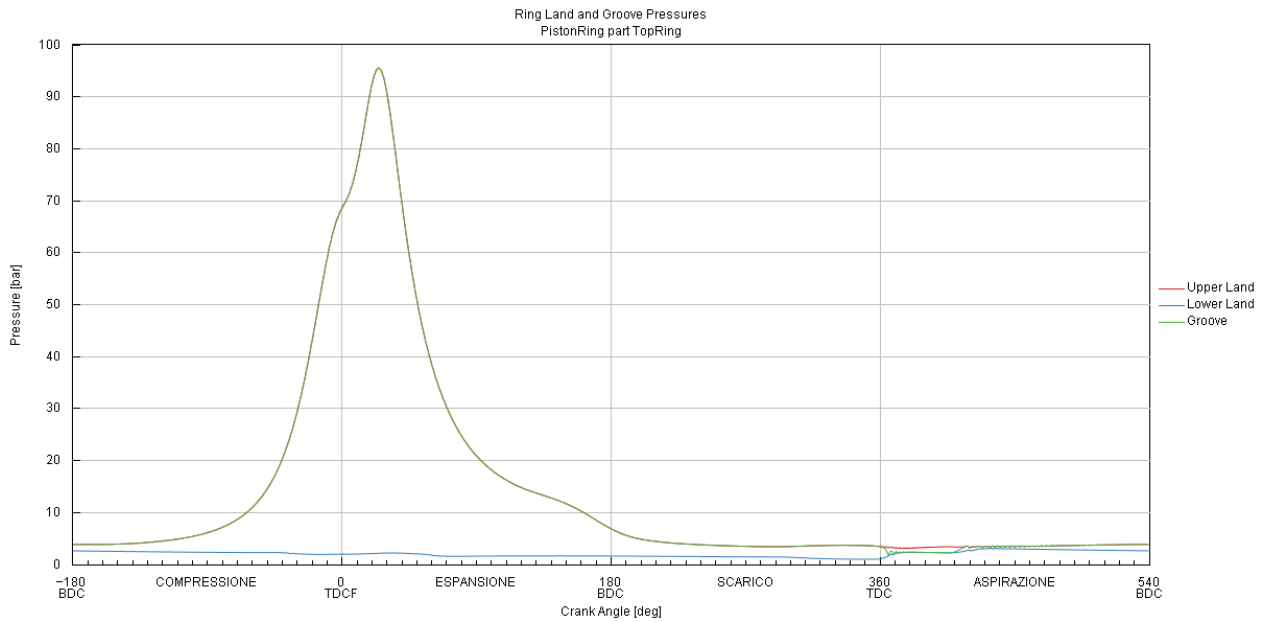


Figure 101. Pressures on first ring's lands

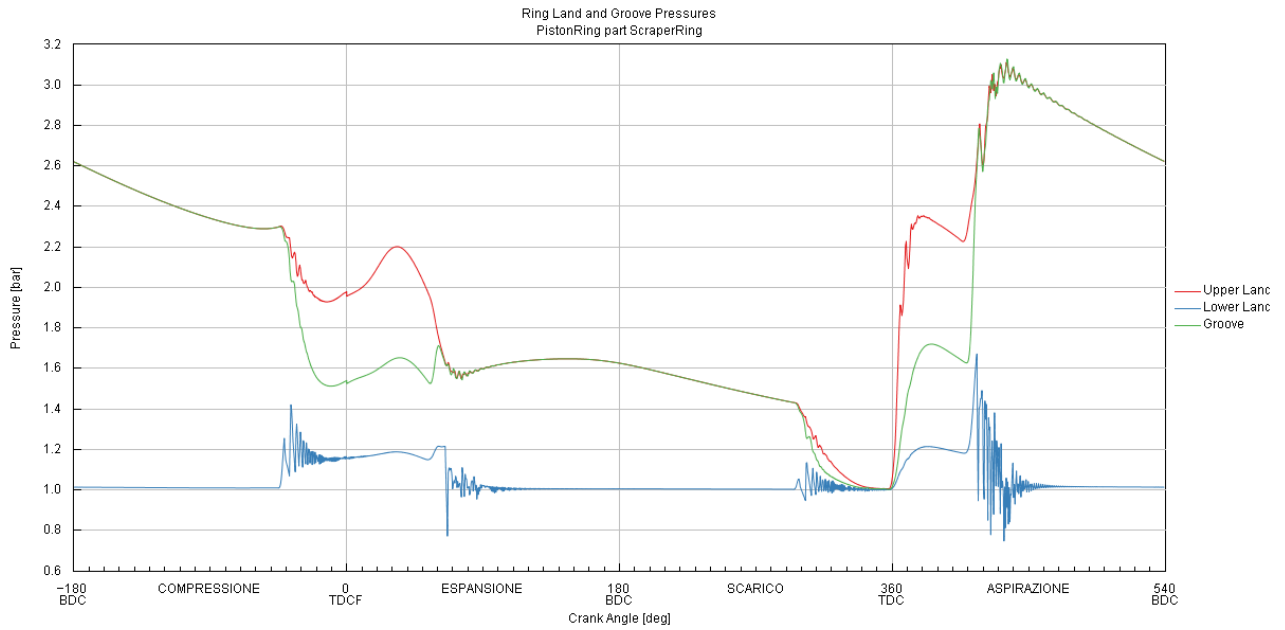


Figure 102. Pressures on second ring's lands

For the first ring the pressure above and behind the ring is the same of the pressure in the combustion chamber, until in proximity of the opening of the first ring around 360 °CA it drops becoming equal to the pressure in the bottom land until the ring closes again. On the other hand, looking at the second ring pressures is important to notice that the one at the top is the same of the one at the bottom of the first ring. From Figure 101 it is not too evident because of the magnitude of the other pressures but isolating only the one at the bottom the trend is shown in Figure 103

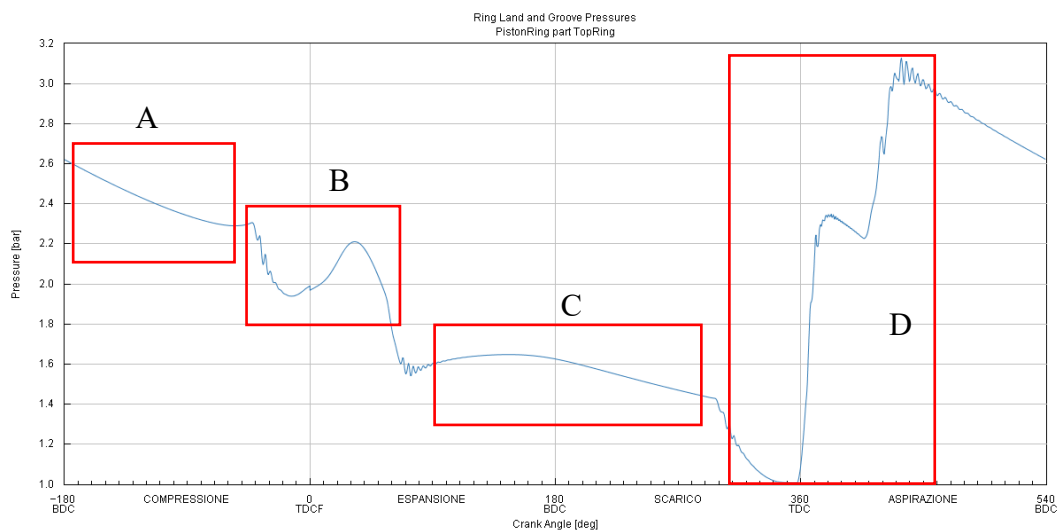


Figure 103. Pressure below first ring

First of all, is necessary to take into account that part of the gases, independently from the ring's displacements, can flow through the end gap of the rings. Referring to Figure 104 and Figure 105 is possible to see how the end gap varied along the cycle taking into account thermal expansion of the ring, local bore distortion and oil film effects. As first consideration, looking at the values of the end gap for both rings, it is always higher than $50 \mu m$, so the target of durability is verified.

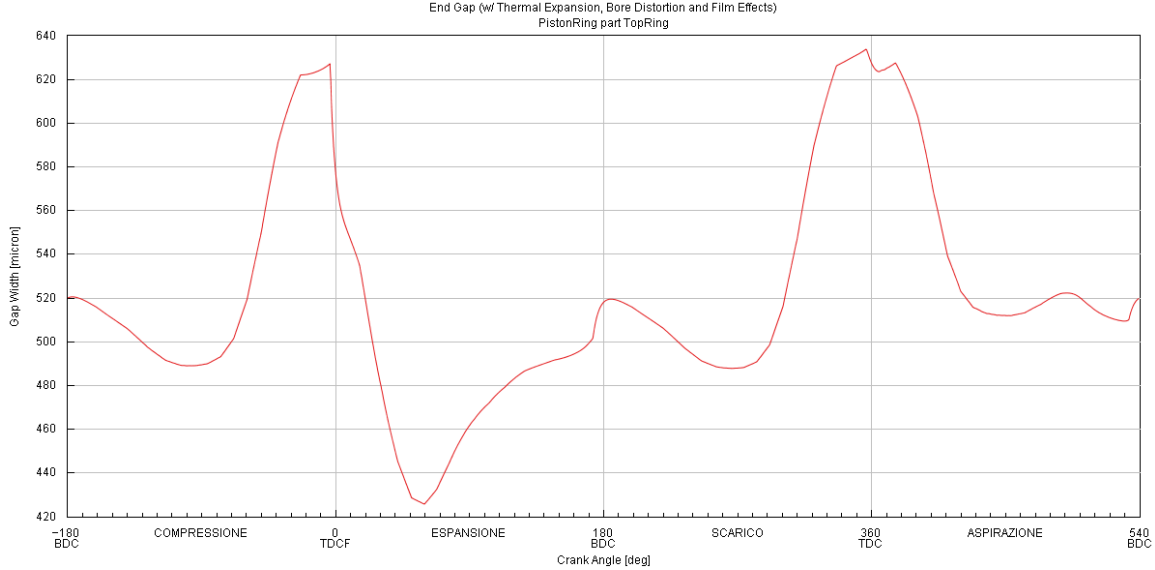


Figure 104. First ring end gap during the cycle

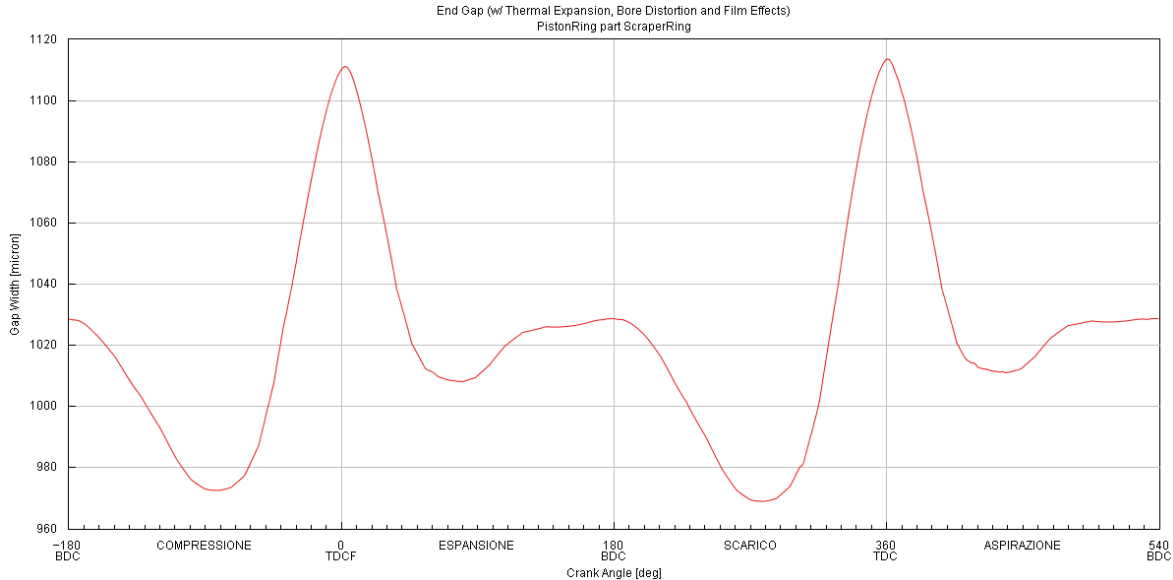


Figure 105. Second ring end gap during the cycle

The pressure normally tends to decrease due to the fact that the end gap of the ring behaves as a passage through which gases can flow. From the figures above it is possible to see that the end gap of the second ring is wider with respect to the first one so what it is expected is that a flow rate of gases goes from second land to third land volume with the pressure that decreases.

At that point to understand properly the trend of the pressure in Figure 103 it is possible to analyze the four areas that have been identified with the letters A, B, C and D.

- Region A: the pressure slightly decreases thanks to the passage of the gas between the end gap of the second ring that is higher with respect to the one of the first ring as shown above.
- Region B: there is a drop of pressure, and it is due to the movement of the second ring relative to the groove. As visible in Figure 97 a path where the gases can flow is created.
- Region C: In that region both the first and second rings are attached to the bottom part of the groove, so the only path of the gases is through the end gap, so there happen the same phenomenon that occurs in region A where the pressure slightly decreases.
- Region D: in this region the pressure overall increases because around 360 °CA both the first and second rings move upward creating a passage for the gases. Due to the fact that above and behind the first ring there is a higher pressure because it faces the combustion chamber the gases tend to move downward with an increment of the pressure in the second land. Moreover, is possible to notice another drop of pressure during the growth because looking at Figure 96 and Figure 97 the first ring moves downward closing the passage for the gases when the second ring is still upward, so for a little amount of time occurs again the phenomenon described for Region B. Finally, when also the second ring moves downward the pressure starts again to decrease until the end of the cycle.

As evidence of what said above about the continuous flow rate through the end gap of the rings it is possible to refer to Figure 106 and Figure 107.

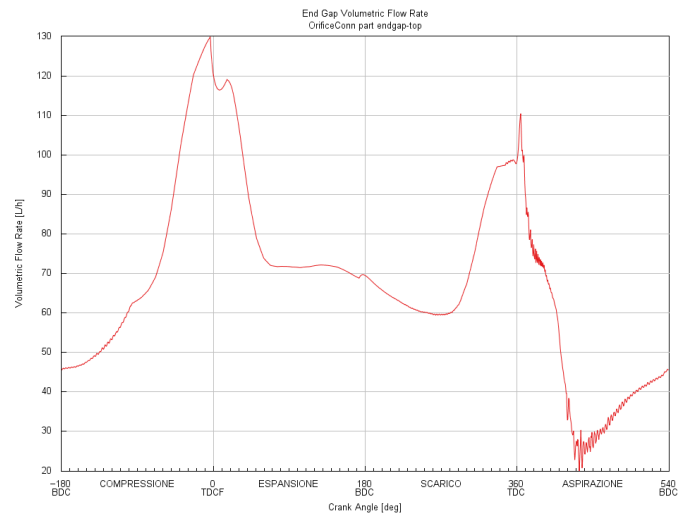


Figure 106. First ring volumetric flow rate through the end gap

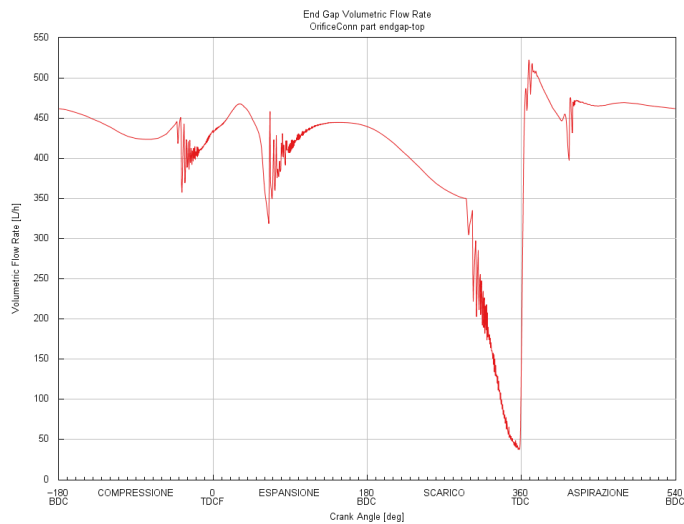


Figure 107. Second ring volumetric flow rate through the end gap

What it is possible to see is that the trend follows the one of the end gaps shown in Figure 104 and Figure 105. In fact, when the end gap is open at its maximum value there is a peak of the flow rate, which is consistent with the fact that through a higher area can pass more gases. On the other hand, looking at Figure 108 and Figure 109 it is possible to see the volumetric flow rate at the top and the bottom of the second ring. Is important to focus on second ring because all the gases escaping from it are responsible for blow-by phenomenon due to the fact that the third ring doesn't behave as a sealing ring.

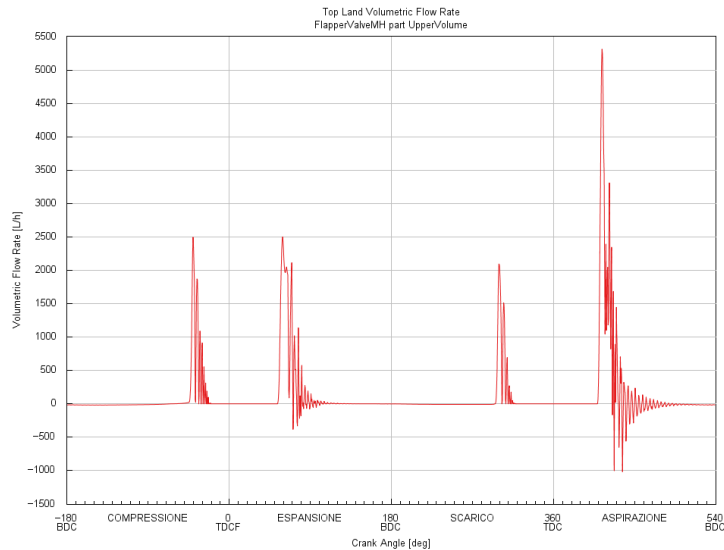


Figure 108. Top land volumetric flow rate of the second ring

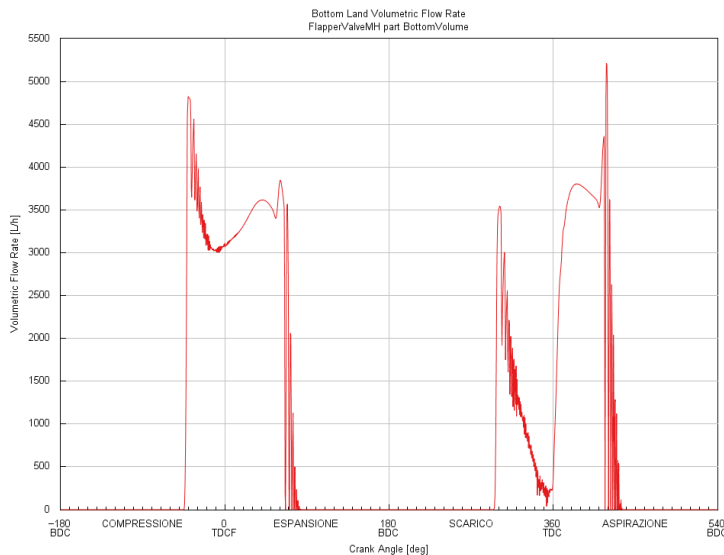


Figure 109. Bottom land volumetric flow rate of the second ring

Looking at Figure 99 where is depicted the variation of the top land volume due to ring displacement in the groove and the Top land volumetric flow rate it is possible to see that the gases move through the top land of the second ring when it moves upward relative to groove. This is due to the fact that in these moments there is a space available for the passage of the gases that is closed when the ring is pressed against the groove. On the other hand, looking at Figure 109, it is possible to see that the gases flow towards the bottom land of the second ring for all the duration of the cycle when the ring moves upward relative to the groove. This is due to the fact that when the ring moves upward a passage where the gases can flow is available.

Finally, a particular behavior is evidenced slightly both at around 0 and 360 ° CA when there is a drop of the bottom volumetric flow rate. This trend is justified because when the ring moves it tends to push the gases that will flow with a higher velocity as evidenced from the sharp rising trend of the flow rate. To keep in mind that the bottom land volumetric flow rate is the one responsible for the blowby flowrate.

The gas flowrate through the bottom flank and the end gap of the second ring according to the results obtained through the model in GT Power are listed in Table 21.

Speed [rpm]	Load [%]	Bottom Flank volumetric flow rate [l/min]	End gap volumetric flow rate [l/min]	Blow-by volumetric flowrate [l/min]
1900	100	15,76	6,83	22,59

Table 21. Blow-by results

The blow-by on the single crank is 22,59 l/min , so it means, considering all the six cylinders of the XC13 a total of 135,54 l/min. In conclusion according to the results obtained with the simulation the target, which imposes a maximum of 150 l/min is verified.

As last step is possible to compare the value obtained through the model in GT Power and the experimental results obtain from bench test. A problem faced with the XC13 with the alternative A of piston rings was an unstable blow-by, which tends to oscillate. In Figure 110 are shown the blow-by flowrate, the crankcase pressure and other values registered during a test.

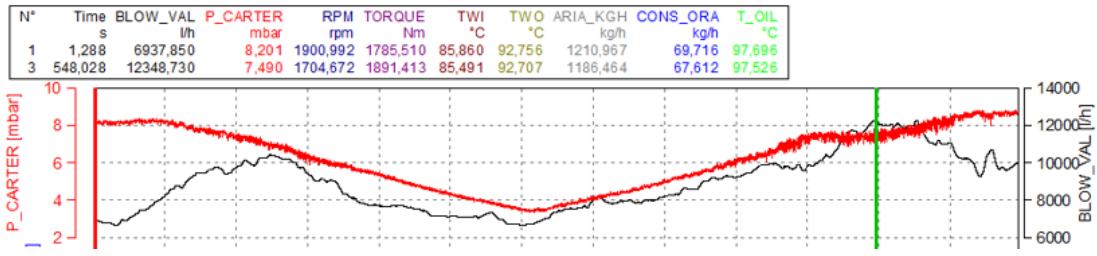


Figure 110. Test bench results

The two values considered are respectively after 1,288 s and 548,028 s and they refer to the red and green vertical lines. Looking in particular to what happen to the blow-by it oscillates between 6937,85 l/h and 12348,73 l/h on the six cylinders. Transforming these values in l/min it means that oscillates between 115 l/min and 205,81 l/min. So, the value calculated through the GT Power model lay between these two bonds, but on the other hand

considering the upper limit it doesn't respect the product target of 150 l/min imposed at the beginning of the project.

7. Conclusions

The PCU system, comprising the piston, liner, and piston rings, plays a crucial role in engine performance. This research has highlighted the importance of optimizing this system to enhance engine efficiency, reduce frictional losses, and minimize blow-by flow rate. Moreover, the work provides an overview of the typical approach used at FPT Industrial to develop a new project and ensure the achievement of the set targets.

The primary function of the piston ring pack is to act as a dynamic seal, preventing gas leakage into the crankcase and vice versa. This is done to improve engine thermal efficiency by reducing blow-by gases. Blow-by and PCU friction analysis have been performed using a GT Power model, which models a single crank and allows us to understand the system's behavior.

In conclusion, this thesis has shed light on the crucial aspects of friction and blow-by flowrate control within the PCU system of a CNG engine. The usage of the GT Power model and the insights gained from this study provide valuable contributions to the field of heavy-duty engine development, with potential implications for reducing the environmental impact of transportation.

In this work some of the targets decided at the beginning of the XC13–CNG project has been investigated. In particular, the target of maximum friction power on the single crank and of the maximum blow-by flowrate of the whole engine at maximum power have been verified.

The results show that the third piston ring has the greatest influence on friction, followed by the first and then the second rings. This is because the third ring experiences the highest tangential load and consistently faces an asperity lubricating condition, resulting in a higher friction coefficient between the ring material and the liner. In contrast, the first ring experiences high pressure from the combustion chamber, pushing it against the liner for most of the time, leading to a hydrodynamic lubricating condition and lower friction power compared to the third ring. The behavior of the second ring is similar to the first, but with significantly lower pressure behind it pushing against the liner.

Regarding the blow-by flow rate, it is closely related to the dynamics of the rings. As the first ring moves upward within its piston groove, some of the gases tend to pass from the first to the second land of the piston. When the second ring also starts to move relative to its piston groove,

the accumulated gases in the second land move towards the third land, where they encounter the third ring. Since the third ring does not have a sealing function, the gases can escape into the crankcase, leading to the blow-by phenomenon.

Several factors influence the piston rings' dynamics, including ring mass, which plays a crucial role as the rings follow the reciprocating movement of the piston and experience acceleration and inertia forces proportional to their mass. These inertia forces are responsible for the relative movement of the ring inside the piston groove when it approaches the TDC and BDC. The tangential load and inertia moment of the cross-section of the rings also significantly influence their twist movement and their ability to prevent blow-by. The volumes between the rings are essential to prevent pressure buildup within the piston lands, and for this reason there is a cavity in the piston between the first and second rings to increase the volume. Another critical aspect related to blow-by flow rate is the end gap of the rings, which generates a continuous flow rate. Minimizing the operating end gap is essential, considering proper design, bore distortion due to the liner's hot deformation, fastening of the cylinder head to the cylinder block, and thermal expansion of the ring.

Focusing on the piston skirt, apart from the TDC and BDC where the speed tends to be negligible, it predominantly experiences a hydrodynamic lubricating condition, so the friction power in this area, while not insignificant, is not exceptionally high due to the wide area of the piston skirt on both the thrust and anti-thrust sides.

As final result is possible to evidence that as the engine speed increase, as expected, the friction power from each single crank component tends to increase, except for the small eye where there is a peak followed by a decrease of friction power.

7.1 Recommendations and future works

This dissertation suggests following issues to be considered for further research:

1. The effect of piston secondary motion on ring pack lubrication needs further investigations. Rings motions such as tilting in the groove has not deeply exploited due to lack of information from the supplier. These motions are affected by piston dynamics that changes the local oil film thickness. A detailed and comprehensive piston ring lubrication model may be useful to address this issue.
2. Pre-twist of the rings, which contributes to reduce blow-by flowrate can be investigated and a model to calculate it according to cross sectional area and the tangential operating load of the ring may be investigated.
3. The accurate prediction of skirt deformation, especially 3D evaluations considering piston ovality and its real geometry may be important due to model hydrodynamic pressure at skirt and liner interface along the piston and skirt deformation subjected to in cylinder pressure and temperature.
4. Implementation of FE model of engine components in the GT Power model in order to exploit better the dynamic behavior of the different parts and predict in a more appropriate way the secondary motion of the piston. With the current model used for the work all the geometrical and dynamic properties have been defined through the dedicated format of the program that tends to simplify the geometries of the parts.
5. Validate through real engine tests the results obtained thanks to the model in order to understand the reliability of the GT Power model.

References

- [1] Prof. Stefano D'Ambrosio, Propulsion Systems and their Application to Vehicle, EXHAUST GAS EMISSIONS OF ICE AFTERTREATMENT SYSTEMS EMISSION REGULATIONS. In: 2022/2023 (Cit. on pp. 22,27)
- [2] AECC – Association for emission control by catalyst. In: 2020 (Cit on pp. 26)
- [3] Technical Guidelines for the preparation of applications for the approval of innovative technologies pursuant to Regulation (EC) No 443/2009 and Regulation (EU) No 510/2011. In: 2018 (Cit on pp. 28)
- [4] Implementation of Regulation (EU) 2017/2400 as regards the determination of the CO₂ emissions and fuel consumption of heavy-duty vehicles. In: 2018 (Cit on pp. 29)
- [5] Pistons and engine testing / Cylinder components, MAHLE GmbH (Ed), 2nd edition, Springer Vieweg (Cit on pp. 42, 46, 50, 65)
- [6] Prof. Stefano D'Ambrosio, Propulsion Systems and their Application to Vehicle, MECHANICAL EFFICIENCY. In: 2022/2023 (Cit. on pp. 67)
- [7] Prof. Carlo Rosso, Powertrain Component Design – Engine, PISTON, In: 2022/2023 (Cit on pp. 62)
- [8] Baelden C., Tian T., A Dual Curved Beam Finite Element Model of Piston Rings for Improved Contact Capabilities, SAE Int. J. Engines, 2014, 7(1): 156-171, doi: 10.4271/2014-01-1085 (Cit on pp. 63)
- [9] Prof. Carlo Rosso, Powertrain Component Design – Engine, BEARINGS, In: 2022/2023 (Cit on pp. 66)